

Aus dem Bereich
Theoretische Medizin und Biowissenschaften
der Medizinischen Fakultät
der Universität des Saarlandes, Homburg/Saar

**Multiphoton Imaging and Nanoprocessing of Stem Cells
with Near Infrared Femtosecond Laser Pulses**

Dissertation zur Erlangung des Grades eines Doktors der Naturwissenschaften

der Medizinischen Fakultät

der UNIVERSITÄT DES SAARLANDES

2009

vorgelegt von: Aisada Uchugonova

geboren am 3. Mai 1977 in Kyrgyzstan

Dekan: Prof. Dr. Michael D. Menger

Erstgutachter: Prof. Dr. Günter R. Fuhr

Zweitgutachter: Prof. Dr. Karsten König

Drittgutachter: Prof. Dr. Berthold Seitz

Tag der Disputation: 26.10.2009

*Бул жазылган илимий эмгегим атам Учугенов Асан менен
апам Миталипова Базирага арналат*

Summary

This dissertation focuses on the application of optical techniques in stem cell research.

Marker-free multiphoton microscopy was employed to study the morphology and the functional activity of stem cells as well as to perform laser nanoprocessing for targeted transfection and optical cleaning of cell clusters.

Stem cells are major research objects in medicine and biotechnology and may revolutionize current therapy. So far, stem cells have to be characterized and sorted by techniques such as FACS (fluorescence-activated cell sorting), MACS (magnetic-activated cell sorting), PCR (polymerase chain reaction), and immunocytochemistry. All these methods require exogenous probes and are often destructive. Also the transfection of stem cells faces problems when using traditional methods such as viral transfection, electrotransfection, or chemotransfection.

Within this work, live adult animal and adult human pancreatic, mesenchymal, salivary gland (*glandula submandibularis*), and dental pulp stem cells have been investigated with specially designed 5D multiphoton microscopes with submicron spatial resolution, picosecond temporal resolution, and 10 nm spectral resolution. Stem cell monolayers as well as stem cell spheroids have been imaged and the biosynthesis of collagen and lipids resulting from chondrogenic, osteogenic, and adipogenic differentiation processes has been detected over time periods up to five weeks. Furthermore, for the first time a sub-20 femtosecond laser scanning microscope was employed to image and nanoprocess single stem cells without any collateral destructive effects. In fact, transient nanoholes could be created and used to realize highly efficient targeted transfection.

From the results of this dissertation can be concluded that near infrared femtosecond laser multiphoton microscopes have the potential to become valuable optical tools in stem cell research for marker-free characterization and precise optical nanomanipulation of living animal and human stem cells.

Zusammenfassung

Thema dieser Dissertation ist die Nutzung optischer Techniken in der Stammzellforschung. Die Marker-freie Multiphotonen-Mikroskopie wurde sowohl für die Untersuchung der Morphologie und der funktionellen Aktivität von Stammzellen als auch für eine Laser-Nanobearbeitung zur gezielten Transfektion und zur optischen Säuberung von Zellclustern eingesetzt.

Stammzellen sind wichtige Forschungsobjekte der Medizin und der Biotechnologie. Sie haben das Potential, gegenwärtige Therapieformen zu revolutionieren. Bislang wurden für die Charakterisierung und die Sortierung von Stammzellen, Techniken wie FACS (Fluoreszenz-aktivierte Zellsortierung), MACS (Magnet-aktivierte Zellsortierung), PCR (Polymerase-Kettenreaktion) und Immunocytochemie eingesetzt. Alle diese Techniken erfordern exogene Marker und sie wirken oftmals destruktiv. Auch die Transfektion von Stammzellen kann problematisch sein, wenn konventionelle Methoden wie die virale Transfektion, die Elektrotransfektion und die Chemotransfektion eingesetzt werden.

Im Rahmen dieser Arbeit, wurden lebende adulte tierische und menschliche pankreatische, mesenchymale, (Unterkiefer-) Speicheldrüsen (*glandula submandibularis*)- und dentale Pulpa- Stammzellen mittels speziell entwickelter 5D Multiphotonen-Mikroskope mit Sub-Mikrometer-Auflösung, Pikosekunden-zeitlicher Auflösung und 10 nm spektraler Auflösung untersucht. Stammzellen in Monolayer- und Spheroid-Kulturen wurden bildgebend detektiert und die Biosynthese von Kollagen und Fetten als Resultat von chondrogenen, osteogenen und adipogenen Differenzierungsprozessen über einen langen Zeitraum von bis zu 5 Wochen dokumentiert. Zudem wurde erstmals ein Sub-20 Femtosekunden-Mikroskop für die Bildgebung und die Nanobearbeitung von einzelnen Stammzellen eingesetzt, ohne kollaterale Schäden zu verursachen. Es konnten transiente Nanoporen erzeugt und für eine äusserst effiziente gezielte Transfektion genutzt werden.

Basierend auf den Ergebnissen dieser Dissertation kann zusammenfassend betont werden, dass nahe-infrarote Femtosekundenlaser-Multiphotonenmikroskope das Potential haben, wertvolle Werkzeuge in der Stammzellforschung für die Marker-freie Charakterisierung und die präzise optische Nanomanipulation tierischer und menschlicher Stammzellen zu werden.

CONTENTS

Summary	v
Zusammenfassung	vi
PREFACE	1
1. INTRODUCTION	3
1.1. Stem cells	3
1.2. State-of-the-art technologies to identify and to characterize stem cells	11
1.3. State-of-the-art technologies for transfection of stem cells	14
1.4. Multiphoton microscopy	18
1.5. Optical nanoprocessing	23
1.6. Aims of the work	26
2. MATERIAL AND METHODS	27
2.1. Cells	27
2.1.1. Cell lines	27
2.1.2. Cell cultures	29
2.1.3. Manufacturing of spheroids	29
2.1.4. Stem cell differentiation	31
2.2. Chemical probes/procedures	31
2.2.1. Reactive oxygen species (ROS) detection	31
2.2.2. DNA break detection	32
2.2.3. Apoptosis detection	32
2.2.4. Vitality tests	33
2.2.5. Detection of collagen	33
2.2.6. Staining of adipocytes	34
2.2.7. Staining of lysosomes	34
2.2.8. Staining of mitochondria	34
2.3. Experimental systems	35
2.3.1. Modified ZEISS LSM510-NLO (META) multiphoton microscope	35
2.3.2. Sub-20 femtosecond laser microscope FemtOgene	37
2.4. Optical sectioning (3D microscopy: x,y,z)	39
2.5. Fluorescence lifetime imaging (4D microscopy: x,y,z,τ) and FLIM data analysis ..	40
2.6. Spectral imaging (5D microscopy: x,y,z,τ, λ) and spectral data analysis	42

2.7. Statistical analysis	43
3. RESULTS	45
3.1. Influence of femtosecond laser radiation on cell viability	45
3.1.1. Damage mechanisms.....	45
3.1.2. Photoinduced modifications of morphology	48
3.1.3. Detection of photoinduced reactive oxygen species	48
3.1.4. Detection of photoinduced DNA strand breaks	50
3.1.5. Detection of photoinduced early apoptosis	50
3.2. Two-photon imaging	52
3.2.1. Autofluorescence imaging of stem cells	52
3.2.2. Spectral measurements of stem cells	54
3.2.3. FLIM measurements	56
3.2.4. SHG imaging.....	66
3.2.5. Two-photon imaging of lysosomes.....	70
3.3. Nanoprocessing	72
3.3.1. Nanosurgery of single cell in cell monolayers.....	72
3.3.2. Optical knock out of single cells in stem cell spheroids/clusters.....	76
3.4. Optical transfection of stem cells	78
3.4.1. Optoinjection of fluorescent molecules	78
3.4.2. Targeted transfection.....	79
4. DISCUSSION AND CONCLUSION	83
5. OUTLOOK/FUTURE DIRECTIONS.....	91
6. BIBLIOGRAPHY	95
Frequently Used Abbreviations	111
List of Figures	113
List of Tables.....	120
Appendix A	121
Appendix B.....	123
Appendix C	125
Acknowledgements.....	127
Own Publication List	129
Declaration.....	131
Curriculum Vitae	133

PREFACE

This dissertation focuses on the usage of optical techniques in particular multiphoton microscopy to study the morphology and the functional activity of stem cells as well as to perform laser nanoprocessing. There is considerable interest in the areas of developmental biology, cell biology, nanobiotechnology, and medicine to understand the functional activity of the stem cells, to track, to isolate, as well as to manipulate them.

Stem cell therapy was first demonstrated on patients with leukemia by the Nobel laureate E. Donall Thomas at MIT in 1956. Now there is substantial hope that in feasible future stem cells can be used to treat degenerative diseases like Parkinson's, Alzheimer's, cancer, diabetes, arthritis, osteoporosis, and heart diseases, where the function or structure of the affected tissues and organs progressively deteriorate over time. In addition, stem cells will be used to engineer tissues and to create novel pharmaceutical components.

So far, stem cells have to be characterized and sorted by techniques which require exogenous probes and which are often destructive. Non-destructive marker-free *in vivo* techniques are required to trace and image the stem cells over a long period of time as well as to study their differentiation process. Multiphoton femtosecond laser microscopy is the ideal technique to image stem cells without a marker. Multiphoton microscopy is based on the simultaneous absorption of two near infrared photons (two-photon microscopy) or more photons.

Two-photon microscopy was introduced by Denk, Strickler, and Webb in 1990. Since then, the microscopy techniques have revolutionized biological sciences including deep tissue imaging, live cell imaging, etc. Two-photon microscopy enables the non-destructive imaging of living cells without any exogenous markers based on nonlinear excitation of endogenous fluorophores such as NAD(P)H and flavins. Furthermore, two-photon microscopy based on second harmonic generation (SHG) allows imaging of the extracellular matrix component collagen.

In this dissertation, adult pancreatic, mesenchymal, salivary gland, and dental pulp stem cells have been investigated with multiphoton microscopy. Working in "five dimensions (5D)", the autofluorescence signals from the specimen were spatially resolved (3D), the fluorescence lifetime determined (4D), and the emission spectrum of the signal depicted (5D). This special multiphoton microscope was employed to study stem cell monolayers as well as stem cell spheroids over time periods of about 5 weeks. The biosynthesis of collagen and lipids as result of the chondrogenic, osteogenic, and adipogenic differentiation processes was monitored. Furthermore, a novel sub-20 femtosecond multiphoton laser scanning microscope

Preface

was used to realize highly efficient targeted transfection. In addition, the optical knock-out of cells was performed without damage to the microenvironment.

The dissertation is organized as follows:

Chapter 1: This chapter *Introduction* covers a review on isolation, characterization and application of stem cells, state-of-the-art transfection technologies, multiphoton microscopy, and optical nanoprocessing. The aims of this dissertation are presented.

Chapter 2: Materials and methods are described in this chapter for the following: (i) the cells, (ii) the probes and procedures such as detection of reactive oxygen species, apoptosis, and DNA breaks, (iii) the experimental systems including the 5D femtosecond laser microscope and the sub-20 femtosecond laser microscope, (iv) optical sectioning, (v) fluorescence lifetime imaging, and (vi) spectral imaging.

Chapter 3: In this chapter, the results of the investigation of cell viability in course of the interaction with femtosecond laser pulses, 5D multiphoton imaging, as well as nanoprocessing for targeted transfection and optical cleaning of stem cell clusters are described.

Chapter 4: This chapter covers the discussion of the results of multiphoton microscopy on stem cells with respect to recent publications and provides conclusions.

Chapter 5: This chapter focuses on future directions of the work and places emphasis on the potential of the multiphoton technology in the current “bench to bedside stage” of stem cell applications.

This dissertation closes with a bibliography, abbreviations, list of figures and tables, appendices with three published papers, acknowledgements, my publication list, the declaration and the CV.

1. INTRODUCTION

This chapter introduction gives an overview of the history of stem cell research, discusses the use of embryonic versus human adult stem cells, and describes state-of-the-art techniques to characterize, to sort, and to transfect stem cells. Furthermore, the method of multiphoton microscopy for high-resolution marker-free imaging and the method of femtosecond laser nanoprocessing are described. Finally, the detailed aims of this dissertation are outlined.

1.1. Stem cells

The Russian histologist A. Maximow predicted the existence of stem cells in 1909 (Maximow 1909). Nearly 50 years after his postulate, McCulloch, Till and Siminovitch demonstrated the presence of stem cells in mouse bone marrow (Siminovitch *et al.* 1963). Currently, stem cells became major research subjects in medicine and biotechnology.

By definition, stem cells are unspecialized cells capable of dividing and self renew. They can give rise to specialized cell types under certain conditions.

Scientists classify stem cells into two groups by their origin: embryonic stem cells and adult stem cells (tissue specific stem cells). Embryonic stem cells (ESCs) are derived from the inner cell mass of a blastocyst (4-5 days old embryo, approximately 64-200 cells) as shown in Fig. 1.1. First ESCs have been isolated in 1981 from mouse (Martin 1981; Evans and Kaufman 1981), the first non-human primate ESCs in 1995 (Thomson *et al.* 1995) and the first human embryonic stem cells in 1998 (Thomson *et al.* 1998) from an *in vitro* fertilized blastocyst. In 2009, the world's first human clinical trial of embryonic stem cell-based therapy was approved on patients with spinal cord injuries (Geron Corp., Menlo Park, CA, USA; www.geron.com). Embryonic stem cells are "pluripotent": they can produce all differentiated cell types of the body (cells from all three germ layers: meso-, endo-, ectoderm) as described in Fig. 1.1. The fertilized egg is known as a totipotent cell, since it can give rise to all the cells and tissues of the developing embryo.

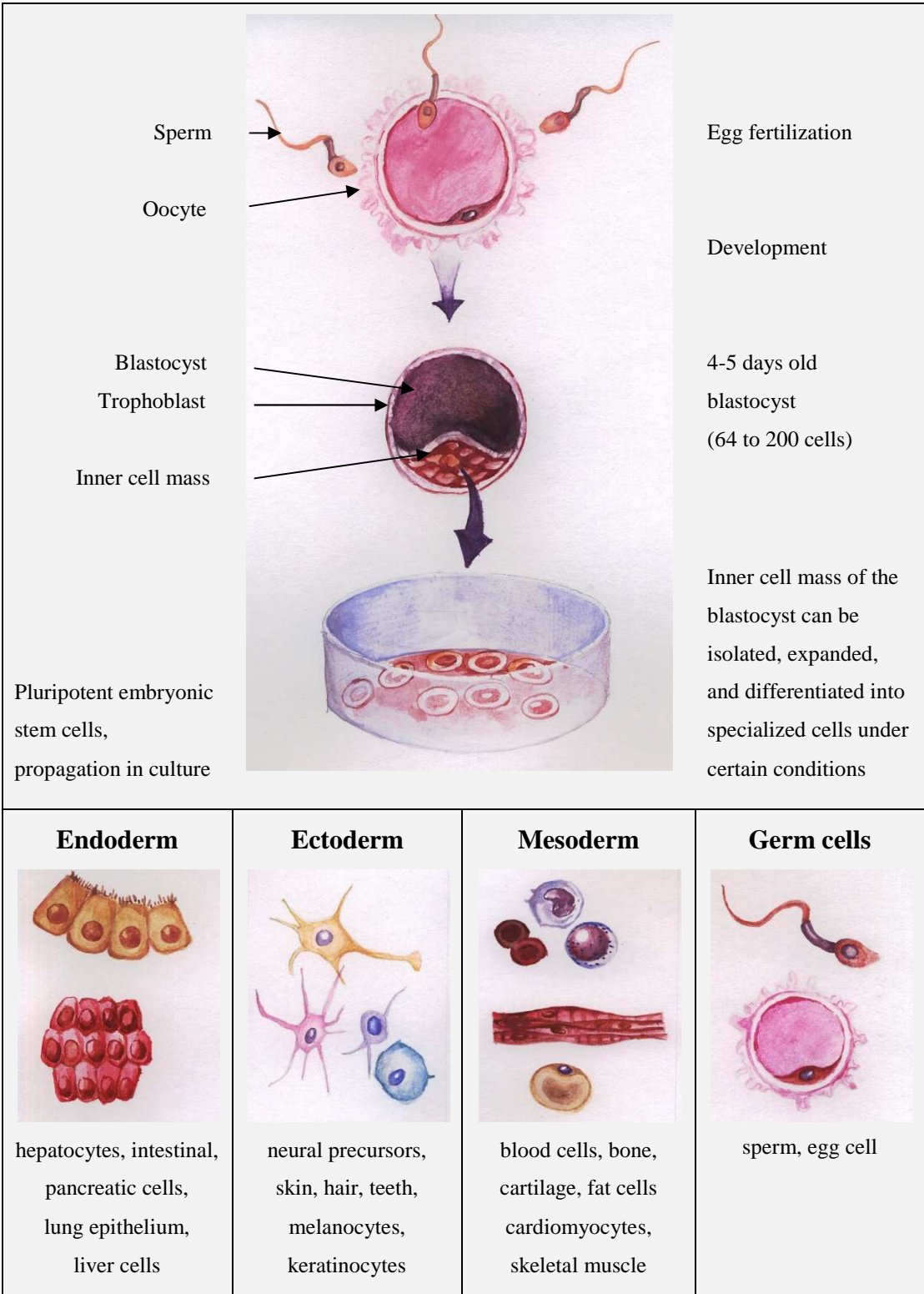


Fig. 1.1: Scheme of the ESCs isolation process and examples for human embryonic stem cell-derived cell types.

The differentiation of stem cells into mature cell types is usually accomplished through the generation of intermediate cell types called progenitors and precursors cells.

Adult stem cells, also termed somatic or tissue specific stem cells, have been found among differentiated cells within fully developed tissues or organs. Fig. 1.2 demonstrates identified stem cell populations in human skin. Mesenchymal stem cells have been isolated in a number of different tissues like bone, skin, muscle, adipose, cartilage, peripheral, and umbilical cord blood (Friedenstein *et al.* 1968; Loncar 1992; Nuttal *et al.* 1998; Zuk *et al.* 2001; Young *et al.* 2001; Gimble and Guilak 2003). Hematopoietic stem cells have been isolated from peripheral blood, umbilical cord blood, and bone marrow (Till and McCulloch 1980). Neural stem cells have been isolated from different parts of the brain. The subventricular zone is considered to be the main source of neural stem cells (Morshead *et al.* 1994; Gritti *et al.* 1996; Weiss *et al.* 1996; Palmer *et al.* 1999). Songtao Shi *et al.* (2003) discovered a source of adult stem cells in children's primary teeth. Stem cells have been found in human hairs (Hoffman 2006), in the retina, the skin, the lung, the liver (In't Anker *et al.* 2003), and from glands like thyroid (Thomas *et al.* 2006), testis (Guan *et al.* 2006), salivary gland (Hisatomi *et al.* 2004), and pancreas (Kruse *et al.* 2004, Seaberg *et al.* 2004). Recently, De Coppy *et al.* (2007) reported on stem cells from umbilical fluid which share markers of embryonic and adult stem cells.

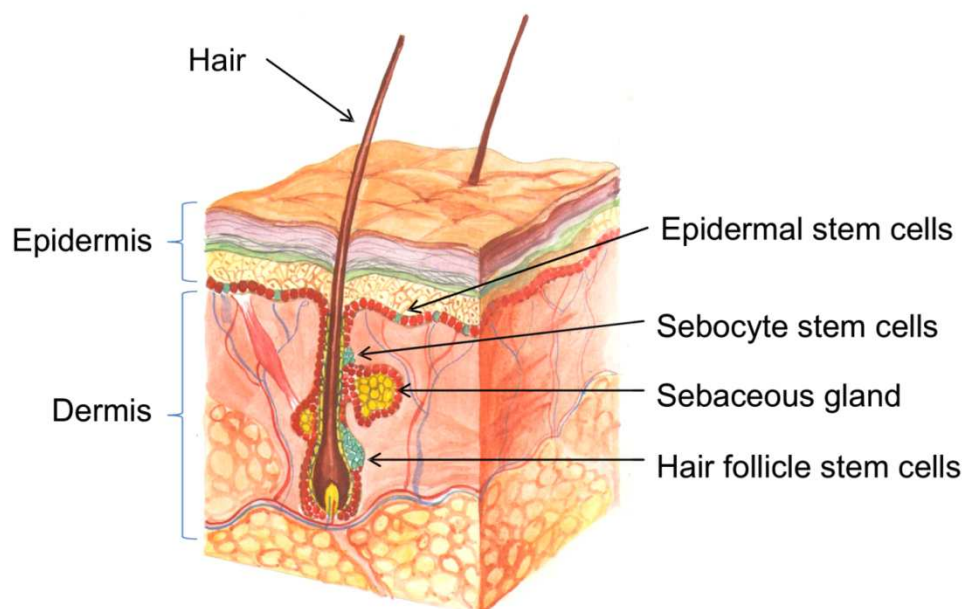


Fig. 1.2: Illustration of tissue specific stem cells from the skin. Stem cell populations have been identified in the epidermis (stratum basale), the hair follicle, and in the sebaceous gland.

Introduction 1

Adult stem cells are found nearly in all adult organs and tissues but in a low abundance. For example, mesenchymal stem cells represent 0.01–0.0001% of the total population of nucleated cells in the bone marrow (Pittenger *et al.* 1999; Sakaguchi *et al.* 2005).

Adult stem cells are considered to differentiate mainly into the specialized cell types depending on the kind of tissue they have been found in. They are “multipotent”. However, several studies have also shown that cells originated from the mesoderm (muscle, blood, bone, fat) can produce cells normally originated from the endoderm (gut, lungs, liver, and pancreas) and the ectoderm (skin, nervous system) germ layer. Also, cells from the endoderm and the ectoderm can generate cells of other germ layers. For instance, bone marrow stem cells have been found to be able to differentiate into brain astrocytes (Eglitis and Mezey 1997), into neurons (Mezey *et al.* 2000), and into myocardial cells (Orlic *et al.* 2001) besides adipocytes, osteoblasts, chondrocytes, and smooth as well as cardiac muscle cells (Minguell *et al.* 2001). Bjornson *et al.* (1999) reported that neural stem cells can be differentiated into blood and into immune cells. Korbling *et al.* (2002) reported on the differentiation ability of hematopoietic stem cells to produce epithelial cells and hepatocytes. Furthermore, pancreatic stem cells can be differentiated into cell types of three embryonic germ layers (Kruse *et al.* 2006; Rapoport *et al.* 2009). This process is called “transdifferentiation”- somatic stem cells have broadened potency and can generate cells of other lineages. The key to transdifferentiation is very controversial in mammals (Jaenisch and Young 2008).

Under laboratory condition, directed differentiation can be reached by stimulation of certain factors and cytokines. For instance, TGF- β has found to be factor for cartilage differentiation, BMP for osteoblasts differentiation, insulin and dexamethasone for adipocytes, and retinoic acid for neural cells differentiation. Nanostructures (topography) (Yim *et al.* 2007; Cecchini *et al.* 2007; Neeley *et al.* 2008), mechanical stress, vibration, temperature, light, pressure and electrical field can induce differentiation (Sauer *et al.* 1999; Zou *et al.* 2006; Wagner *et al.* 2008; Ge *et al.* 2009). Differentiated cells can be evaluated by their morphology, function, and gene profiles (chapter 1.2).

Different types of stem cells can be identified by antigens. For instance, mesenchymal stem cells express Stro-1, and SH-2, whereas hemotopoetic stem cells express CD34, Sca-1, and c-Kit. Neural stem cells can be distinguished by the intermediate filament protein-nestin, and the neurotrophin receptor. ESCs can be identified by cell surface SSEA-1, nanog, and Oct4 and expression of other early antigenes. These markers are detected by immunocytochemistry staining or FACS (chapter 1.2).

However, in most cases stem cells are not well defined by markers. Neural stem cells isolated from different parts of the brain behave differently and molecularly distinct from each other. Nestin was believed to be a marker of neural stem/progenitor cells. However, nestin positive cells have been isolated from human islet too (Kruse *et al.* 2006). Also, some mesenchymal stem cells have been found to be able to express nestin. Pancreatic stem cells isolated from the exocrine (Kruse *et al.* 2004) express embryonic stem cell markers Oct4 and nanog. There is a need to provide more specific markers for identification of stem cell types.

Interestingly, stem cells are able to proliferate in cell cultures while retaining the differentiation capacity. ESCs can be grown in their non-differentiated state for many generations and large quantities of cells can be produced in the laboratory. It has been proven that ESCs can be used to produce cells from the three germ layers including germ cells under laboratory condition. The high potential of ESCs to treat diseases has been tested on animal models successfully. Not so many studies have been conducted on human ESCs because of ethical constraints.

A tumorigenicity of ESCs has been reported upon transplantation (Chung *et al.* 2006). Even a single non-differentiated cell can initiate a tumor. Because of this tumorigenicity, it is recommended to differentiate cells in laboratory before performing the transplantation.

Non-invasive tools are required to control and monitor the growth, the proliferation and the differentiation of stem cells.

The use of adult stem cells is preferred because of legal and ethical concerns about the employment of ESCs (Camporesi 2007). Compared to ESCs, the proliferation and differentiation capacity of adult stem cells is limited. Under laboratory condition, adult stem cells stop to divide after some passages. This phenomenon is explained with the decrease of telomerase activity and the shortening of the telomere length (Suwa *et al.* 2001; Oh *et al.* 2004; Ju and Rudolph 2006). Furthermore, a prolonged culture of adult stem cells can induce tumorigenicity (Rubio 2005). Freshly isolated adult stem cells do not show a propensity for tumor formation. Case *et al.* (2008) demonstrated that clonally derived cell lines retain heterogeneous potential. Undesired differentiation occurs under laboratory condition (Bruder 1997).

Spontaneous differentiation remains a big problem of adult stem cell cultures. Main advantages of adult stem cells are: (i) they are easily accessible and obtainable in large quantities (e.g. stem cells from adipose tissue, peripheral and umbilical cord blood) and (ii) they provoke less ethical controversy than embryonic stem cells.

Introduction 1

Research on stem cells attracts considerable attention in developmental biology, nanobiotechnology, and medicine. Major research topics include the understanding of mammalian development, the onset of diseases, and the development of novel pharmaceutical substances. The most attractive application field is the stem cell therapy.

For the first time stem cells have been used in clinical therapy and demonstrated on patients with leukemia by Nobel laureate E. Donall Thomas (1956) and his colleagues at the Massachusetts Institute of Technology (MIT). Nowadays, hematopoietic and bone marrow stem cell transplantation have become the standard therapy to treat patients with leukemia and lymphoma in combination with chemo- and radiation therapy. Chemo- and radiation therapy are used to eradicate malignant cells. Afterwards stem/precursor cells are transplanted to repopulate the bone marrow. Patient's own cells can be transplanted (autologous). An alternative source is stem cells from an identical twin (syngeneic), or from a human leukocyte antigen (HLA)-matched donor (allogeneic).

Currently many studies show the high potential of stem cells to cure many diseases which are still considered incurable. Neurological diseases are related with a loss of functional nerve cells after injury or related with age (nerve cells are considered to be not able to divide and replace themselves). They can be treated with stem cells. Stem cells can generate neurotransmitter producing neurons which is important to treat Parkinson's disease and Alzheimer's disease. It was successfully conducted that stem cells can replace dopamine producing neuron cells, as well as other functional nerve cells (Miller 2006; Yu and Silva 2008). Mezey *et al.* (2000; 2003) have verified that transplanted bone marrow stem cells generated new neurons in human brain.

Hematopoietic and mesenchymal stem cells could have also a high potential to cure cardiac diseases. A recent study demonstrated an autologous implantation of stem cells derived from bone marrow to patients who had a myocardial infarction (Stamm *et al.* 2003). Transplanted stem cells were capable to regenerate infarcted myocardium and to induce angio- and myogenesis, and to recover cardiac function.

The transplantation of autologous stem cells has the advantage that the patient becomes his own donor which avoids the problem of immunological incompatibility of tissues.

Furthermore, stem cells have been used to generate insulin-producing pancreatic β cells to treat diabetes (Lechner and Habener 2003; Hussain and Theise 2004). Recent research has shown essential roles of stem cells for the treatment of immunodeficiency diseases and cancer (Joshi *et al.* 2000).

Stem cells from bone marrow (or from peripheral blood) have to be purified from red blood cells, white blood cells, and blood plasma before transplantation. The separation of stem cells from these other cell types is based on their specific adherence to plastics. After separation they are tested on viability and finally transplanted to patients.

There are several approaches to transplant stem cells. Cells are administered to patients intravenously, intrathecally (injected directly in the liquor), or transplanted directly to the damaged organ.

Stem cells injected intravenously could migrate to all parts of the body. They can reach damaged tissues including the brain, with its high limits of the access of serum constituents and circulating cells due to the blood-brain barrier containing endothelial tight junctions (Priller 2001). The transplantation process of the cells into the organs like heart, brain, liver, and pancreas is invasive and could cause inflammation. However, this direct application of stem cells is preferred in order to get the maximum available amount of cells into the damaged tissue.

Till 2009, more than 2000 patients with different diagnosis such as Parkinson's disease, Alzheimer's disease, cerebral palsy, diabetes Mellitus, spinal cord injury, cardiac infarction etc. have been successfully treated with adult stem cells from bone marrow in Germany (X-Cell Center at the Institute of Regenerative Medicine, Germany; www.xcell-center.de).

According to these results, the autologous stem cell treatment obviously seems to be advantageous. No side effects have been reported. However, the exact clinical (repair) phenomenon remains not understood. It would be helpful to trace individual stem cells in culture as well as *in vivo* to study their interaction with the microenvironment over a long period of time.

Autologous stem cell transplantation may revolutionize current therapy. It would be of great advantage to use a variety of adult stem cell types from different parts of the body. Unfortunately, so far it is difficult to identify, to isolate, and to purify adult stem cells from the tissue (chapter 1.2).

Besides stem cell therapy based on the direct application of stem cells to the human body, tissue engineering is a further major application field. New tissues can be generated from the patient's own cells and can be transplanted to treat organ failure or to replace a tissue loss (Muschler *et al.* 2004). In that case, a donor is not needed and there is no problem of immunological biocompatibility. The goal is to engineer tissues which are nearly identical to natural and physiological functional tissues (Murry *et al.* 1996; Taylor *et al.* 1998; Tomita *et*

Introduction 1

al. 1999) which would overcome the problem of the transplanted purely artificial and mechanical prostheses (e.g. ceramics and metals are used as knee joints, polymer heart valves, and teeth prosthesis) that cannot display physiological function and are not able to self-repair. So far a variety of tissues/organs like bladder, blood vessels, skin, cartilage, heart valve, kidney, liver, salivary glands, pancreas, ear, bone have been generated by tissue engineering and clinical trials have been conducted (Schenke-Layland *et al.* 2006).

Stem cells can be genetically modified for stem cell therapy (chapter 1.3). Specific cell populations can be developed. Due to the restriction of the isolation of ESCs from blastocytes, scientists are interested to produce ESC like cells from somatic cells through reprogramming and nuclear transfer. In 2007, Kazutoshi Takahachi at the Kyoto University demonstrated that induced pluripotent stem cells (iPSC) can be generated from adult dermal fibroblasts. They could reprogram murine and human somatic cells into embryonic-like pluripotent cells by introducing four genes Oct3/4, Sox2, Klf4, and c-Myc using viral transduction methods (Takahashi *et al.* 2007). Kim *et al.* (2009) reported that Oct4 is sufficient to generate pluripotent stem cells from adult mouse neural stem cells (NSCs). These one-factor induced pluripotent stem cells are similar to embryonic stem cells *in vitro* and *in vivo* and can be efficiently differentiated into NSCs, cardiomyocytes, and germ cells *in vitro*, but they are also capable of teratoma formation and germline transmission *in vivo*. However, the authors faced problems with an extremely low efficiency. The use of viruses can cause significant risk for human therapy. Zhou *et al.* (2009) demonstrated the iPSC generation using recombinant proteins without using DNA. Kaji *et al.* (2009) reported on the removal of such transgenes once reprogramming has been achieved.

1.2. State-of-the-art technologies to identify and to characterize stem cells

Stem cells exist only in low abundancies among the heterogeneous cell population of tissues. For example, one stem cell is present among 100,000 cells in the circulating blood. In most cases stem cells appear morphologically just like any other cells in the tissues. Therefore “markers” are required to identify them. These identified stem cells should be isolated and sorted in order to obtain purified stem cell populations.

A particular stem cell can be characterized either by specific surface molecules (receptors) or by their specific genetic profile.

The special protein - cell surface receptors (antigens) can be identified by “signaling” molecules (antibodies). Typically, a combination of multiple markers is required to identify a particular type of stem cell. For example, the hematopoietic stem cell type SP is described as (CD34^{-/low}, c-Kit⁺, Sca-1⁺) where the receptor CD34 is absent and the receptors c-Kit and stem cell antigen -1 are present (Kirschstein and Skirboll 2001). The markers (antibodies) are often tagged with a fluorophore (Fig. 1.3). It is also possible to tag the antibodies with magnetic nanobeads or gold nanoparticles.

In order to find stem cells in tissues, biopsies have to be taken, sliced into microsections, and tagged with the marker. Typically, fluorophores with a high quantum yield are employed in this immunocytochemistry approach. Fluorescence images, taken with a microscope, provide information with submicron resolution about the presence and the location of the stem cells within the tissue qualitatively. Typically, stem cells have to be fixed and are no longer alive.

The genetic approach requires procedures to gain, to amplify, and to stain DNA which also destroy the stem cell. Polymerase chain reaction (PCR) is employed in order to provide larger quantities of DNA. Specific genomic regions can be stained with fluorophores based on fluorescence *in situ* hybridization (FISH).

In order to identify living stem cells in suspension, to obtain quantitative information, and to isolate them from mature cells, fluorescence-assisted cell sorting (FACS) as a special type of flow cytometry is applied. Hundred thousands of cells within a fast jet stream pass a laser beam induces fluorescence from the cells tagged with specific fluorescent markers. Non-tagged cells remain non-fluorescent. When fluorescence occurs (selection criteria), an electromagnetic field is switched on which charges the fluorescent cell. This particular cell within a droplet can be deflected by a strong electrostatic field and can be collected. FACS enables precise counting and accurate sorting of stem cells of interest (e.g. one rare stem cell

Introduction 1

out of 10^5 cells) and provides a nearly purified stem cell suspension. The major disadvantages of FACS are the required use of exogenous dyes and the possible destructive effects during droplet generation due to high fluid pressure (low viability of sorted cells).

An alternative technology to FACS is MACS (magnetic-assisted cell sorting). The technology is based on the use of nanometer- and micrometer sized magnetic particles which are coated with monoclonal antibodies. Cells can be sorted by the application of magnetic fields. MACS systems are simpler and inexpensive compared to FACS systems. Up to 10^8 cells can be analyzed in one second that makes it possible to separate large cell numbers (David *et al.* 2005). A major advantage is the relatively easy removal of the bead including the antibody after sorting e.g. by temperature increase. These sorted stem cells can be used for further growth and cell culturing.

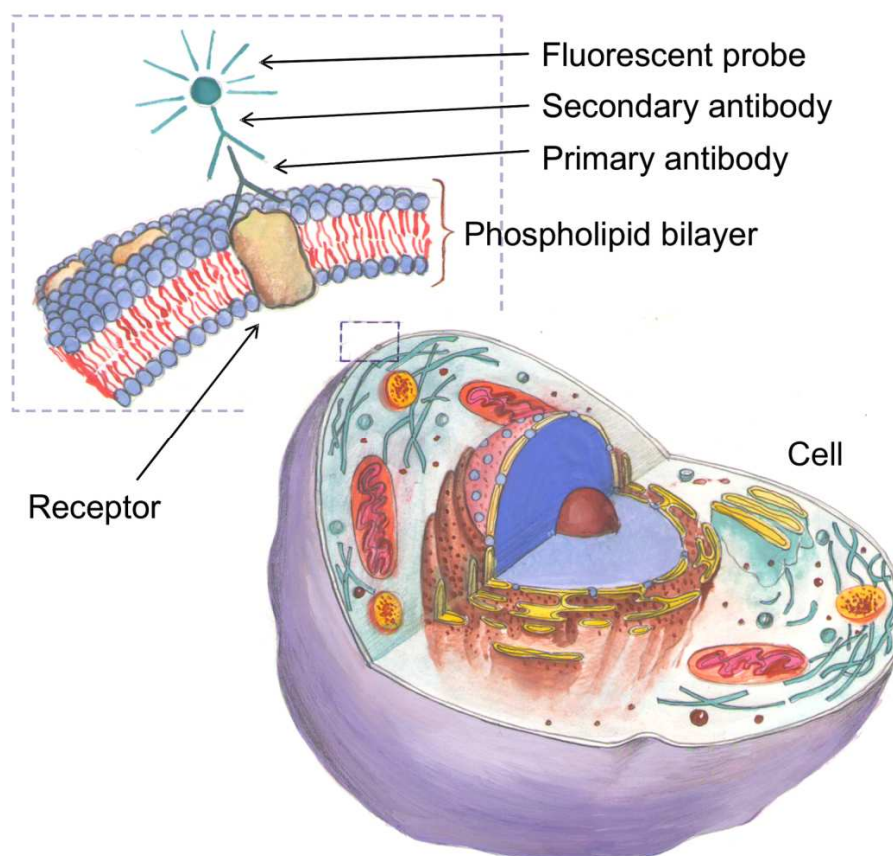


Fig. 1.3: Immunocytochemistry approach. Cells are stained with fluorophore-labeled antibodies. A primary antibody binds to a cellular specific antigen (receptor). This complex binds to a secondary fluorescent antibody which can be detected by fluorescence microscopy and FACS.

Further techniques for stem cell separation include density gradient separation, clonal isolation, and plating strategies (e.g. with special coated plates). The major advantage is the absence of chemical agents such as antibodies and fluorophores. However, these techniques lack purity of sorted cells and additional control is needed.

All these techniques possess a variety of disadvantages. FACS and MACS require cell suspensions and chemical agents such as antibodies and magnetic or fluorescent markers. Not all cells survive the analyzing procedure and the sorting procedure.

The diagnosis of stem cells in tissues slices suffer from the absence of their physiological environment and the extent use of chemicals for fixation and staining. DNA analysis requires cell destruction. Density gradient separation, clonal isolation, and plating strategies require also cell suspensions and apriori knowledge about differences between the cells in the heterogenous solution such as adherence to special coating, reproduction cycle (clonal isolation) and density (density gradient). Unfortunately, these methods enable only rough cell separation without a high purification output.

In view of the various disadvantages of the different techniques mentioned, it would be of great importance to find other chemical-free methods to identify stem cells in their native 3D tissue environment as well as in *in vitro* cell suspensions and biopsies. It would also be of tremendous interest if a marker-free imaging method could be employed to monitor stem cells and their differentiation over a long period of time under physiological conditions.

As a consequent, two-photon imaging as a marker-free high-resolution *in vivo* imaging technique is employed in this work for the imaging of human stem cells. Two-photon images possess the highest spatial resolution compared to other marker-free imaging techniques such as magnet resonance tomography, high-frequency ultrasound microscopy, and optical coherence microscopy. This work focuses on the employment of two-photon imaging of animal and human stem cells.

1.3. State-of-the-art technologies for transfection of stem cells

Stem cells can be manipulated by recombinant gene technologies to achieve a high differentiation efficiency, to produce stable and pure stem cell lines, and to transfer genetic information into tissue for the elimination of disease genes.

For a variety of stem cells, problems occur when applying the state-of-the-art non-optical transfection technologies.

Current transfection methods include (i) chemical methods such as DEAE-dextran, calcium phosphate, and liposome-mediated transfection, (ii) physical methods such as electroporation, magnet assisted transfection, DNA guns, ultrasound, and microinjection, and (iii) biological methods such as transfection using viruses (Fig. 1.4).

DEAE-dextran is a cationic polymer that associates with negatively charged nucleic acid. The cell can uptake the complex by endocytosis when they come into close contact with the negatively charged cell membrane. However, this technique is useful only for transient transfection and not for stable transfection. Another disadvantage is the high cytotoxicity.

Calcium phosphate co-precipitation is used for both transient and stable transfections of a variety of cell types. The precipitate is taken up via endocytosis or phagocytosis.

In liposome-mediated transfection, positively charged lipid molecules are associated with negatively charged nucleic acids to deliver DNA by fusing to the cell membrane and further incorporation into the cell. The method is limited in the type of DNA which can be delivered.

Viral transfection is called also viral transduction. Different viruses can be used: retroviruses, adenoviruses, herpes simplex viruses, and lenti viruses. This method can provide high transfection efficiencies and can deliver a wide variety of DNA. However, viruses can carry limited DNA sequences only and viruses can have unwanted immunogenicity and cytopathic effects.

Electroporation (electro-permeabilization) is based upon perturbation of the cell membrane by electrical pulses that allow the passage of nucleic acids into the cell. This method is appropriate for transfection of large cell numbers, however, they may alter the cell phenotype. Moreover, not all cells will survive the procedure.

The DNA gun relies upon high velocity delivery of nucleic acids on microprojectiles. Transfection based on ultrasound (sonoporation) faces problems of cell damage and low transfection efficiency.

All these described methods do not allow targeted transfection.

They lack the possibility to transfect a certain cell or cell cluster without influencing surrounding cells.

Targeted transfection is possible by direct mechanical microinjection into cells or nuclei using needles or micropipettes. This method has been used to transfer DNA into particular embryonic stem cells to produce transgenic organisms. Mechanical microinjection is not appropriate for studies that require a large number of transfected cells. It requires skilled personal and faces problems due to the contact procedure.

An alternative to the mechanical targeted transfection is targeted non-contact optical transfection with highly focused laser beams (Fig. 1.4).

Typically, a tiny hole is “drilled” in to the cellular membrane, allowing diffusion of extracellular foreign DNA plasmids into the cytoplasm of the cell of interest. Passive introduction into the nucleus may occur during cell division when the nuclear envelope is disintegrated. Targeted transfection has been demonstrated with UV and visible laser microbeams (Palumbo *et al.* 1996; Shirahata *et al.* 2001; Schneckenburger *et al.* 2002; Paterson *et al.* 2005). Laser beams in this wavelength range may face problems due to heating effects and destructive photochemical UV effects. More elegant is the use of less harmful near infrared (NIR) laser light and the employment of very short pulses, in particular femtosecond laser pulses. Highly focused femtosecond laser radiation provides for short moments extremely high light intensities which are able to create nanoholes without collateral damage by multiphoton-induced optoporation. These nanoholes in the submicron range are transient due to a successful self-repair of the membrane within seconds (Tirlapur and König *et al.* 2002).

Femtosecond laser pulses have been used to demonstrate efficient targeted transfection of Chinese hamster ovary (CHO) cells (Tirlapur and König 2002; Tsampoula *et al.* 2007). Typically, mean powers of about 100 mW (~1 nJ pulse) and high NA 1.3 objectives were required. All laser-exposed cells survived and the transfection efficiency was nearly 100% in the case of CHO cells. When using low NA 0.85 objectives in an upright beam path where the laser beam has to be transmitted through the medium, the transfection efficiency dropped down to about 50% likely due to relatively large laser-induced holes of 2.2 – 10 μm in the cell membrane (Stevenson *et al.* 2006).

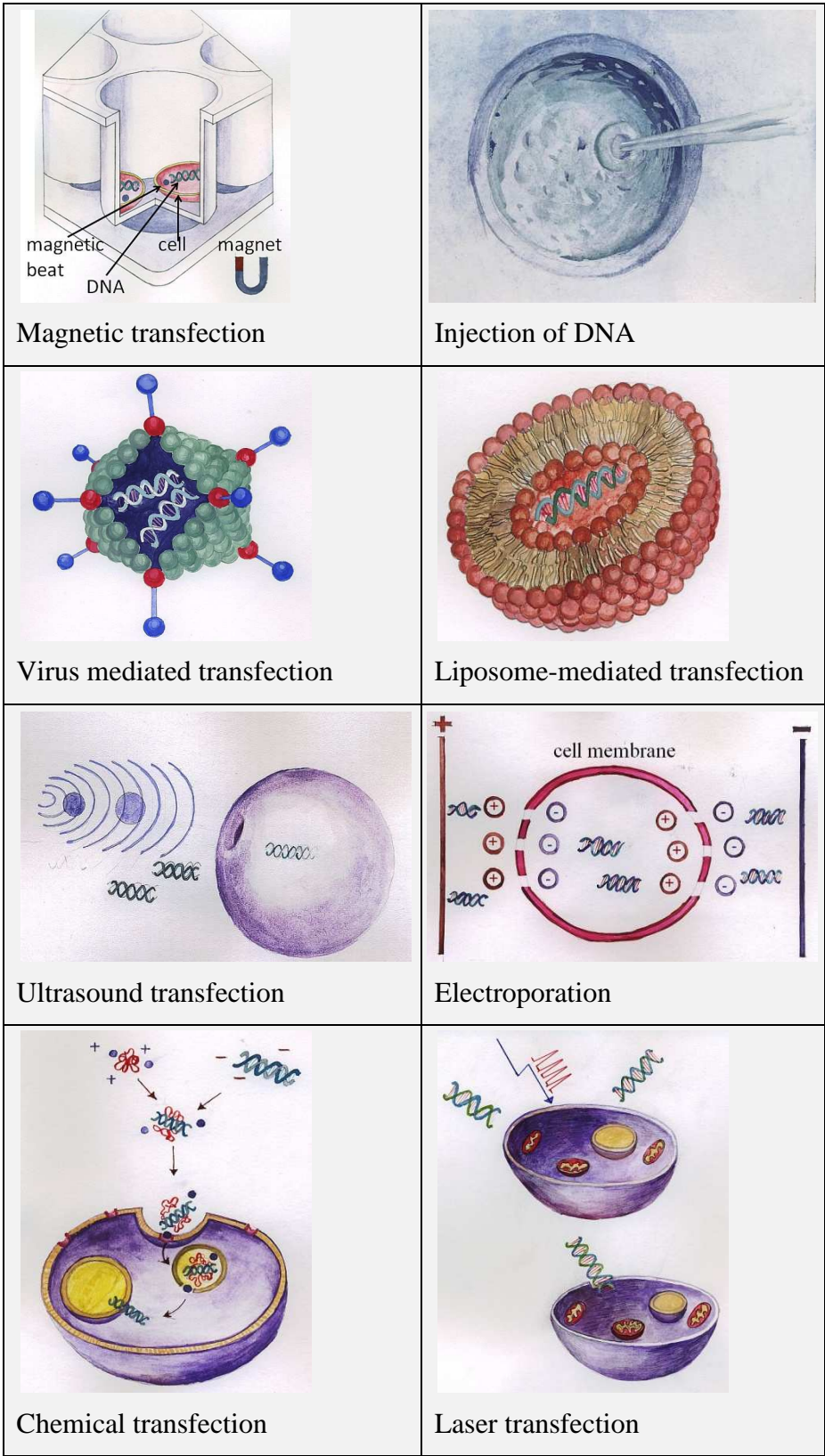


Fig. 1.4: Methods for cell transfection.

In the case of transfection of a variety of stem cells, significant problems have occurred with all state-of-the-art transfection technologies. Whereas the transfection efficiency by optoporation and by non-optical transfection methods may be up to 70% and higher (Hamm *et al.* 2002) in the laboratory routine in certain commonly used cell lines, transfection failed to be effective in stem cells. Typical transfection rates are 0.5 – 12% for human smooth muscle cells with conventional methods such as electroporation, viral transport, liposome-mediated transfer and calcium phosphate treatment, while up to 29% was achieved when using a combination of electroporation with chemical methods (amexa chemical Nucleofector technology) as demonstrated by Hamm *et al.* (2002). After optimization, even higher efficiencies were obtained for the case of human mesenchymal stem cells which survived the treatment. However, nearly 50% of the stem cell population died (Haleem-Smith *et al.* 2005). Within this work, targeted transfection of individual human stem cells of interest with femtosecond laser pulses at extremely short pulse durations of less than 20 fs and mean powers of even less than 7 mW was investigated.

1.4. Multiphoton microscopy

Principle

Especially in stem cell research there is a high demand for techniques for the non-invasive, marker-free observation of the growth, proliferation, differentiation, and stability of stem cells under physiological conditions. The use of exogenous markers has the disadvantage that it may alter the metabolic balance and hinders further therapeutic application.

Multiphoton microscopy which uses nonlinear absorption to excite fluorophores can overcome the problem. The theoretical basis of multiphoton excitation was established by Maria Göppert-Mayer in 1929. For the first time, two-photon absorption was experimentally demonstrated by Kaiser and Garrett in 1961.

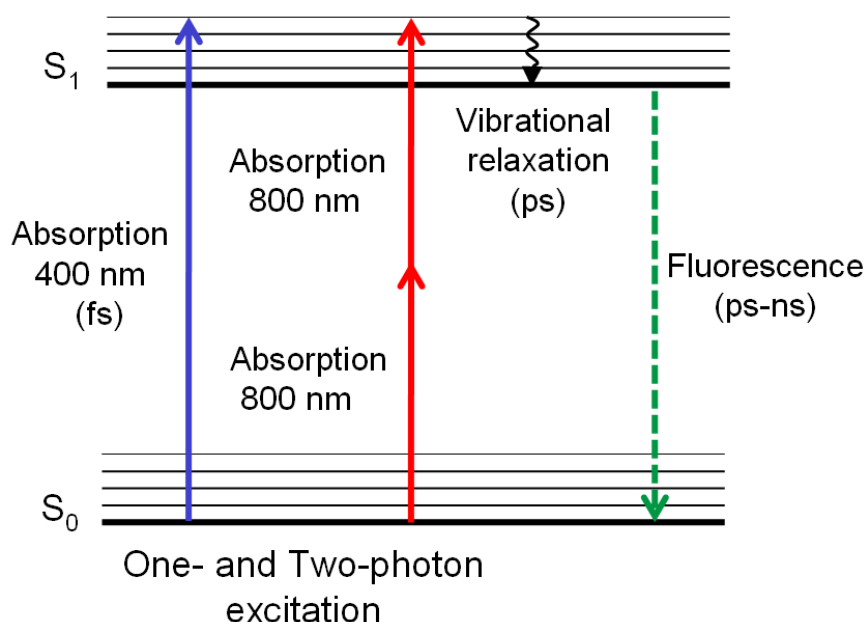


Fig. 1.5: Principle of one- and two-photon excitation. In the case of one-photon excitation of molecules, short-wavelength radiation with high energy photons are required. In two-photon excitation, two low-energy photons are absorbed simultaneously. The absorption from the ground state S_0 to the first excited electronic state S_1 occurs within femtoseconds (fs), whereas the vibrational relaxation within S_1 takes picoseconds (ps). The fluorescence of biomolecules occurs typically within some hundred picoseconds up to 10 nanoseconds (ns) after excitation.

Wilson and Sheppard proposed in 1984 the application to microscopy and Denk, Strickler, and Webb demonstrated practically the first two-photon microscope in 1990 (Denk *et al.* 1990).

The principle of multiphoton excitation is based on the simultaneous absorption of multiple low energy photons (Fig. 1.5).

Multiphoton microscopy has many advantages: (i) the laser wavelength is typically centered in the NIR which enables deep light penetration into tissues, (ii) the excitation volume is limited to a sub-femtoliter focal volume and provides therefore the possibility of “pinhole-free” optical sectioning of three dimensional biological objects (Fig. 1.6), (iii) it is very suitable for non-destructive long term analysis of living cells due to the absence of out-of-focus absorption, out-of-focus photobleaching, and out-of-focus phototoxicity, and (iii) accessibility of multicolor imaging with one laser excitation wavelength due to broad multiphoton absorption bands of multiple fluorophores.

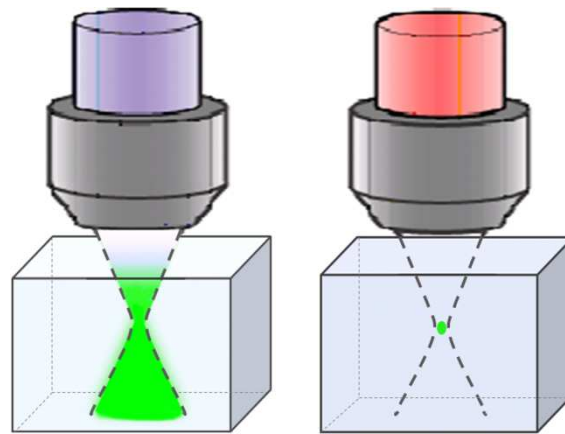


Fig. 1.6: Comparison of excitation volumes. In contrast to one-photon excitation (left), two-photon excitation occurs in a tiny sub-femtoliter focal volume only due to the required high GW/cm^2 light intensity. In one-photon microscopy, excitation (fluorescence) occurs in a large double cone shaped excitation volume.

In addition to multiphoton fluorescence, multiphoton microscopes enable second harmonic generation (SHG) imaging. In SHG, two photons interact simultaneously with non-centrosymmetrical structures and generate coherent radiation at exactly half of the excitation wavelength in forward direction (Fig. 1.7). There is no light absorption. Therefore, photobleaching and photodamage are excluded. SHG enables deep three dimensional imaging due to backscattered light.

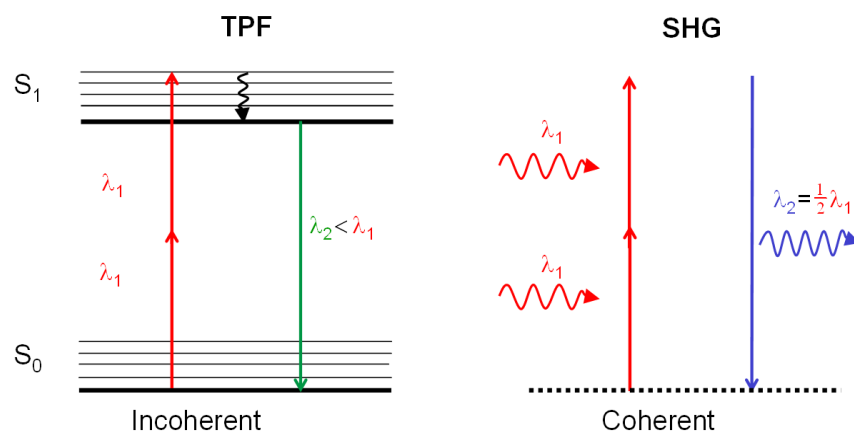


Fig. 1.7: Two photon excited fluorescence (TPF) versus SHG. SHG occurs immediately, at exactly half the laser wavelength λ_1 , and in forward direction whereas the fluorescence occurs some nanoseconds after excitation, at a wavelength range between $\lambda_1/2$ and λ_1 , and in isotropic direction.

Major endogenous cellular fluorophores and SHG active biomolecule structures

Non-invasive multiphoton microscopes with NIR femtosecond laser sources (König 2000a; Rebecca *et al.* 2001; Zipfel *et al.* 2003) have been applied to image living single cells and different tissues with a high spatial resolution without any staining. Two-photon autofluorescence is obtained from intrinsic fluorophores such as NAD(P)H, flavins, porphyrins, elastin, and melanin (König and Schneckenburger 1994). In addition, SHG images can be obtained from certain biomolecule structures such as collagen and myosin (Freund and Deutsch 1996; Master *et al.* 1997; Squirrell *et al.* 1999; Zoumi *et al.* 2002; König *et al.* 2005a, Cox *et al.* 2005).

The most important endogenous cellular fluorophores for two-photon imaging are the reduced coenzymes nicotinamide adenine dinucleotide NADH and nicotinamide adenine dinucleotide phosphate NADPH, referred as NAD(P)H, with a broad emission in the blue/green spectral range. The oxidized form NAD(P) shows no significant fluorescence in the visible spectral range. The reduced coenzymes possess a folded and an unfolded configuration with the unfolded ones to bound NAD(P)H. The emission maximum of the unfolded configuration shows a blue-shifted maximum 450 nm and a higher fluorescence quantum yield compared to free NAD(P)H with its maximum at 470 nm (König and Schneckenburger 1994). The hydrogen-transferring pyridine coenzymes are mainly located in the mitochondria. They play a key role in the respiratory chain activity and act as sensitive indicators of the cellular

metabolism since the metabolic activity of cells is given by the ratios of the concentrations of free and protein-bound NAD(P)H and of NAD(P)H to flavins (Chance *et al.* 1979; König and Schneckenburger 1994; Huang *et al.* 2002; Niesner *et al.* 2004). Normally, the excitation of NAD(P)H requires UV light at around 340 nm. However, the use of UV exposure should be avoided due to photoinduced cytotoxic reactions and the limited light penetration depth. Two-photon excitation based on near infrared radiation is the ideal method to image intracellular and intratissue NAD(P)H without the disadvantages of UV microscopy.

Cellular flavins such as flavin adenine dinucleotide (FAD), flavin mononucleotide (FMN), lipoamide dehydrogenase (LipDH), riboflavin, and electron transfer flavoprotein (ETF) are also fluorescent coenzymes that are involved in oxidation-reduction reactions (Huang *et al.* 2002). Within this work, they are referred as flavins/flavoproteins. The spectra of the flavins/flavoproteins possess major electronic transitions at 260 nm, 370 nm, and 450 nm as well as an emission peak around 530 nm. The fluorescence intensity decreases when covalently attached to proteins (flavoprotein) as reported by König and Schneckenburger (1994).

Besides the measurement of the fluorescence/SHG intensity by optical sectioning (3D imaging), fluorescence lifetime imaging (FLIM, 4D) and spectral imaging (5D) can be performed. In particular, the arrival times of the fluorescence photons with respect to the excitation of the molecule and the particular location (pixel) can be determined by time-correlated single photon counting (TCSPC) and the use of photomultipliers with short rise time. When using a PMT array in combination with a polychromator, the “color” of the emitted photon per pixel can be also determined (spectral imaging). Recent developments involve PMT arrays with fast picosecond rise time and a polychromator or other wavelength-selective components to realize spectral FLIM within one scan (Dimitrow *et al.* 2009).

Intrinsic cellular fluorophores deliver information on the cell structure as well as on cell activities. Authors could distinguish certain cancer cells from normal cells (Demos *et al.* 2005; Salomatina *et al.* 2006) and even malignant from benign tumors (Fournier *et al.* 2006) by optical properties of native fluorescent molecules. Many studies on the intrinsic metabolic state show that cellular autofluorescence has the potential to discriminate proliferating and from non-proliferating cell populations (Zhang *et al.* 1997) and to monitor metabolic changes of self-renewing and differentiating cells (Smith *et al.* 2000; Reyes *et al.* 2006).

Introduction 1

The differentiation process of human mesenchymal stem cells into an adipogenic pathway (formation of lipid droplets, changes of morphology and autofluorescence) has been investigated recently by two-photon microscopy (Rice *et al.* 2007).

A unique feature of stem cells is the extended self renewal of the cell population and their differentiation potency. The aim of the present study is to investigate the two-photon excited autofluorescence of human stem cells and the onset of collagen production of differentiated cells by the detection of SHG signals. The interesting question arises if it is possible to select differentiated cells from non-differentiated cells without interfering with the native environment and without the use of external markers.

Within this work, 5D two-photon microscopy has been employed for imaging different human and animal stem cell lines by autofluorescence and SHG in monolayers and spheroids.

1.5. Optical nanoprocessing

Principle and mechanism of femtosecond laser nanoprocessing

Femtosecond laser microscopes combine the opportunity of three dimensional optical imaging and precise nanosurgery of tissues, cells, and intracellular compartments in three dimensions. Disruption occurs when using TW/cm^2 intensities, which result in ionization and plasma formation by multiphoton processes. The simultaneous absorption of several photons, e.g. 5 photons, induces ionization of molecules and the generation of free electrons. Onset of plasma occurs if a density of 10^{21} electrons/ cm^3 is achieved (Vogel *et al.* 2005). In the case of water, where a “bandgap” of 6.5 eV has to be overcome, this value is achieved at $10 \text{ TW}/\text{cm}^2$ for 100 fs pulses at 580 nm. 800 nm photons have a photon energy of 1.55 eV. Therefore 5 photons are required for multiphoton ionization of water molecules (Vogel *et al.* 2005). The application of 750 nm photons (1.65 eV) requires 4 photons. The formation of plasma in aqueous solution results in the formation of plasma-filled cavitation bubbles which can be video-imaged. Interestingly, nanoprocessing of cells can be performed at thresholds below the threshold for multiphoton ionization of water. Intensities of about $1 \text{ TW}/\text{cm}^2$ are required (König *et al.* 2005b; König 2006). The formation of bubbles have been observed in the area of cells but not in the aqueous surroundings (medium).

The bubbles expand and can induce an implosion. This creates destructive jet streams of the medium. In addition, shock waves can be produced. Both, shockwaves and destructive bubble kinetics are called photodisruptive effects. These effects result in the destruction of the microenvironment. The onset of the photodisruptive effects depends on the transient laser intensity whereas the amount of damage depends on the pulse energy. The smaller the applied pulse energy the smaller the photodisruptive effects (König *et al.* 1999a). Therefore, low pulse energies are required to perform nanoprocessing without collateral destructive effects. The procedure should therefore be performed near the threshold of multiphoton ionization and plasma formation of cellular structures. This can be realized by fine-tuning of the laser power. In early studies on chromosome cutting, pulse energies of about 1 nJ were applied when using 200-300 femtosecond laser pulses at 80 MHz repetition rate (König *et al.* 2001).

Precise laser nanosurgery depends on laser wavelength, laser intensity, pulse duration, repetition rate, and irradiation time.

Application of femtosecond laser nanoprocessing in biomedicine

Focused femtosecond laser pulses have been successfully used to manipulate intracellular structures without causing collateral damage to the cell. One of the first femtosecond laser subcellular nanosurgery was demonstrated by König's group in 1999 by dissections of single chromosomes in living cells (König *et al.* 1999b, König 2000b, König *et al.* 2001, König *et al.* 2005b). The group also demonstrated single cell gene transfection by creating transient holes in the cell membrane (König *et al.* 2002) (Fig 1.8). Femtosecond laser pulses have been applied to dissect single dendrites and cytoskeletons, to optically knock out intracellular mitochondria (Watanabe *et al.* 2005; Heisterkamp *et al.* 2005; Shimada *et al.* 2005), for membrane and microtubules surgery (Sacconi *et al.* 2005) as well as for ocular refractive surgery (König *et al.* 2002).

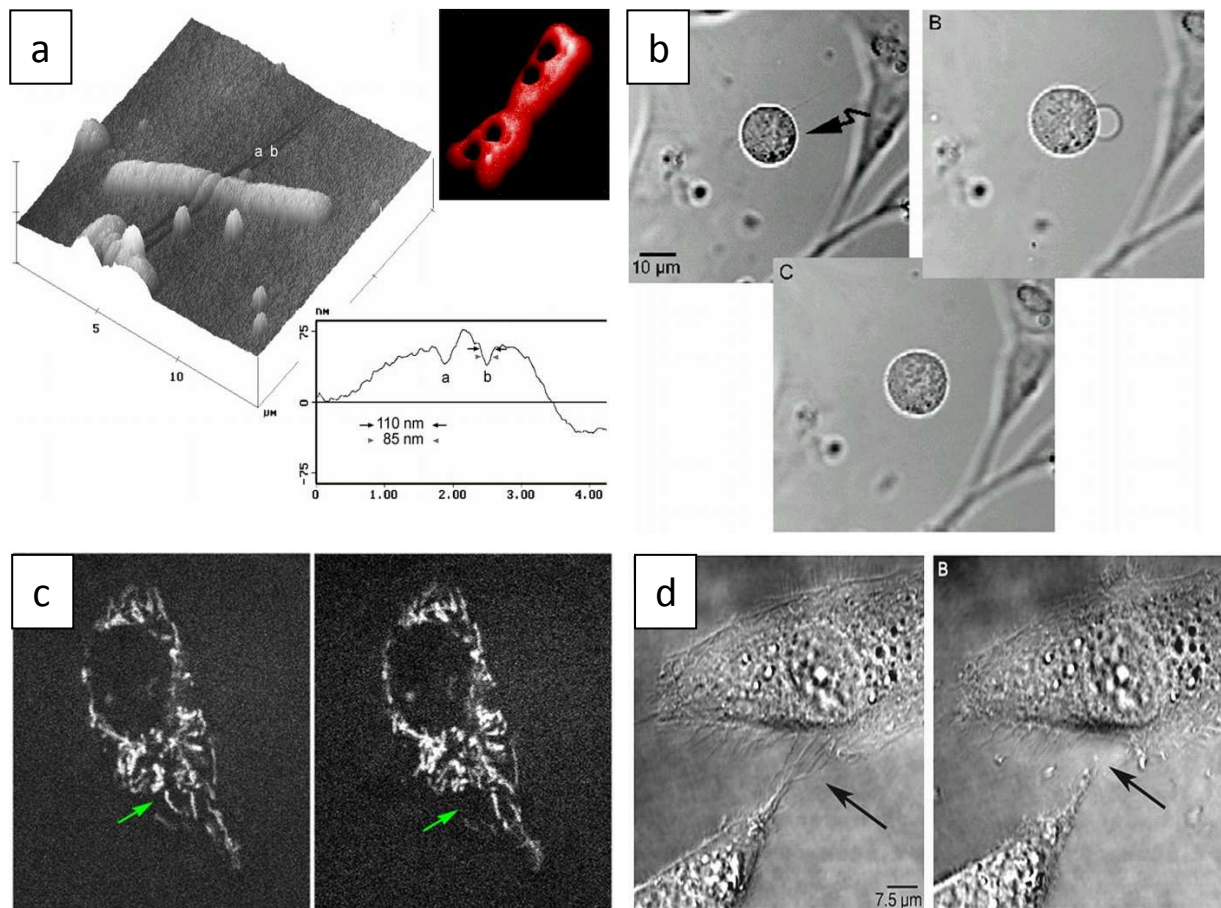


Fig. 1.8: (a) Femtosecond laser nanodissection and nanodrilling of human chromosomes. (b) Femtosecond-laser induced nanoholes in the cellular membrane for targeted transfection. (c) Ablation of single mitochondria in a living cell. (d) Disruption of cell-cell connections by femtosecond laser pulses (Tirlapur and König 2002; König *et al.* 2005b).

In the last few years, the application of extremely ultrashort femtosecond laser pulses (sub-20 fs) has been demonstrated as a non-invasive tool for manipulation of living cells. Kohli *et al.* (2005) reported on single cell isolation by the ablation of focal adhesions and precise membrane surgery without evidence of membrane reorientation, cell collapse and bleb formation when using a 10 femtosecond laser source. Also exogenous material has been delivered into developing zebrafish embryos (Kohli and Elezzabi 2008) by such short femtosecond laser pulses.

However, the use of ultrashort laser pulses faces the major problem of pulse broadening. In fact, the *in situ* pulse width at the sample can be as long as picoseconds when not employing pulse compression units (Stingl *et al.* 1994, Müller *et al.* 1997, Jasara and Rudolph 1999).

The use of inherently compact, low loss dispersive-mirror pulse compression units is a novel opportunity in contrast to the application of bulky prism and grating compressors. The dispersive mirror technology (chirped mirrors) enables accurate compensation of high order dispersion (HOD) and avoids problems due to beam pointing drifts. *In situ* sub-20 fs pulses can be achieved in the focal plane of a high numerical aperture objective.

The use of these extremely ultrashort laser pulses should be in particular useful for nanoprocessing based on higher order multiphoton processes. Recently, we have demonstrated the efficient optical transfection of stem cells by sub-20 fs laser microscopy (Uchugonova *et al.* 2008a).

Spontaneous differentiation occurs in stem cell cultures and within 3D tissue-like microenvironments. It is very difficult to control the purity of a stem cell population and to avoid undesired cell differentiation.

It would be of interest to provide methods to isolate pure stem cells of interest from their surroundings for further biomedical application. Also the occurrence of single non-differentiated cells within well-differentiated cell clusters may cause problems since this can lead to unregulated growth such as the formation of teratomas (Gerecht-Nir and Itskovitz-Eldor 2004; Rubio *et al.* 2005; Kruse *et al.* 2006).

In this work, optical cleaning of stem cells based on highly precise multiphoton processing using ultrashort NIR femtosecond laser pulses is reported. In particular this new method was used to isolate single cells of interest to inactivate undesirable single cells within 3D stem cell clusters.

1.6. Aims of the work

The aim of this dissertation is to investigate adult stem cells as monolayers and as spheroids by means of marker-free, high-resolution 5D multiphoton femtosecond laser scanning microscopy. Two-photon excitation of endogenous cellular fluorophores has to be used to realize nonlinear imaging with submicron spatial resolution (3D), picosecond temporal resolution (4D), and 10 nm spectral resolution (5D) over a long period of time without destructive effects.

It should be investigated, whether the parameters autofluorescence intensity, fluorescence lifetime, and emission spectrum can be used to distinguish stem cells from their differentiated state and whether it is possible to monitor the differentiation process.

Finally, the potential of sub-20 femtosecond laser scanning microscopes as novel nanoprocessing tools at high transient TW/cm^2 laser intensities should be explored. In particular, it has to be investigated (i) if a lethal effect on a specific cell can be induced without collateral side effects and (ii) if an efficient targeted transfection of stem cells can be realized.

The specific aims are the following:

1. Investigation of femtosecond laser-induced effects in stem cells. In particular, thresholds for long-term two-photon imaging without collateral destructive effects have to be determined.
2. Exploration of high resolution 5D two-photon microscopy and its potential to image stem cells and their differentiation process without any exogenous markers based on autofluorescence intensity, luminescence decay, and spectral features of the intracellular fluorescent molecules NAD(P)H and flavoproteins.
3. Investigation of the biosynthesis of collagen and fat droplets in long-term multiphoton studies as results of chondrogenic, osteogenic, and adipogenic differentiation processes.
4. Isolation and knock-out of single stem cells within a 3D microenvironment (spheroid) without destructive effects to neighbour cells.
5. Investigation of highly efficient targeted transfection of adult human stem cells with sub-20 fs laser pulses.

2. MATERIAL AND METHODS

2.1. Cells

Different human and animal stem (non-differentiated) cell lines and mature (differentiated) cell lines have been used within this work. Cell lines and culturing procedures are described below.

2.1.1. Cell lines

CHO-K1 (Chinese hamster ovary) cell line was derived as a subclone from an ovary of an adult Chinese hamster (*Cricetulus griseus*) (ATCC No. CCL-61™). These cells have an epithelial-like morphology and grow as an adherent monolayer. They proliferate in approximately 12-hours intervals. These cells were used for transfection and for studies on damage mechanisms induced by femtosecond laser pulses.

PtK2 (rat kangaroo kidney epithelial cells) cells derived from kidney of *Potorous tridactylis* (ATCC No. CCL-56™) have an epithelial-like morphology and grow as a very thin adherent monolayer. They proliferate in approximately 24-hours intervals. These cells were used for studies on damage mechanisms induced by femtosecond laser pulses.

rPSCs (rat pancreatic stem cells) were derived from the pancreas of male Sprague-Dawley rats (Kruse *et al.* 2004). These cells were donated by Dr. Kruse (Fraunhofer IBMT). The morphological features of these cells resembled non-differentiated fibroblast-like cells. They grow as a monolayer. rPSCs cells were able to form “bodies” by hanging drop technology (Kruse *et al.* 2004). The population doubling time interval is 24 to 48 hours. These cells are characterized by the markers CD9⁺, CD44⁺, Nestin⁺, Oct 4⁺, SSEA-1⁺, and Pax6⁺ (Kruse *et al.*

Material and Methods 2

2006). These cells were used for autofluorescence-, SHG-, and FLIM measurements as well as for transfection studies.

hPSCs (human pancreatic stem cells) were isolated from the pancreas of patients with pancreatic diseases (Kruse *et al.* 2004). These cells were donated by Dr. Kruse (Fraunhofer IBMT). The morphological features of these cells resembled non-differentiated fibroblast-like cells. They grow as a monolayer and were able to form “bodies”. The population doubling time interval is 3 to 9 days. These cells are characterized by the markers CD105⁺, CD29⁺, CD44⁺, CD90⁺, CD15⁻, CD34⁻, CD31⁻, and CD133⁻ (Gorjup *et al.* 2009). These cells were used for autofluorescence-, SHG-, and FLIM measurements as well as for transfection studies.

hSGSCs (human salivary gland stem cells) were isolated from patients with diseases of submandibular glands (Kruse *et al.* 2004). These cells were kindly provided by Dr. Kruse (Fraunhofer IBMT). They have a fibroblast-like morphology, and grow as a monolayer and were able to form “bodies”. The population doubling time interval is 2 to 4 days. These cells are characterized by the markers CD105⁺, CD29⁺, CD44⁺, CD90⁺, CD15⁻, CD34⁻, CD31⁻ and CD133⁻ (Gorjup *et al.* 2009). These cells were used for autofluorescence-, SHG-, and FLIM measurements, and transfection studies.

hDPSCs (human dental pulp stem cells) were kindly provided by Prof. König who received them from the NIH (National Institute of Health, Bethesda, USA). These cells were used for two-photon autofluorescence studies.

hBM-MSCs (human bone marrow mesenchymal stem cells) were isolated from human bone marrow, in particular from the posterior iliac crest of the pelvic bone of volunteers (Lonza Sales Ltd, Basel, Switzerland, No. PT-2501). They have a fibroblast-like morphology, and grow as a monolayer. These cells are characterized by the markers CD105⁺, CD166⁺, CD29⁺, CD44⁺, CD34⁻, and CD45⁻. The population doubling time interval is 48 to 74 hours. These cells were used for SHG imaging.

2.1.2. Cell cultures

25 cm² and 75 cm² flasks were used to culture the cells at 37° C in a 5% CO₂ humidified atmosphere (CO₂-incubator: Binder GmbH, Tuttlingen, Germany). All cultivation procedures were done in a laminar flow safety cabinet (Kendro Laboratory Products GmbH, Langenselbord, Germany). Cells were passaged when they reached a 90% confluence. After removal of the growth media, the cells were washed with PBS (No. 14040, Gibco, Germany) and treated with trypsin/EDTA (No. 25300, Gibco, Germany) for up to 5 minutes to detach the cells from the bottom of the plate. The cell release from the plate was confirmed by microscopic visualization.

The solution was replaced in a centrifuge tube and spun for 5 min (1000x) at room temperature. The supernatant was removed aseptically by pipettes. Afterwards the cells were resuspended in fresh culture medium. An appropriate number of cells in suspension was transferred to cell chambers for further imaging or to culture for future passages.

The stem cell lines hSGSCs, hPSC, and rPSC were cultured in Dulbecco's modified Eagle's medium (No. 41965, DMEM, GIBCO, Germany) containing 4.5 g/l glucose, L-glutamine and 15 % fetal calf serum Gold (FCS-Gold, PAA Laboratories GmbH). hDPSC were cultured in α -MEM (No. F 0915, Biochrom AG, Berlin, Germany) with 10% FCS, 100 μ M L-ascorbic acid 2-phosphate, and 2 mM L-glutamine. CHO-K1 cells were cultured in HAM's F-12 (Gibco, Germany). PtK2 cells were cultured in RPMI 1640 medium (No. 21675, Gibco). All media contained 100 U/ml penicillin and 100 μ g/ml streptomycin. hBM-MSCs were cultured in medium provided by the same company where the cells were purchased (mixture of PT-3001, PT-3238 and PT-4105, Lonza Sales Ltd, Basel, Switzerland).

For imaging, cells were transferred (confluence: 80-90%) into sterile miniaturized cell chambers with two 0.17 mm thick glass windows with etched grids (MiniCeM-grid, JenLab GmbH, Jena, Germany) and additionally incubated for another day until they were attached to the glass surface.

2.1.3. Manufacturing of spheroids

Hanging drop technology

Cells were trypsinized using trypsin/EDTA, washed and resuspended in culture medium to a concentration of 200,000 cells/ml. The cell concentration in the suspensions was counted with

Material and Methods 2

an automatic counter (Casy, Schärfe System GmbH, Germany). Drops of the suspension were placed on the lid of a plastic culture dish. The lid was turned upside down and placed on the bottom part of the dish which was filled with sterile water creating hanging drops. Dishes were incubated at 37°C in 5% CO₂ in air for 3-4 days. For experiments, spheroids were transferred into sterile miniaturized cell chambers (MiniCeM-grid, JenLab GmbH, Jena, Germany) (Fig. 2.1).

Pellet culture system technology

Approximately 200,000-300,000 cells were placed in a 15 ml polypropylene tube and centrifuged to a pellet for 5 min (1000x/min). The flattened pellet at the bottom of the tube was cultured at 37°C with 5% CO₂ in the culture medium for 5-6 days until a spherical form (spheroid) was formed.

For the differentiation studies, the spheroids were cultured in an appropriate differentiation medium for 3-5 weeks (Fig. 2.1).

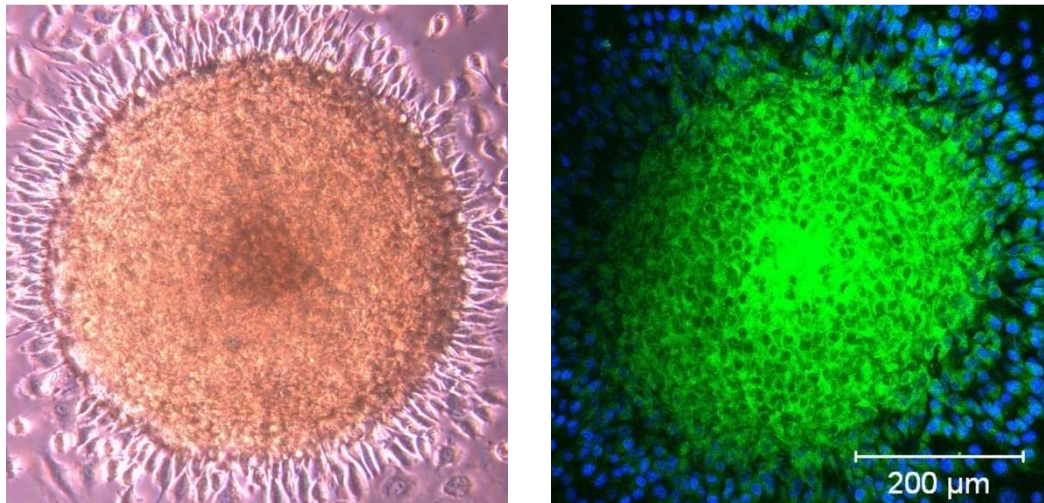


Fig. 2.1: Images of a stem cell spheroid attached to a cover slip.

Left: phase contrast image, Right: fluorescence image (blue: Hoechst 33342, green: Rhodamine 123).

2.1.4. Stem cell differentiation

Stem cells were differentiated in adipogenic, chondrogenic, and osteogenic pathways using monolayer cultures and spheroids (“bodies”). To induce differentiation within monolayers, cells were counted and an appropriate number of cells was replaced to the cell chamber and incubated for about 2-3 days to adhere and to obtain a high confluence. Afterwards the culture medium was replaced with the differentiation medium.

To induce differentiation within “bodies”, pellet cultures were manufactured as described in (chapter 2.1.3) and incubated in the differentiation medium. The medium was replaced every 3-4 days.

For adipogenic differentiation, cells were cultured in α -MEM containing 10% FCS, 100 U/ml penicillin, 100 mg/ml streptomycin, 100 nM dexamethasone, 5 μ M 1-methyl-3-isobutylxanthine, 200 μ M indomethacin, and 100 ng/ml insulin (Sigma-Aldrich, Hamburg, Germany). Osteogenic differentiation was induced by 5 mM β -glycerolphosphate, 100 nM dexamethasone, 100 μ g/ml L-ascorbic acid-phosphate, and 100 μ g/ml bone morphogenic growth factor-2 (BMP-2). For chondrogenic differentiation, cells were cultured in chondrogenic medium DMEM (GIBCO, Germany) supplemented with 10 mg/ml transforming growth factor (TGF)- β 3, 100 nM dexamethasone, 50 mg/ml ascorbic acid-phosphate, 4 mg/ml L-proline, 100 mg/ml natrium piruvate, 15% FCS-Gold, 100 U/ml penicillin, and 100 mg/ml streptomycin.

2.2. Chemical probes/procedures

2.2.1. Reactive oxygen species (ROS) detection

ROS are molecules or ions formed as a result of the incomplete one-electron reduction of oxygen. ROS include singlet oxygen, superoxides, peroxides, hydroxyl radicals, and hypochlorous acid. ROS generation occurs at a controlled rate in healthy cells. ROS contribute to the microbicidal activity of phagocytes, the regulation of signal transduction, and gene expression. Under conditions of oxidative stress, ROS production is dramatically increased which results in subsequent alteration of membrane lipids, proteins, and nucleic acids, the loss of organelle functions, the reduction of metabolic activities, in chromatin breaks, mutation, and cell death.

Material and Methods 2

Oxidation induced by light is known as photooxidation process. Type I photooxidation results in oxygen radicals whereas type II photooxidation generates singlet oxygen via an energy transfer from a photo-excited molecule to molecular oxygen (Henderson and Dougherty 1992, Foote 1999).

Photooxidation effects induced by NIR femtosecond laser pulses were probed by *The Image-iT™ LIVE Green Reactive Oxygen Species (ROS) Detection Kit*. The assay is based on 5-(and-6)-carboxy-2',7'-dichlorodihydrofluorescein diacetate (carboxy-H₂DCFDA), a reliable fluorescent marker for ROS production in live cells. Cells were washed with PBS and incubated in 25 µM carboxy-H₂DCFDA solution (Biochrom AG, Berlin, Germany) for 30 min at 37°C before laser exposure. As control, cells were exposed to the ROS generator tert-butyl hydroperoxide (TBHP) diluted with PBS (1:1000) for 60 min. ROS positive cells exhibited a green fluorescence (fluorescence excitation maximum at 495 nm, emission maximum at 529 nm). Detailed information of this procedure is described in the company's Product Protocol (Biochrom AG No. 136007, Berlin). To visualize all cells within the chamber, an additional staining was employed based on the nucleus marker Hoechst 33342 (excitation maximum at 350 nm, emission maximum at 461 nm).

2.2.2. DNA break detection

Laser radiation can cause breakage of DNA. Fragmented DNA strands have been detected using the terminal deoxynucleotidyl transferase (TdT) – mediated dUTP nick-end labeling (TUNEL) assay. Laser-exposed cells were fixed 30 min after irradiation with 1% paraformaldehyde in PBS for 60 min at 25°C, permeabilized with 0.1% TritonX-100 in 0.1% sodium citrate, and labeled with TUNEL solution for 60 min at 30°C. Cells with DNA strands breaks showed green fluorescence in the nucleus (excitation wavelength: 488 nm, emission: 515-565 nm). Detailed information of this probe and procedure can be obtained from the Product Protocol provided by the company (Roche No. 11 684 795 910, Germany).

2.2.3. Apoptosis detection

Apoptosis is the process of programmed cell death which involves a series of biochemical events leading to characteristic cell morphology changes including blebbing, loss of

membrane asymmetry, loss of attachment, cell shrinkage, nuclear fragmentation, chromatin condensation, and chromosomal DNA fragmentation.

To detect laser-induced early apoptosis, annexin V labeled with the fluorophore Alexa Fluor 488 (excitation: 495 nm, emission maximum: 519 nm) was employed. Annexin V protein binds to phosphatidyl-serine (PS). PS is normally located on the cytoplasmic inner surface of the membrane. However, in the case of apoptosis PS is translocated to the outer leaflet of the membrane. Now it can be detected by extracellular annexin V. Detailed information of this probe and procedure is given in the Product Protocol provided by the producer (Molecular Probe No. A13201). Additionally 10 μ M Hoechst 33342 was used to stain the nuclei from vital and apoptotic cells.

2.2.4. Vitality tests

To determine laser effects on cell viability, 3 μ M Ethidium bromide (Molecular Probe, Netherland) was used as a dead cell marker to stain the nucleus from necrotic cells. Ethidium bromide is non-permeable through the intact membrane. When the membrane is disintegrated the dye can enter the cell nucleus and can bind to DNA. The dye-DNA complex is fluorescent.

2.2.5. Detection of collagen

After differentiation, adherent cells grown in chambers were washed with PBS, fixed with cooled (-20°C) methanol-acetone solution (7:3) for 5 min, and permeabilized with 0.1 % Triton X-100 + 10% normal goat serum (NGS) in PBS/pH 7.3 for 2 min. Afterwards, the cells were labeled with monoclonal antibodies. To detect collagen II produced from rat PSCs the chambers were incubated at 4°C overnight with the primary antibody rabbit anti-rat collagen type II (Chemicon No. AB2036) (1:400) and with the secondary antibody Alexa Fluor 568 (Rabbit) goat anti-rabbit IgG (Molecular Probe No. A11036) for 60 min at room temperature in the dark. To detect collagen I, the primary antibody mouse anti-collagen type I (Sigma-Aldrich No. C2456) and the secondary antibody FITC mouse IgG (Sigma-Aldrich No. F5897) were used.

2.2.6. Staining of adipocytes

After adipogenic differentiation, cells were rinsed twice with DPBS and fixed with 10% formalin for 30 min and then stained with 0.18% oil red O solution (60% isopropanol in water) for 5 min (preparation details described in the manufacture's protocol, Sigma-Aldrich, Germany, No. O-0625). Additionally, the nucleus has been stained with hemotoxylin for 1 min.

2.2.7. Staining of lysosomes

The red-fluorescent LysoTracker Red DND-99 (Invitrogen No. L-7528, absorption maximum at 577, emission maximum at 590 nm) that stains acidic compartments in live cells has been employed. Cells were stained with 30 nM solution for 25 min at 37°C and washed with fresh medium before observation under the fluorescence microscope.

2.2.8. Staining of mitochondria

The green-fluorescent MitoTracker Green FM (Invitrogen No. M-7514, absorption maximum at 490 nm, emission maximum at 516 nm) was used to stain mitochondria in living cells. Cells were stained with 30 nM solution for 25 min at 37°C and loading solution was replaced with fresh medium before observation under the microscope.

2.3. Experimental systems

2.3.1. Modified ZEISS LSM510-NLO (META) multiphoton microscope

The ZEISS LSM510-NLO (META) microscope consists of an inverted epi-fluorescence microscope Axiovert 200M, two visible lasers (Argon ion laser at 458 nm, 488 nm, and 514 nm; HeNe laser at 543 nm and 633 nm), and a high-pressure mercury lamp for one-photon fluorescence excitation and reflectance microscopy as well as a femtosecond laser for multiphoton excitation. The femtosecond laser is a tunable (680-1080 nm) mode-locked 80 MHz (>3.3 W peak power) Ti:sapphire oscillator Chameleon with (140 ± 20) fs output pulse duration and a typical pulse width at the sample of 250 fs. The femtosecond laser beam is typically focused into the sample using a Plan Neofluar 40x/1.3 oil objective (ZEISS, Germany). A mechanical shutter in the beam path was used to control the number of pulses that irradiate the sample during nanoprocessing experiments. The mean laser power was measured after transmission through the objective by means of the Field Master power meter (Coherent, Santa Clara, USA). The microscope employs galvoscan for x-y scanning and a motorized stage to vary the focal plane. Photons are detected by a variety of single photomultipliers as well as a 32 channel PMT array for spectral imaging. The beam splitter HFT KP 650 and the short pass filter KP 685 were employed for two-photon imaging.

For second harmonic (SHG) detection, the external PMT GaAsP (H7422P-40, Hamamatsu, Japan) was mounted onto the microscope in forward beam direction. A SP 610 filter was installed in front of the detector to avoid scattered laser light onto the detector. SHG signals were collected by passing a (435 ± 5) nm band pass filter at an excitation wavelength of 870 nm. Fig. 2.2 shows the experimental setup of the modified microscope for one-photon and multiphoton microscopy.

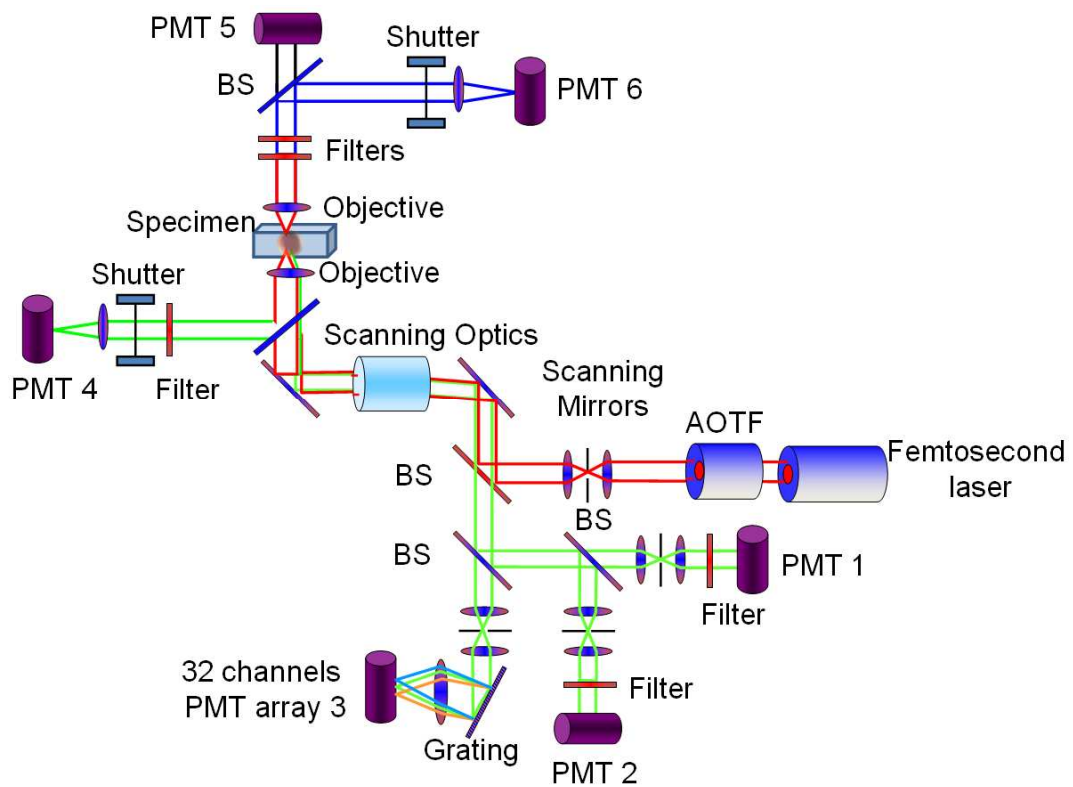


Fig. 2.2: Experimental setup of the modified ZEISS LSM510-NLO (META) multiphoton microscope and photograph of the microscope with the SHG detection module. BS-beam splitter; PMT-photomultiplier tube; AOTF-acousto-optical tunable filter; SP-short pass filter; BP-bandpass filter.

2.3.2. Sub-20 femtosecond laser microscope FemtOgene

The ultracompact scanning microscope FemtOgene™ (JenLab GmbH, Jena, Germany) with galvoscanners for beam scanning and piezodriven focussing optics equipped with highly-dispersive, large-NA objectives (Zeiss EC Plan-Neofluar 40x/1.3 oil, 63x/1.25 oil) was used. Two femtosecond lasers which provided extremely short pulses (<10 fs, Femtolasers Produktions GmbH, Vienna, Austria) were employed (Fig. 2.3). The first one was the passively mode-locked dispersive-mirror-based *Integral Pro* oscillator (0.2 MW peak power, 85 MHz, $M^2 < 1.3$, 180 mW mean power output (2 nJ per pulse)), the second one was a Kerr-lens passively mode-locked dispersive-mirror-based Ti:Sapphire *Synergy Pro* oscillator (0.67 MW peak power, 75 MHz, $M^2 < 1.3$, 600 mW mean power output (8 nJ per pulse), 5 W/532 nm cw pump Spectra Physics *Millenia V*). For dispersion pre-compensation of the whole microscope including the beam expander, the polarizer for beam attenuation, the tube lens, the objective, filters etc., the optical module *Mosaik™* was used. The *in situ* pulse duration was measured by means of a second order interferometric scanning autocorrelator (FEMTOMETER, Femtolasers Produktions GmbH) using a non-linear photodiode at the focus of the objectives. A typical short pulse duration of 10 - 12 fs (*in situ* pulse width) and a bandwidth of 80 - 97 nm, respectively, were measured at the sample plane (Fig. 2.4)

The microscope was used in the two-photon fluorescence excitation mode at mean powers in the microwatt range for nondestructive imaging of the stem cell of interest and to monitor the biosynthesis of fluorescent proteins after laser processing. It was employed in the milliwatt range for nanoprocessing in two exposure modes: (i) scanning of a region of interest (ROI) and (ii) by single point illumination where the galvoscanners were fixed to a point of interest. A CC-12 (“ColorCube”) CCD camera (Soft Imaging System GmbH, Muenster, Germany) attached to the side port enabled on-line imaging of the cells, the laser beam, and the formation of plasma-filled cavitation bubbles. A photomultiplier tube PMC-100 (Becker&Hickl GmbH) with fast rise time attached to the front port was employed to image two-photon fluorescence.

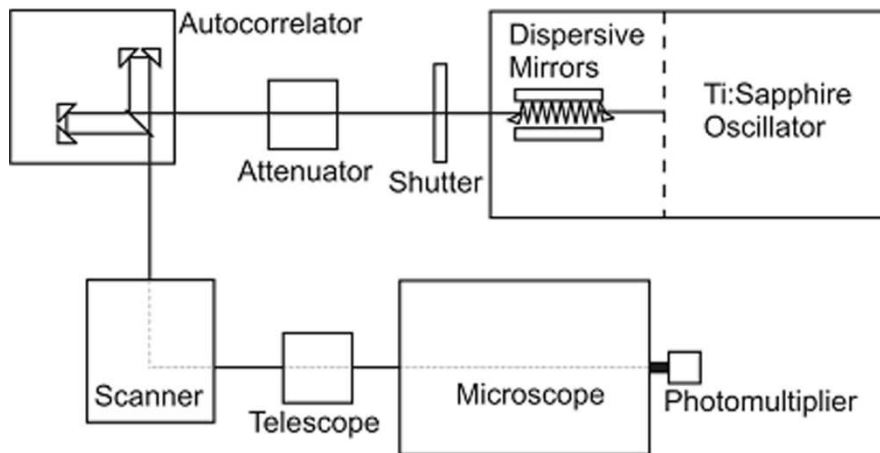


Fig. 2.3: Experimental setup and photograph of the sub-20 femtosecond laser microscope FemtOgene. The beam emitted by the 12-fs oscillator passes a pair of high dispersion mirrors (HDM) before coupling into the scanning microscope via a dispersion-balanced Michelson scanning interferometer.

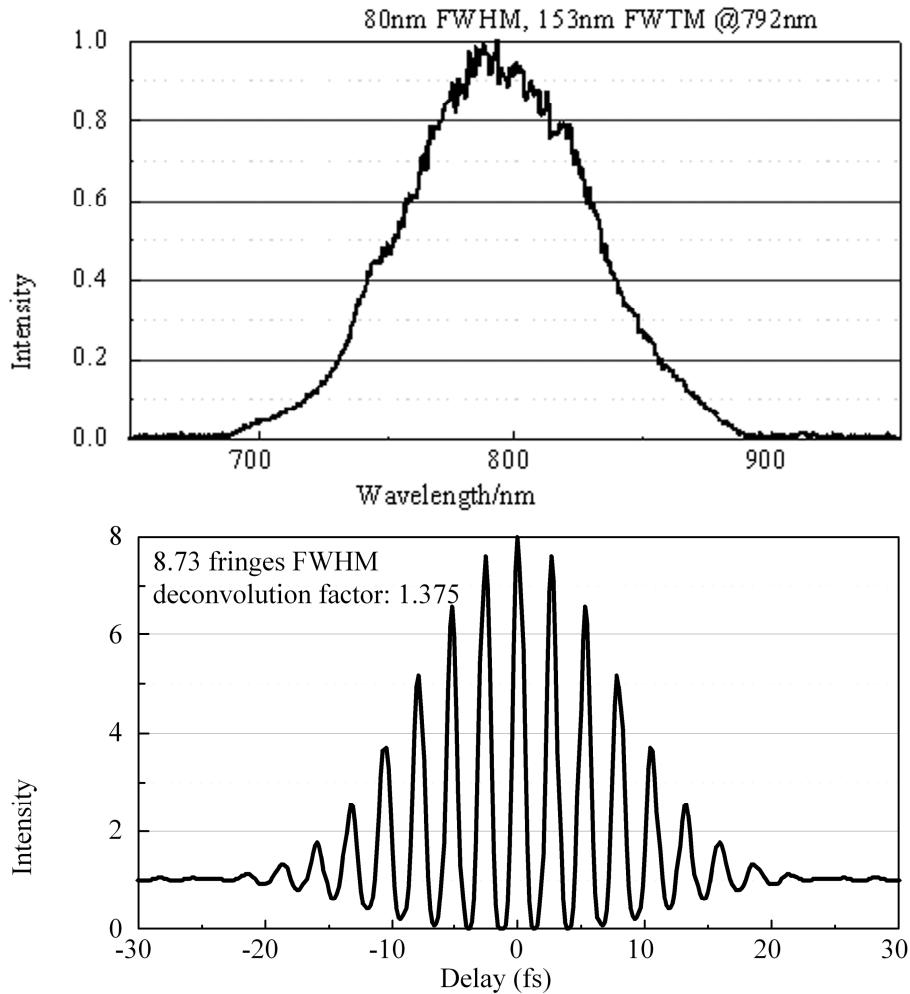


Fig. 2.4: The spectrum and the autocorrelation function demonstrate the output laser parameters 12 fs, 80 nm full-width half-maximum (FWHM), 153 nm full-width tenth-maximum (FWTM), and the emission maximum at 792 nm.

2.4. Optical sectioning (3D microscopy: x,y,z)

Both laser scanning microscopes (250 fs microscope, sub-20 fs microscope) employed x-y galvoscanners to scan the target with the highly focused laser beams. Typically, the target was scanned in a 512x512 pixel field correspondingly to an area of 230x230 μm^2 at 25.6 μs pixel dwell time. In contrast to confocal microscopy, pinholes as spatial filters are not required to perform 3D two-photon imaging. In order to change the focal plane either the motorized stage was moved in axial (z) direction (ZEISS LSM510-NLO) or the focusing optics was moved by a piezosystem (FemtOgeneTM, MIPOS 5, 500 μm working distance, Piezosystems Jena, Germany).

3D images were obtained by the correlation of the PMT signal with the position of the x-y galvoscaners and the z-position of the stage/focusing optics. Most optical sections were taken at mean powers of 5 mW (250 fs microscope).

2.5. Fluorescence lifetime imaging (4D microscopy: x,y,z, τ) and FLIM data analysis

Upon photoexcitation within femtoseconds from the ground state S_0 to a higher electronic state S_1 , the molecule will remain in the excited state only transiently for some picoseconds up to tens of nanoseconds. The average time a fluorescent molecule remains in the excited state is referred to as the “fluorescence lifetime τ ”. The parameter τ is a signature of the fluorescent material and independent of the fluorophore concentration, the illumination intensity, the light path of the optical system, and the detector which makes fluorescence lifetime measurements more robust than measurements of the fluorescence intensity (Becker 2005). However, the fluorescence lifetime depends strongly on the microenvironment and may change as a result of the interaction with other molecules due to the loss of their excited state energy by additional decay pathways. This enables the study of the binding status of a molecule. In the case of fluorescent protein-protein interactions, Förster resonance energy transfer (FRET) can occur which decreases the fluorescence lifetime of the donor molecule. Of high interest is the combination of the measurement of the fluorescence lifetime with high spatial resolution. Since its introduction to Life Sciences 20 years ago (Bugiel *et al.* 1989), Fluorescence lifetime imaging microscopy (FLIM) has become a key technique for imaging cellular processes, protein-protein interactions, and tissue compartments (Periasamy 2001; König 2008; Periasamy and Clegg 2009). There are two major methods to map the spatial distribution of the fluorescence lifetime, the frequency-domain method and the time-domain method. The frequency-domain method requires a modulated (cw) light excitation source (10-100 MHz) and a modulated detector (image intensifier). The fluorescence signal occurs with a phase shift and with demodulation compared to the excitation light. τ can be calculated from these parameters.

Within this work, FLIM measurements were performed in the time-domain where 80 MHz ultrashort femtosecond laser pulses as excitation light and special detectors with a short rise time in the picosecond range were employed. The fluorescence was detected by time-correlated single photon counting (TCSPC) where the arrival times of photons were measured

with respect to the excitation pulse. Thousands of photons are counted per pixel and placed into different “time channels” to build up a histogram and a fluorescence decay curve $F(t) = F_0e^{-t/\tau}$, respectively. From this decay curve, the fluorescence lifetime can be calculated. The accuracy follows the Poisson statistics (Becker 2005). Often, the fluorescence decay curve represents a multi-exponential decay due to the presence of different fluorophores or a fluorophore in the free and its bound form. Within this work, a fitting procedure was employed which can consider a mono-exponential as well as a bi-exponential behavior $F(t) = A_1e^{-t/\tau_1} + A_2e^{-t/\tau_2}$ (Fig. 2.5).

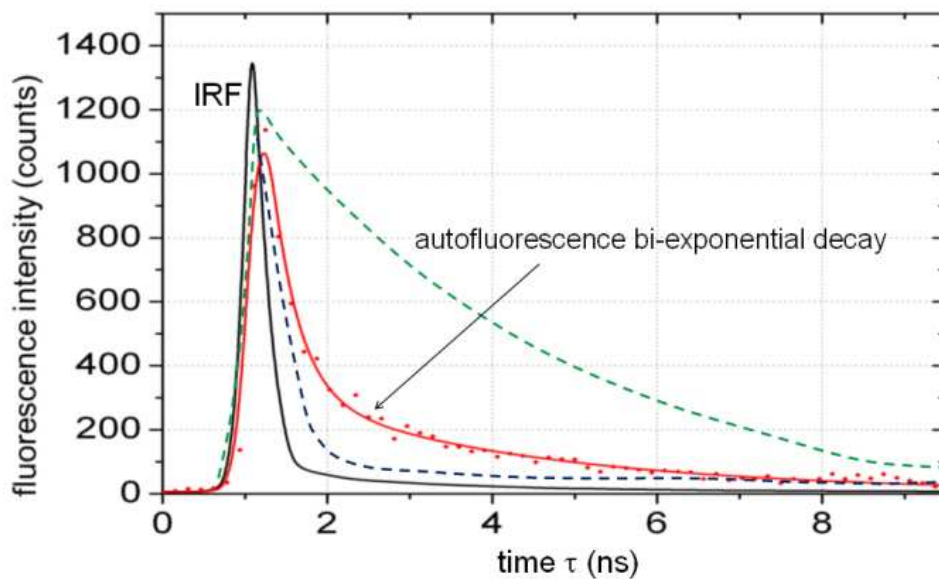


Fig. 2.5: Fluorescence decay curves. The green dotted curve reflects the mono-exponential fluorescence decay with a long fluorescence lifetime of 4.0 ns, whereas the blue dotted mono-exponential curve reflects a fluorophore with a short lifetime of 1.6 ns. Typically, the “real” autofluorescence decay of a stem cell is a bi-exponential (red curve) with two fluorophores with lifetimes $\tau_1 \approx 0.30$ ns and $\tau_2 \approx 2$ ns, respectively. The black curve reflects the instrument response function (IRF).

TCSPC was performed by means of the PC boards SPC-830 and SPC-730 (Becker&Hickl GmbH, Germany). A detailed description is given in the reference Becker, 2008. Fast photon counting detectors such as the PMC-100 were used for autofluorescence/SHG FLIM imaging. They were mounted to the external boards of the microscopes.

The instrumental function (IRF) of the optical system was measured using the SHG signal from collagen II (Sigma-Aldrich, Germany). The measured full-width half-maximum (FWHM) of the IRF was determined to be ~250 picoseconds (Fig 2.6).

The SPCImage software from the Becker&Hickl GmbH company was used to analyze the fluorescence lifetime decay curves as well as to perform the calculation of histograms.

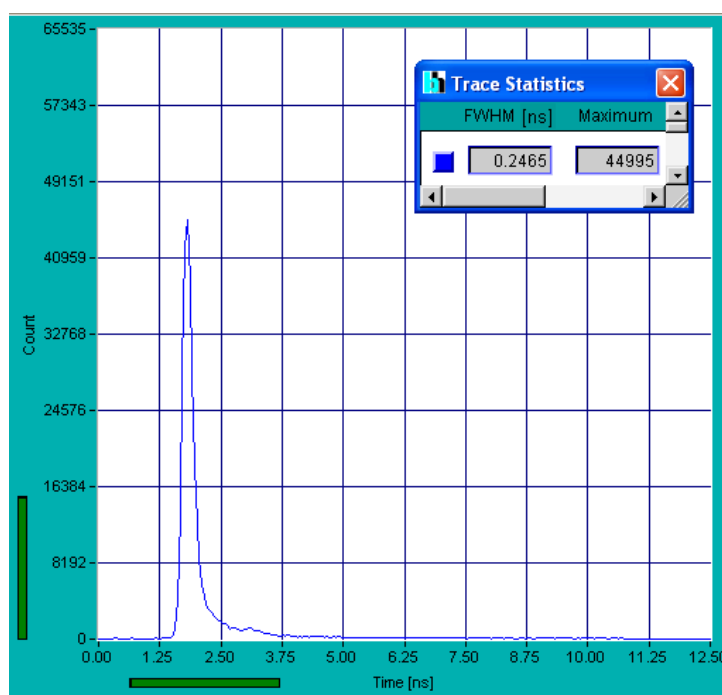


Fig. 2.6: Measured IRF from collagen II.

2.6. Spectral imaging (5D microscopy: x, y, z, τ, λ) and spectral data analysis

Sometimes, the fluorescence lifetimes of two different fluorophores are similar. It would be helpful to have another criterion to distinguish between them. This can be for example the “color” of the emitted photon. The spectral characteristics of the fluorescence can be determined by separation of the photons into “spectral channels”. The method is also called “emission fingerprinting” (Dickinson *et al.* 2001). The combination with microscopy enables “spectral imaging”. Within this work, spectral imaging was performed with a 32 channel PMT array (ZEISS-META, Hamamatsu) in combination with a polychromator. The grating in the

polychromator provided a resolution of 10.5 nm per channel. A full 512x512 lambda stack of data from all 32 channels (the full visible spectrum 382-714 nm) can be acquired in 0.8 s. The scanning speed can be increased in accordance with x-y scans with fewer pixels or lambda stacks, including data from fewer channels. The LSM 510 software program (ZEISS, Germany) enables the following analysis of the spectral data: to determine the spectral signature from a single image pixel or from a region of interest (ROI) of the scanned image, to subtract background spectral profiles, to visualize a spectral color image, and to export spectral images as a TIFF file. Fig. 2.2 shows the experimental setup. Fitting of the emission spectrum was performed with the software OriginPro 7.5.

2.7. Statistical analysis

Statistical analysis was done for a variety of studies based on the student's test which provided the parameter means \pm SD (standard deviation) and mean \pm SEM (standard error of the mean). In the case of two-exponential fitting of the fluorescence decay curves, the parameter χ^2 was provided by the SPCImage software. The accuracy of FLIM data follows the Poisson statistics.

3. RESULTS

3.1. Influence of femtosecond laser radiation on cell viability

3.1.1. Damage mechanisms

Light exposure can induce destructive photothermal, photochemical, and photomechanical effects based on one-photon absorption and multiphoton absorption. Animal and human cells (except red blood cells and cells with melanin) do not possess efficient NIR absorbers. For example, the absorption coefficient of water at around 1000 nm is less than 0.1 cm^{-1} .

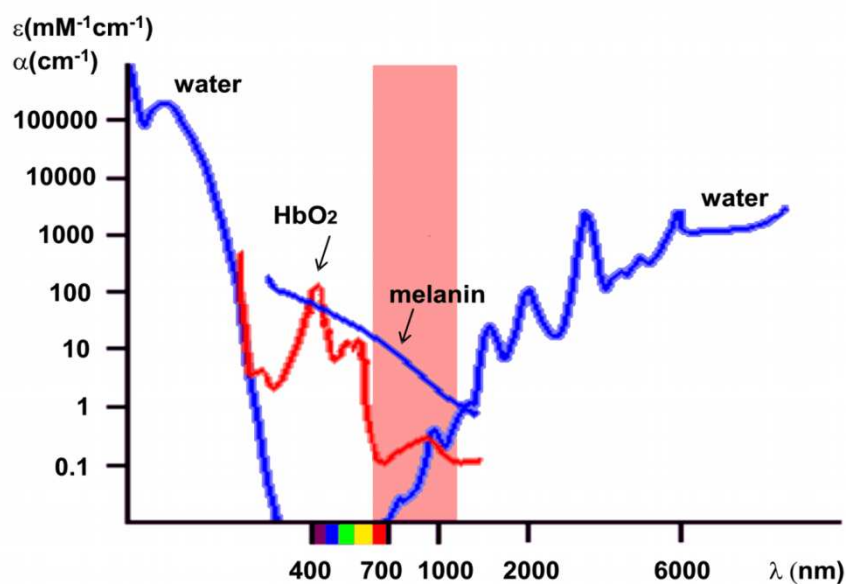


Fig. 3.1: Absorption spectra of the major tissue components water, oxidized hemoglobin (HbO₂), and melanin. The molar extinction coefficients and the absorption coefficient of water are depicted. The region of 600 nm – 1200 nm is referred as optical window due to the low absorption/extinction coefficients and the low scattering coefficients (König 1999).

Results 3

Therefore, one-photon destructive effects such as heating of water can be excluded when NIR radiation at reasonable powers (milliwatt) is used (Fig. 3.1).

However, multiphoton absorption of NIR photons may occur in the focal volume of a high NA objective due to the high light intensities of more than 1 GW/cm^2 which is more than 10 orders higher than the sun light intensity on earth. In particular, two-photon absorption can induce UV-like photochemical reactions including the formation of reactive oxygen species (ROS). ROS can induce DNA strand breaks and apoptosis. Multiphoton ionization and the formation of free electrons, respectively, occur when high TW/cm^2 intensities are applied. Photoinduced plasma exists when the free electron density reaches values of more than 10^{21} cm^{-3} (Vogel *et al.* 2005). The formation of the plasma induces photodisruptive effects such as shockwaves and destructive bubble formation which can cause immediate cell death e.g. by fragmentation.

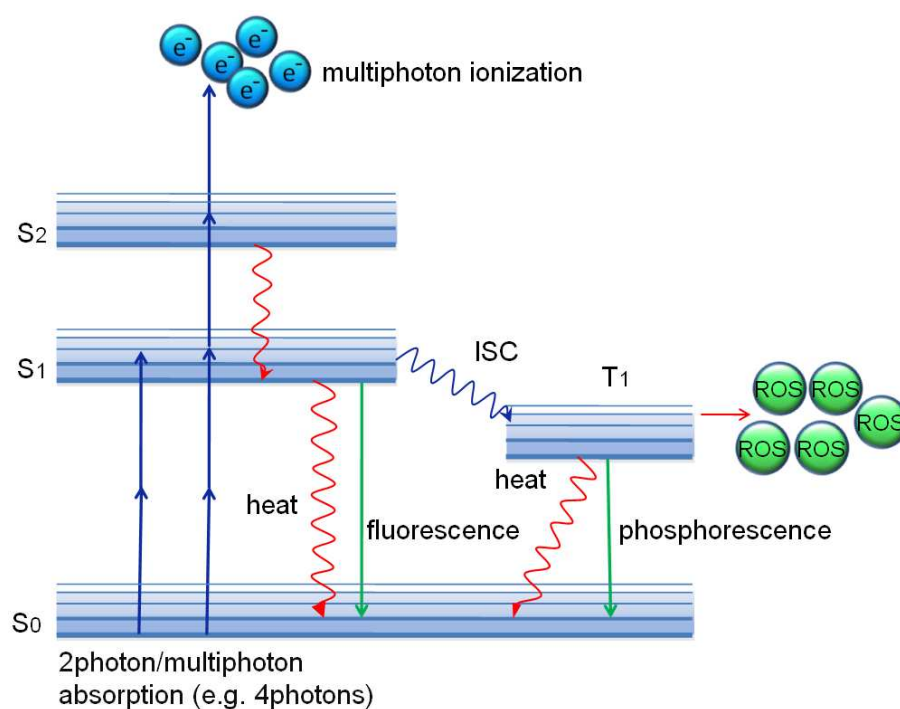


Fig. 3.2: Principle of multiphoton ionization (generation of free electrons and ions) and ROS formation during the multiphoton absorption process. S₀, S₁, and S₂ are the ground state and higher energy excited electronic states, and T₁ is the lowest energy triplet state for the molecule. ISC is intersystem crossing to the triplet state. Multiphoton ionization requires multiple photons (e.g. 4) and TW/cm^2 intensities, respectively, to remove electrons from the molecule. Two-photon excitation at lower GW/cm^2 intensities results in heat, fluorescence, and the occupation of the triplet state. The triplet state with a relatively long lifetime of some microseconds enables chemical reactions including oxygen which results in the formation of ROS.

Fig. 3.2 shows the major destructive photoinduced effects which are (i) two-photon photochemical reactions as well as (ii) multiphoton ionization and plasma formation. Tab. 3.1 exhibits typical laser and exposure parameters used within this work. Two laser microscopes were employed: one system with “long” laser pulses of 250 femtoseconds and the second one with extremely ultrashort pulses of 12 femtoseconds. The spot size “d” was calculated based on the formula $d = \lambda/NA$. Typically, a numerical aperture of 1.3 was used in most of the studies (40x/NA 1.3 oil, $\infty/0.17$, ZEISS objective). The mean laser power P was measured with a standard power meter (FieldMate, Coherent Inc., USA) with a detector PM3 (PowerMax, USA). The laser peak power P_{max} was calculated with $P_{max} = E/\tau$ and $E=P/f$. The pulse width was measured with an autocorrelator at the focal plane. The peak light intensity was calculated as $4P_{max}/(\pi d^2)$, the laser pulse number n as the product of the repetition frequency f and exposure time t ($n=ft$). As demonstrated in the Tab. 3.1, very low pulse energies in the range of pJ are employed for two-photon imaging.

Within this work, a variety of studies have been performed on stem cells and other cell types to understand the influence of NIR femtosecond laser pulses provided by laser scanning microscopes on cell metabolism and cell viability as well as to define an optical window for safe long-term two-photon imaging of stem cells.

Tab. 3.1: Typical laser and exposure parameters used for two-photon imaging of stem cells.

Pulse width, τ (fs)	Mean power, P (mW)	Wavelength, λ (nm)	Spot size, d (μm)	Repetition frequency, f (MHz)	Pulse energy, E (pJ)	Peak power, P_{max} (kW)	Mean light intensity, I (MW/cm ²)	Peak light intensity, I_{peak} (GW/cm ²)	Exposure time, t (μs)	Energy density (J/cm ²)	Laser pulse number, n	Applied energy (nJ)
Microscope 1 250	5	750	0.58 (NA 1.3)	80	62.5	0.25	1.9	95	6	11.4	480	30
Microscope 2 12	0.5	800	0.62 (NA 1.3)	75	6.6	0.55	0.2	182	6	1.2	450	3

3.1.2. Photoinduced modifications of morphology

Stem cells and mature cells have been laser-exposed by multiple scanning. Typically, cells were scanned 10 times with 4-16 s per frame (6-26 μ s beam dwell time) within one focal plane (512x512 pixel, 230x230 μ m²). The effects of the laser beam on the cell morphology were on-line monitored with a CCD camera. The laser power was increased in typical steps of 1 mW. When using 250 fs laser pulses, scanning at mean laser powers of up to 7 mW (n=500) did not induce any morphological alteration. However, when further increasing the mean power up to 10 mW, the shape of the majority of the cells changed (shrinkage) and some cells (30%) lost their attachment to the cover glass within few minutes. When applying even higher average laser powers, the formation of transient bubbles, membrane disruption, and fragmentation of the cells were monitored.

The application of the sub-20 fs laser pulses has been found to be more destructive compared to 250 fs laser pulses. Using the same scanning parameters, cell damage by bubble formation and disruption has been monitored already at mean powers as low as 7 mW. Mean powers of 5 mW laser radiation induced changes of the cell morphology. A power less than 2 mW did not cause any morphological changes. Typically, microwatt powers were sufficient for two-photon imaging as described in the following chapters (chapter 3.3 and appendix C).

3.1.3. Detection of photoinduced reactive oxygen species

Two control experiments have been performed to obtain information on the possible formation of reactive oxygen species (ROS). The first control experiment was based on UV illumination with the mercury lamp HBO50 (ZEISS, Germany). UV light induced ROS was monitored immediately after (15-60) s UV exposure using the two-photon excited probe carboxy-H₂ DCFDA which emitted in the green spectral range (maximum at 529 nm). As another control experiment, PtK2 cells were treated with tert-butyl hydroperoxide (TBHP) which is known to induce oxygen radicals (Fig. 3.3). Green fluorescence of the ROS probe was detected in the cytoplasm of the cell.

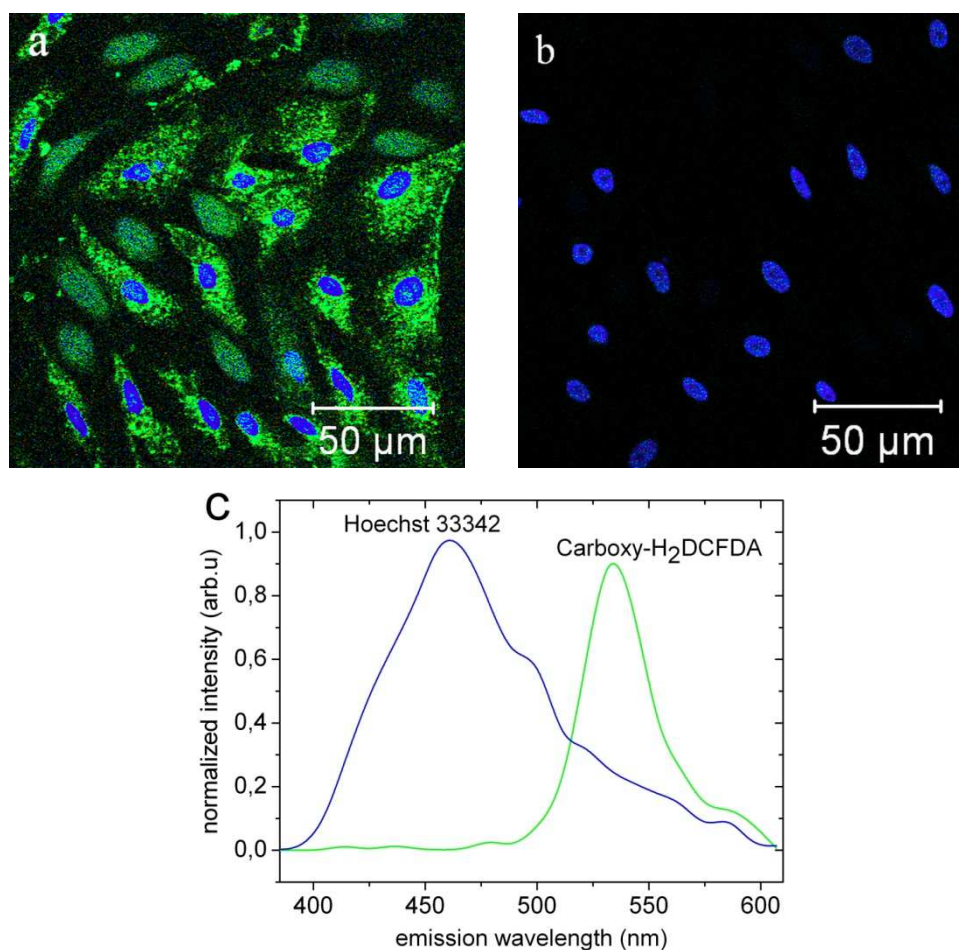


Fig. 3.3: (a) Positive control of ROS formation. Green fluorescence indicates generation of ROS. Additionally, the nuclei were stained with blue-fluorescent Hoechst 33342. (b) ROS negative cells after femtosecond laser exposure at 800 nm. The nuclear fluorescence due to Hoechst shows up only. (c) Normalized fluorescence spectra of carboxy-H₂DCFDA and Hoechst at 800 nm excitation.

The studies on the influence of NIR 250 fs laser pulses have been performed at mean powers of up to 7 mW and pulse energy of 0.088 nJ, respectively. No ROS signal was detected. Even repeated frame scanning up to 10 times of the PtK2 cells (n=100) did not induce any ROS probe fluorescence (Fig. 3.3).

However, significant ROS formation was detected when single point illumination on a particular cell was performed with high pulse energy of about 2.6 nJ which was later applied for nanoprocessing (chapter 3.3.2).

The results on the formation of ROS are consistent with the results on morphological modifications. No significant fs laser induced effects occurred when the mean powers were kept at a low level of less than 7 mW.

3.1.4. Detection of photoinduced DNA strand breaks

In order to investigate possible photo-induced DNA damage, cells were scanned at different mean powers in a 512x512 pixel field at 26 μ s beam dwell time per pixel. The probe for detecting DNA strand breaks was applied 30 min after laser exposure. When using mean powers up to 7 mW, no DNA damage was monitored.

Only at very high mean powers, DNA strand breaks could be detected as demonstrated in Fig. 3.4. In this case, cells were exposed to 250 fs laser pulses at an average power of 60 mW (one scan).

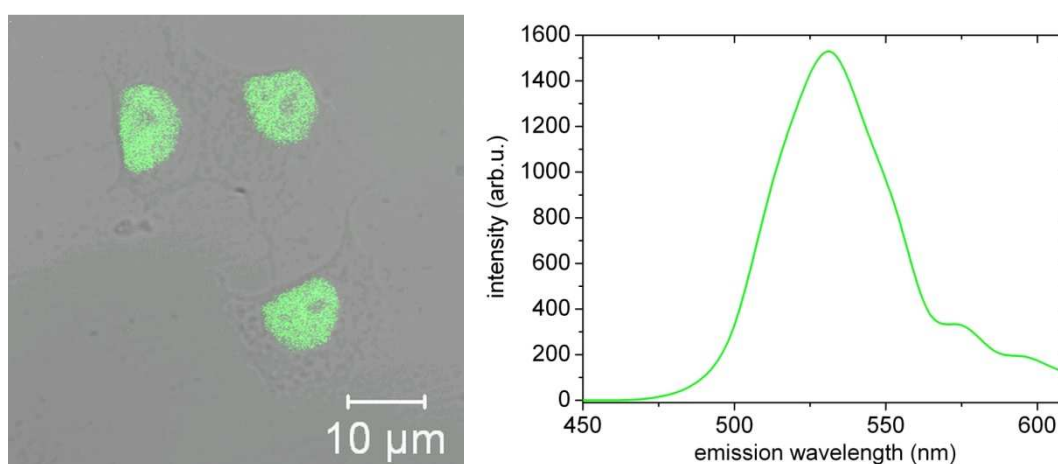


Fig. 3.4: Overlay of the green nuclear fluorescence and the transmission image of TUNEL positive cells after exposure to 250 fs laser pulses at 800 nm (60 mW, 1 scan). The spectrum shows the emission of the two-photon excited TUNEL assay probe.

3.1.5. Detection of photoinduced early apoptosis

The cells were scanned at different average powers in a 512x512 pixel field at 26 μ s beam dwell time. As shown in Fig. 3.5, signs of early apoptosis have been detected at 10 mW laser power (250 fs) by the green-fluorescent annexin probe which binds to extracellular phosphatidyl-serine as a result of laser-induced membrane modifications. At 7 mW average power, no signs of early apoptosis were found (n=100).

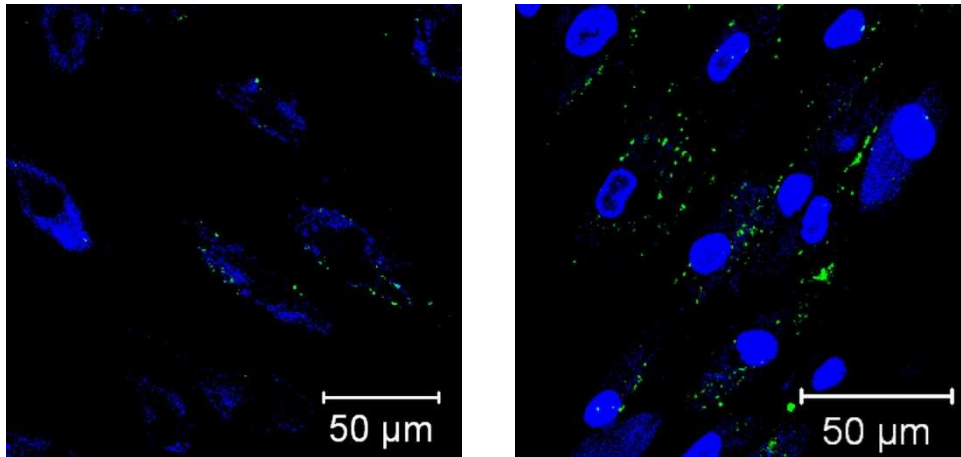


Fig. 3.5: The green fluorescence indicates laser-induced alterations of the membrane structure. The blue fluorescence in the cytoplasm depicts autofluorescence, whereas the nuclear fluorescence in the right image originates from the DNA stain Hoechst.

According to the results, it can be stated that the exposure of cells with 250 femtosecond NIR pulses at 80 MHz repetition rate with mean powers of up to 7 mW and beam dwell times of up to 26 μ s (16 s per frame) allows non-destructive two-photon imaging. When applying extremely ultrashort laser pulses of sub-20 femtoseconds, the mean power should be kept at values less than 2 mW. As shown in the next chapters, most of the two-photon studies within this work have been performed at mean power levels of 5 mW and 0.5 mW, respectively.

3.2. Two-photon imaging

Two-photon excitation of endogenous fluorophores enables non-destructive high resolution imaging of living cells over a long period of time. Within this chapter, the potential of marker-free two-photon imaging of endogenous intracellular fluorophores of stem cells as well as of collagen as end product of differentiated cells was studied. The method of 3D autofluorescence/SHG imaging was expanded to a 5D imaging modality by the exploration of the fluorescence lifetime per pixel (FLIM) and the spectral characteristics of the emitted photons (spectral imaging). The modifications of the autofluorescence/SHG parameters during the differentiation processes were measured.

3.2.1. Autofluorescence imaging of stem cells

The application of near infrared femtosecond laser pulses induced a cellular autofluorescence mainly in the blue/green spectral range. 3D autofluorescence imaging provided information on the cell morphology and cell size as well as enabled visualization of some cell structures and extracellular matrix components with submicron resolution without exogenous markers. Intense fluorescent structures were found to be the mitochondria. Fig. 3.6 shows autofluorescence images of human salivary gland stem cells (hSGSCs) and rat pancreatic stem cells (rPSCs) acquired at 750 nm excitation wavelength. The ellipsoidal/round non-fluorescent nucleus and the fluorescent mitochondrial network were clearly seen. The cellular membrane was not observed.

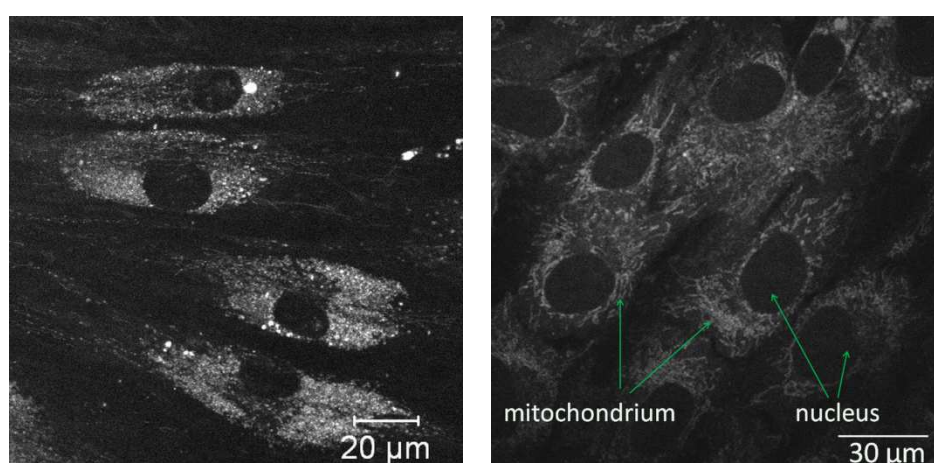


Fig. 3.6: 750 nm excited autofluorescence images of hSGSCs (left) and rPSCs (right). The beam splitter HFT KP 650 and the short pass filter KP 685 were employed for the detection.

Two-photon imaging showed that different stem cell lines have an autofluorescence with different intensity. hDPSC, hPSC, and hSGSC human stem cells exhibited a more intense autofluorescence compared to rPSC rat cells. Fig. 3.7 demonstrates the differences in the fluorescence intensity between human and rat stem cells. Also significant fluorescence intensity variations between cells of the same cell line were observed (Fig. 3.8).

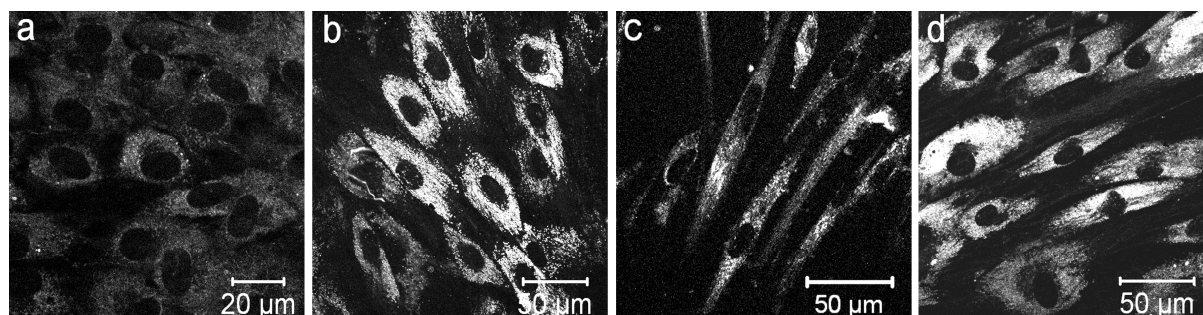


Fig. 3.7: Autofluorescence images of (a) rat pancreatic stem cells (rPSC), (b) human pancreatic stem cells (hPSC), (c) human dental pulp stem cells (hDPSC) and (d) human salivary gland stem cells (hSGSC) at 750 nm excitation wavelength (Uchugonova and König 2008).

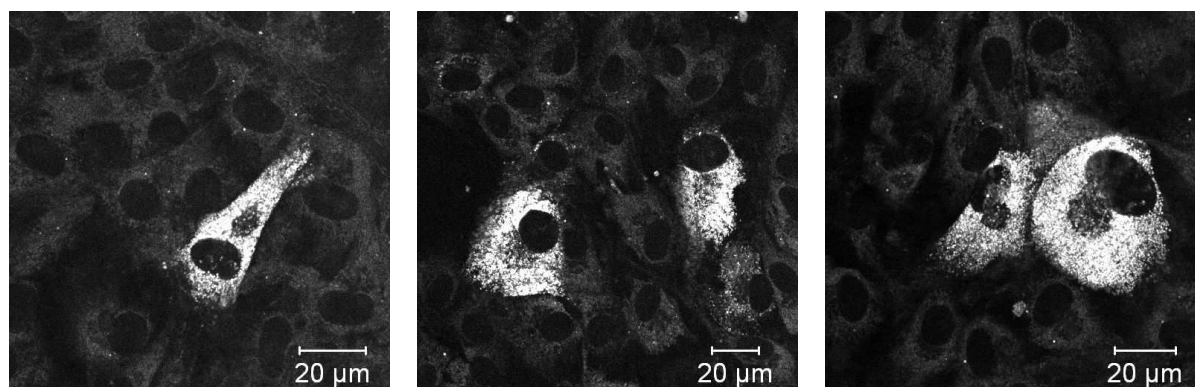


Fig. 3.8: Autofluorescence images of rPSC cells. Note that some cells (<5 %) exhibited a very intense autofluorescence (750 nm excitation wavelength).

Some of the bright cells had a different morphology than the main cell population. Most of them showed a dividing nucleus. In order to obtain more information on the natural fluorescent components and their alterations, spectral and time-correlated SPC measurements have been performed.

3.2.2. Spectral measurements of stem cells

Spectral imaging was performed with the ZEISS META system which is based on the 32 channel PMT array with 10.5 nm resolution. Natural fluorescence from living stem cells was detected at different NIR excitation wavelengths (750 nm, 800 nm, 850 nm, 900 nm) in order to separate different native fluorescence molecules. When using 750 and 800 nm, NAD(P)H as well flavins/flavoproteins were efficiently excited by a two-photon process. The intensity of the detected fluorescence was high compared to other excitation wavelengths. However, when changing to 850 nm or even 900 nm, flavins/flavoproteins (e.g. FAD) only and not NAD(P)H were efficiently excited.

Spectral measurements (Fig. 3.9) showed that the detected fluorescence light was intense in the blue/green spectral region. The maximum of the fluorescence was found to be at 460-470 nm when excited with 750 nm light which is consistent with the emission behavior of free and protein bound NADH.

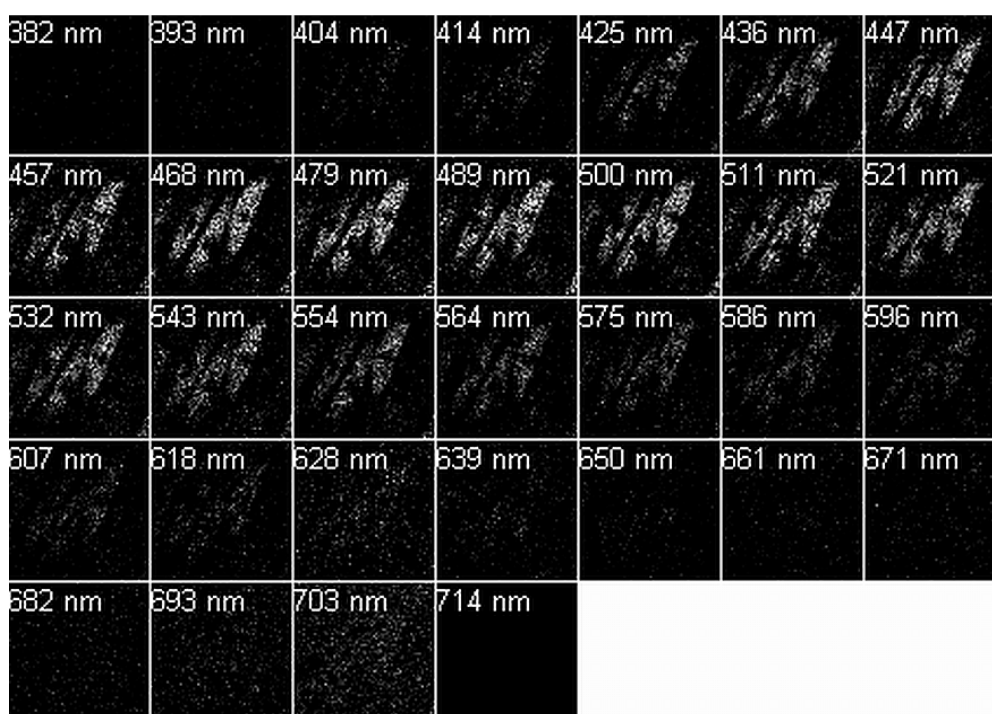


Fig. 3.9: Spectral analysis of hSGSC stem cells obtained from 32 images in the spectral range of 382 nm to 714 nm. Excitation wavelength was 750 nm (40x objective, the beam splitter HFT KP 650 was employed in front of the PMT array to avoid the detection of backscattered laser light).

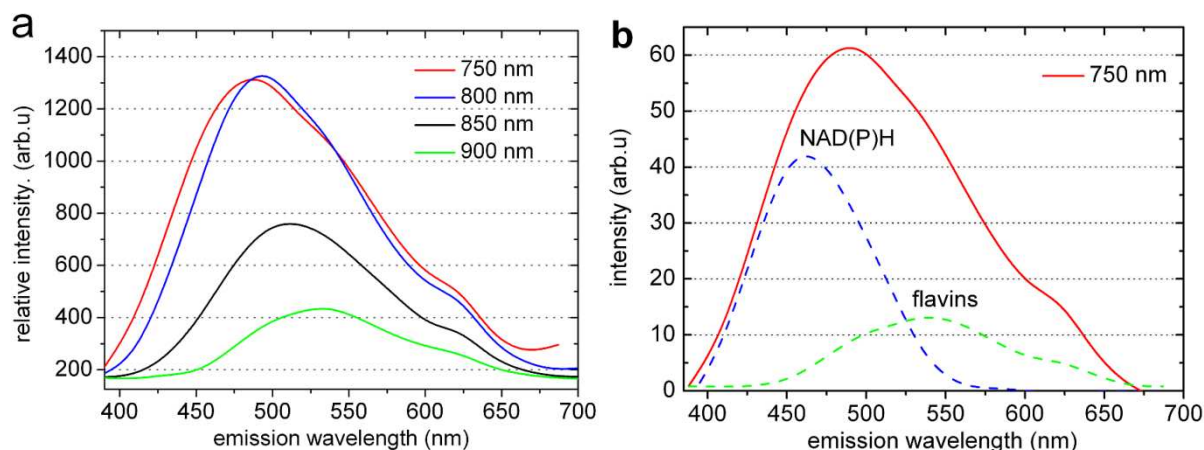


Fig. 3.10: (a) Spectral measurement of hSGSC stem cells. Four excitation wavelengths were employed. The emission peak shows a red-shift with increasing excitation wavelength due to the preferred two-photon excitation of flavins versus NAD(P)H. (b) The 750 nm/800 nm excited emission spectra can be considered as an overlay of the two fluorophores NAD(P)H and flavins (dotted lines, spectral unmixing).

The maximum shifted to 530-535 nm when using 900 nm light which is consistent with flavin emission (Fig. 3.10a). The 750 nm excited emission curve was analyzed using the software OriginPro 7.5. According to the fitting procedure (spectral unmixing), the fluorescence consists of the major component NAD(P)H and a minor component flavin (Fig. 3.10b).

The presence of the culture medium did not add significant background to the autofluorescence signals from the cells.

Because of the broad and variable fluorescence spectra of endogenous chromophores, it is difficult to disentangle the fluorescence components by their emission spectra alone. It would be helpful to add another parameter such as the fluorescence lifetime (chapter 3.2.3).

3.2.3. FLIM measurements

Measurements on human adult stem cells

Spatially resolved autofluorescence decay curves from stem cells have been obtained using time-correlated single photon counting in combination with x, y, z scanning. For this data collection, the laser excitation wavelengths 750 nm and 900 nm and a scanning time of up to 30 s per frame were used. Fitting of the decay curves (non-linear least square curve fitting method) enabled the analysis of up to two fluorescence components per pixel and provided fluorescence lifetime data and amplitudes per pixel. The two fluorescence lifetimes as well as the mean fluorescence lifetime per pixel were depicted as false color. Fig. 3.11 represents a typical FLIM image, a histogram and a particular intramitochondrial fluorescence decay curve of 750 nm-excited hSGSC stem cells based on 6740 detected photons. The bi-exponential fit with the excellent fitting parameter $\chi^2 = 1.00$ revealed a fast decaying fluorophore with a short lifetime (τ_1) of 0.17 ns and an amplitude of $a_1 = 72\%$ and a second component with $\tau_2 = 1.8$ ns and the amplitude $a_2 = 28\%$. Although the amplitude is lower, the longer component provides $\tau_2 a_2 / \tau_1 a_1 = 4$ times more fluorescence intensity than the short-lived fluorophore.

In order to get statistical information on the variance of intracellular decay curves, the curves of 10 different perinuclear fluorescence regions of a single cell within Fig. 3.11 have been analyzed. The results are listed in Tab. 3.2. Interestingly, only one major short as well as one major long component with an average value of $\tau_1 = 0.202$ ns (standard deviation SD: 0.019 ns, amplitude: 70.5%) was found in this particular cell. The long component τ_2 had an average value of 2.014 ns with a standard deviation value of about 0.077 ns which corresponds to a value of <5% of τ_2 .

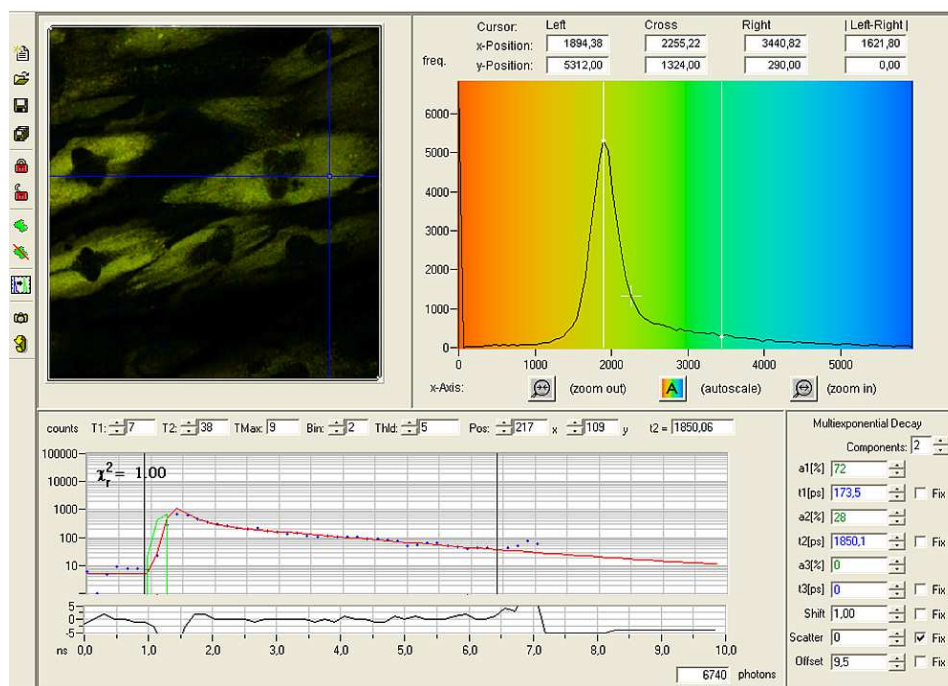


Fig. 3.11: FLIM of stem cells (hSGSC). The depicted decay curve is from an intracellular “pixel” of the right cell (cross), the τ_2 -histogram from the whole frame.

Tab. 3.2: Intracellular FLIM data obtained from 10 decay curves within the cytoplasm of the stem cell with the cross in Fig. 3.11 (Uchugonova and König 2008).

Location	τ_1 (ns)	τ_2 (ns)	τ_m (ns)	a_1 (%)	χ^2
1	0.193	1.892	0.729	68.5	1.01
2	0.244	2.004	0.778	69.7	1.14
3	0.202	2.089	0.722	72.4	1.44
4	0.208	2.087	0.736	71.9	1.40
5	0.197	2.060	0.721	71.9	1.22
6	0.169	1.933	0.731	68.1	1.48
7	0.203	1.979	0.717	70.5	1.08
8	0.211	2.128	0.776	70.5	1.59
9	0.214	2.025	0.729	71.6	1.65
10	0.186	1.945	0.722	69.6	1.56
Average	0.202	2.014	0.736	70.5	1.36
SD	0.019	0.077	0.022	1.5	0.2

Results 3

Next, the variance of FLIM data of different cells was investigated. When calculating the average fluorescence lifetime τ_2 within the frame of about 10 cells of Fig. 3.11, a major value of 1.87 ns as depicted in the histogram (Fig. 3.12) was obtained.

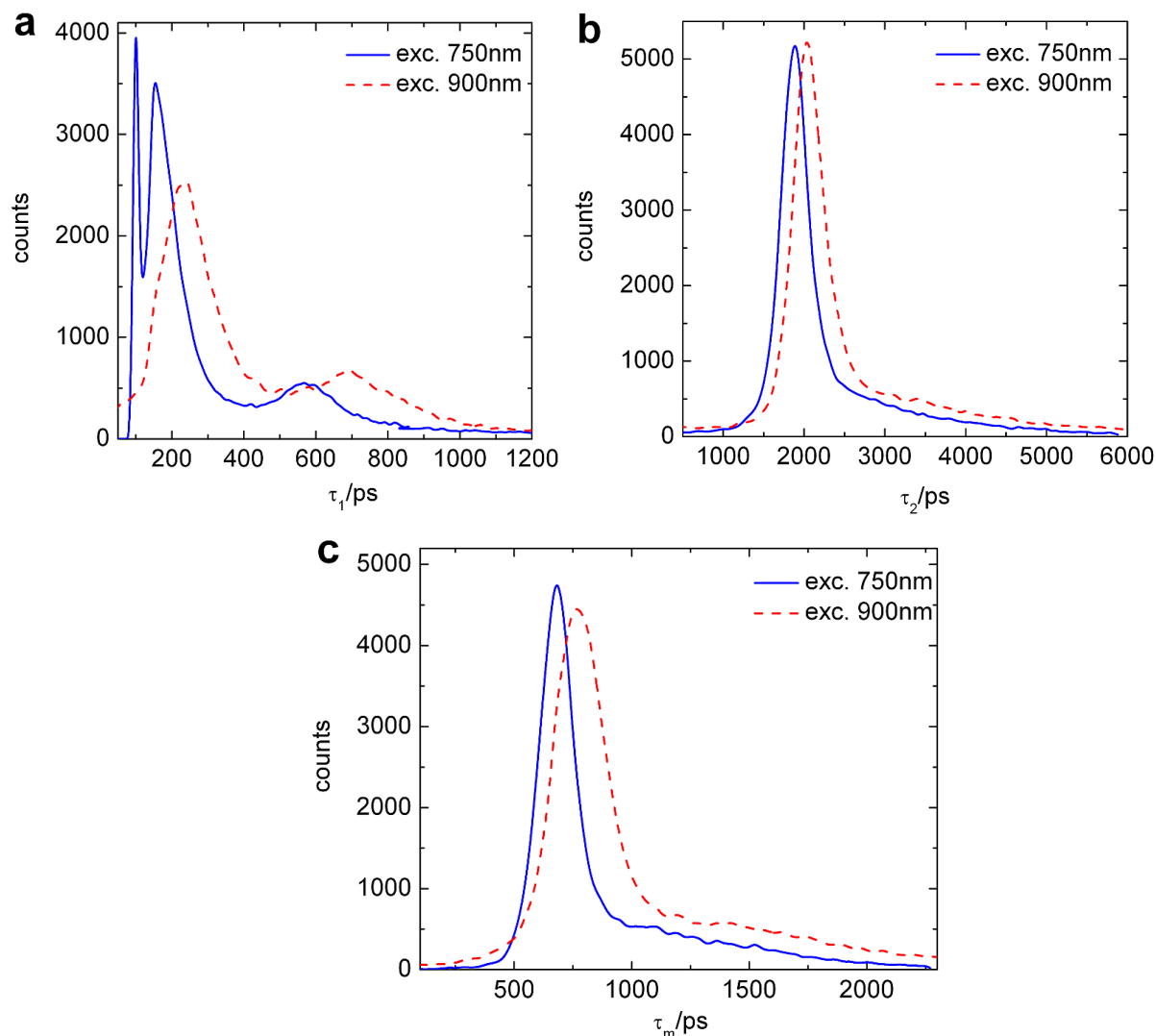


Fig. 3.12: Histograms for the distribution of the fluorescent components (a) τ_1 , (b) τ_2 and (c) τ_m at 750 nm and 900 nm of hSGSC stem cells calculated from the frame in Fig. 3.11.

When analyzing 10 frames of about 100 cells in total of the same cell line, a mean τ_2 value of (1.82 ± 0.02) ns and a mean value τ_m of (0.680 ± 0.04) ns has been obtained. In contrast, when changing the excitation wavelength to 900 nm, values of (2.00 ± 0.03) ns and (0.820 ± 0.05) ns, respectively, were calculated.

Interestingly, when analyzing the short fluorescent components within these FLIM images, (frames) up to 3 maxima have been obtained in the τ_1 –histogram (Fig. 3.12). The first one at around 0.07 ns reflects the influence of backscattered laser light which was partially able to transmit through the optics (beamsplitter and the short pass filter SP 610). When adding a second short pass filter this peak nearly disappeared. The other two peaks occurred around (0.170 ± 0.015) ns and (0.660 ± 0.05) ns at 750 nm excitation wavelength and shifted to (0.200 ± 0.015) ns and (0.800 ± 0.05) ns, respectively, at 900 nm. Control measurements were done in culture medium as well as after washing the cells with phosphate buffered saline (PBS). No significant fluorescence signal was found.

The two short components were therefore of biological origin. When performing a statistical analysis of the histograms on ten single fluorescent cells (Tab. 3.3), differences in the fluorescence decay characteristics were found. According to the table, just three cells exhibited only a single short fluorescence lifetime component of about 0.2 ns, whereas seven out of 10 cells possessed two short components at 0.2 ns and 0.7 ns, respectively. Using false-color coded imaging, the presence of two different short components can be depicted as shown in Fig. 3.13.

Tab. 3.3: Average FLIM data calculated from 10 regions of interest covering one single cell in each region.

“x”- no component was detected.

Cells	τ_{1a} (ns)	τ_{1b} (ns)	τ_2 (ns)	τ_m (ns)	a_{1a} (%)	a_{1b} (%)	ratio	χ^2
1	0.208	x	2.059	0.795	72.1	x	x	1.02
2	0.215	x	2.118	0.781	72.9	x	x	1.08
3	0.216	0.687	2.103	0.798	71.9	79.7	2.216	1.13
4	0.201	0.673	2.118	0.785	71.9	79.9	1.792	1.11
5	0.241	0.695	2.133	0.781	72.3	79.9	1.367	1.10
6	0.283	0.708	1.952	0.785	73.3	79.9	1.815	1.13
7	0.230	x	1.977	0.708	72.9	x	x	1.13
8	0.181	0.696	1.941	0.661	73.9	79.9	1.244	1.13
9	0.197	0.764	2.046	0.701	72.9	79.7	1.219	1.17
10	0.226	0.730	2.097	0.768	71.1	79.3	5.834	1.31
Average	0.220	0.708	2.054	0.756	72.5	79.8	2.212	1.13
SD	0.028	0.031	0.073	0.048	0.8	0.2	1.638	0.07

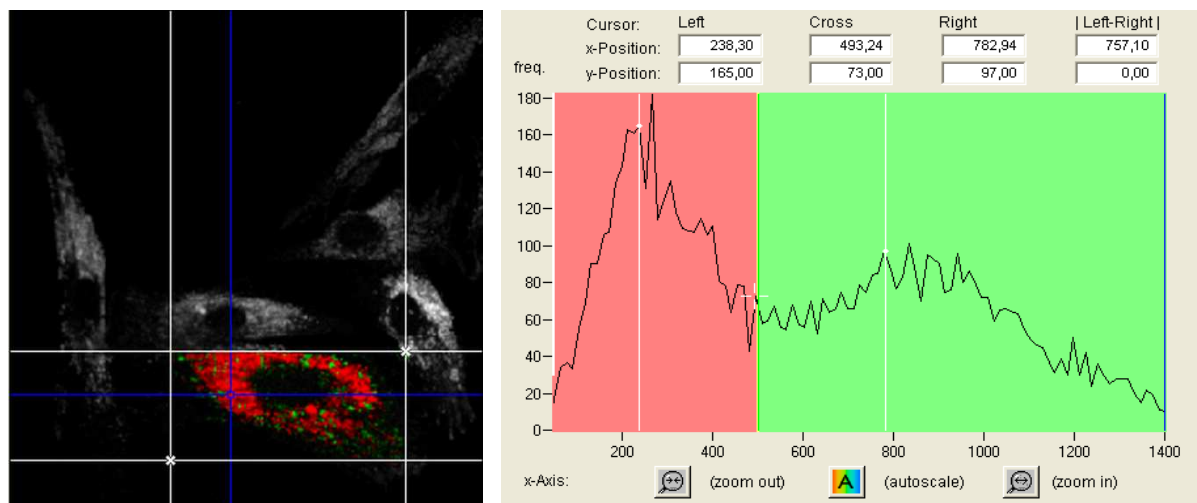


Fig. 3.13: Left: Average FLIM data of a particular cell were obtained from a region of interest (white rectangle). Right: The histogram reveals two short-lived components with two fluorescence lifetime maxima at 0.238 ns and 0.783 ns, respectively. The fluorophores with a lifetime in the range of 0.00-0.50 ns are depicted red and the fluorophores with a lifetime of 0.51-1.40 ns are shown green in the false color τ_1 image.

A more detailed description of the two-photon imaging results regarding the endogenous fluorophores in stem cells can be found in the appendix A.

FLIM and spectral measurements during adipogenic differentiation

Human SGSCs stem cells can undergo adipogenic differentiation resulting into the formation of mature adipocytes (Rotter *et al.* 2008; Gorjup *et al.* 2009). The differentiation process can be initiated by the administration of a specific adipogenic differentiation medium. Fig. 3.14 demonstrates directed adipogenic differentiation of human salivary gland stem cells.

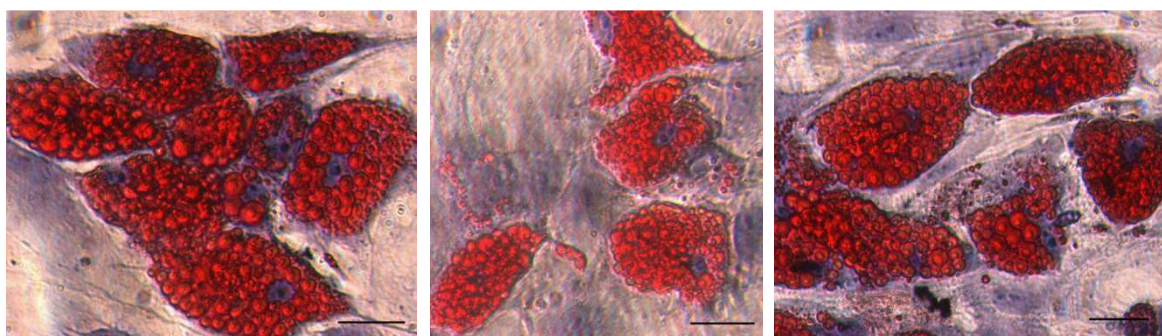


Fig. 3.14: Adipocytes stained with red oil O (scale bar: 30 μ m).

Within this work, the modifications of FLIM and spectral data during the differentiation process were studied. Fig. 3.15 shows images of about 10 stem cells inside a spheroid taken 7 days after administration of adipogenic differentiation factors. Two of them are differentiated into about 100 μm long adipocytes with lipid vacuoles (fat droplets) which synthesize and store fat. The typical diameter of the fat droplets was measured to be in the order of 7-10 μm . A typical cell contained more than 20 of these organelles. The nucleus was found to be not longer in the central part of the cell. The left cell (Fig. 3.15) which is on an earlier stage of development contained organelles with typical diameters of less than 5 μm . When analyzing the autofluorescence pattern, the differentiated cells were found to possess lower fluorescence intensity than cells without fat droplets.

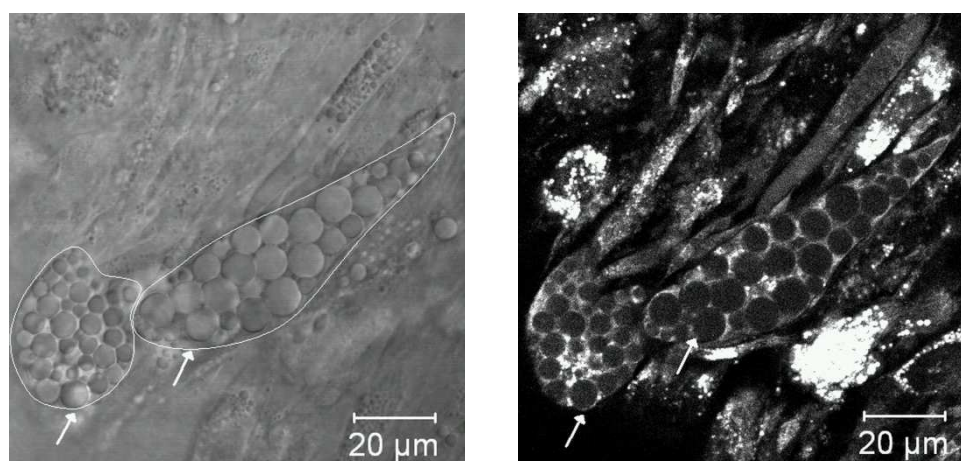


Fig. 3.15: Transmission and two-photon autofluorescence images of cells after adipogenic differentiation. In the transmission image the cell membrane of two adipocytes are marked (white line).

Interestingly, some cells without organelles (e.g. 3 cells in Fig. 3.15) exhibited a very bright fluorescence after incubation with the differentiation factor. Very likely these highly fluorescent cells are in very early stages of differentiation and possess a high metabolic activity. After formation of the fat droplets the total fluorescence intensity decreases because no visible autofluorescence was found inside the organelles. It was possible to monitor the onset of the formation of the organelles already 3 days after administration of the differentiation medium.

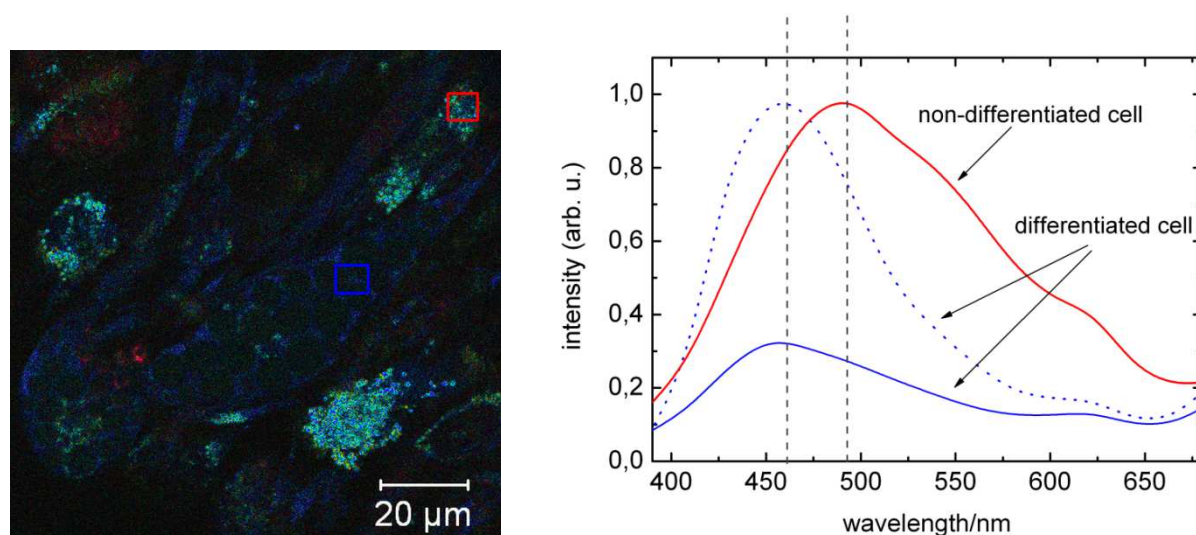


Fig. 3.16: Spectral image (left) and spectra (right) of the cells 7 days after incubation in the adipogenic medium. Differentiated cells showed an increase of NAD(P)H and a decrease of flavin/flavoproteins compared to the non-differentiated cells as well as a decrease of the total fluorescence intensity of more than 60%. The dotted line is the normalized spectrum of the differentiated cells in order to indicate the blue shift compared to the non-differentiated cells (750 nm excitation wavelength).

When analyzing the cells with the method of spectral imaging, significant changes of the emission spectrum were found. Non-differentiated highly-fluorescent cells exhibited a maximum at 490 nm with shoulders at 540 nm and 620 nm, whereas the differentiated cells emitted at 455 nm with a less pronounced shoulder at 620 nm (Fig. 3.16). The maximum at 455 nm corresponds to the typical emission maximum of NAD(P)H. FLIM data were measured by defining a region of interest (ROI) that covers the highly fluorescent vacuole-free cell of interest. A τ_m -value of 0.59 ns, a short 0.22 ns component with amplitude of 78 % as well as a slow 1.93 ns component (22 %) were calculated. In contrast, the mean lifetime of cells with fat droplets was found to be much longer with typical values of more than 0.85 ns (Fig. 3.17).

Tab. 3.4: FLIM data obtained from 750 nm excited non-differentiated cells and cells with fat droplets.

Cells	τ_1 (ns)	τ_2 (ns)	τ_m (ns)	a_1 (%)	Ratio: a_1/a_2
Non-differentiated cells	0.22±0.03	2.00±0.26	0.60±0.03	78.0±1.4	3.5
Differentiated cells	0.26±0.04	2.33±0.16	0.85±0.04	67.0±2.3	2

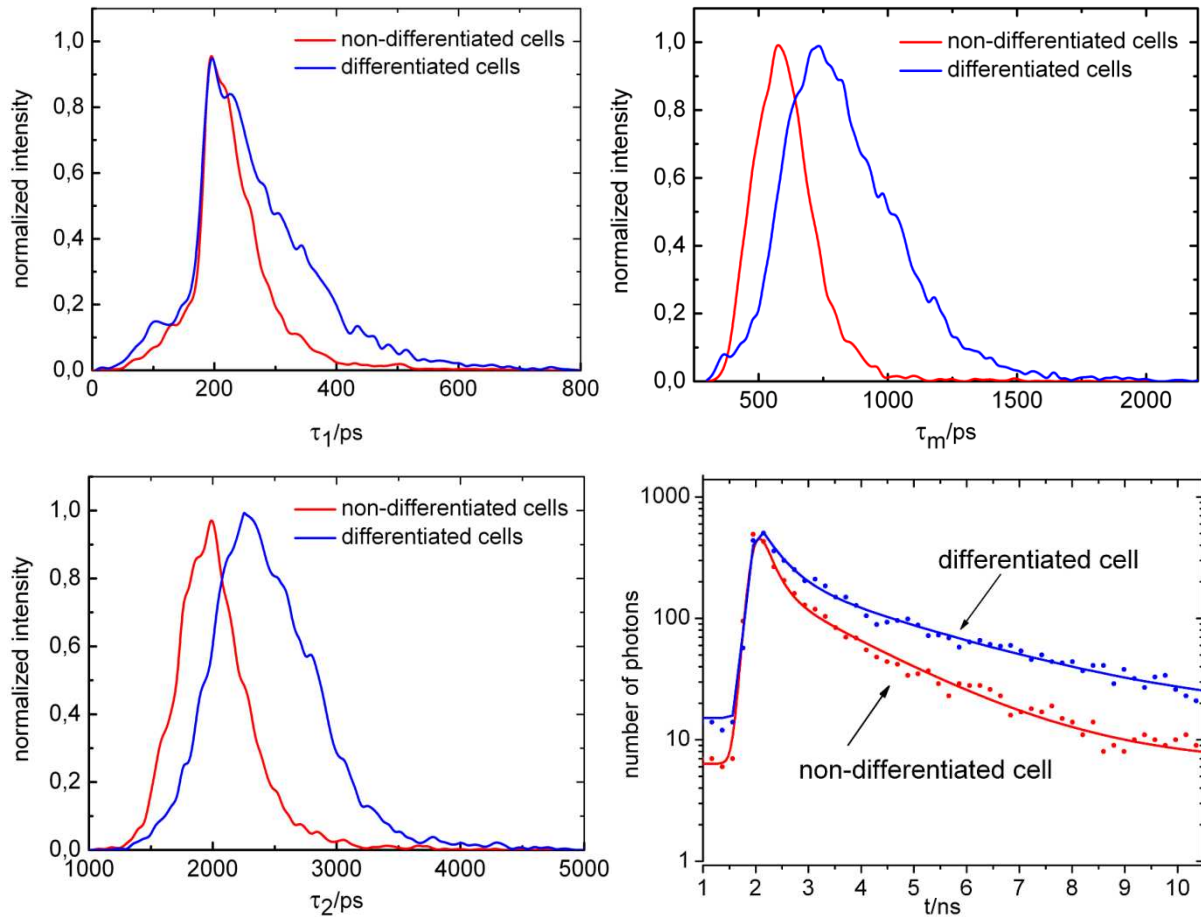


Fig. 3.17: ROI histogram distributions (τ_1 , τ_m , τ_2) and typical decay curves from differentiated cells and non-differentiated cells. Differentiated cells have a larger distribution of the short and long fluorescent component (large FWHM of the histogram) and a significantly longer fluorescence lifetime τ_2 compared to the non-differentiated cells.

Interestingly, also significant modifications of the fluorescence decay characteristics were found in different cytoplasmic regions within one differentiated cell. For example, typical fluorescence lifetime values in an intracellular area between large fat droplets were determined to be (0.26 ± 0.04) ns with amplitude of (67.0 ± 2.3) % and a strong long-lived component with lifetimes of (2.33 ± 0.16) ns (Tab. 3.4).

In contrast, a typical differentiated cell possessed also a small area where the mean fluorescence decay time became significantly shorter, e.g. $\tau_m = (0.60 \pm 0.03)$ ns, $\tau_1 = (0.17 \pm 0.04)$ ns, $a_1 = (78 \pm 1.4)\%$, and $\tau_2 = (2.0 \pm 0.26)$ ns (Fig. 3.18).

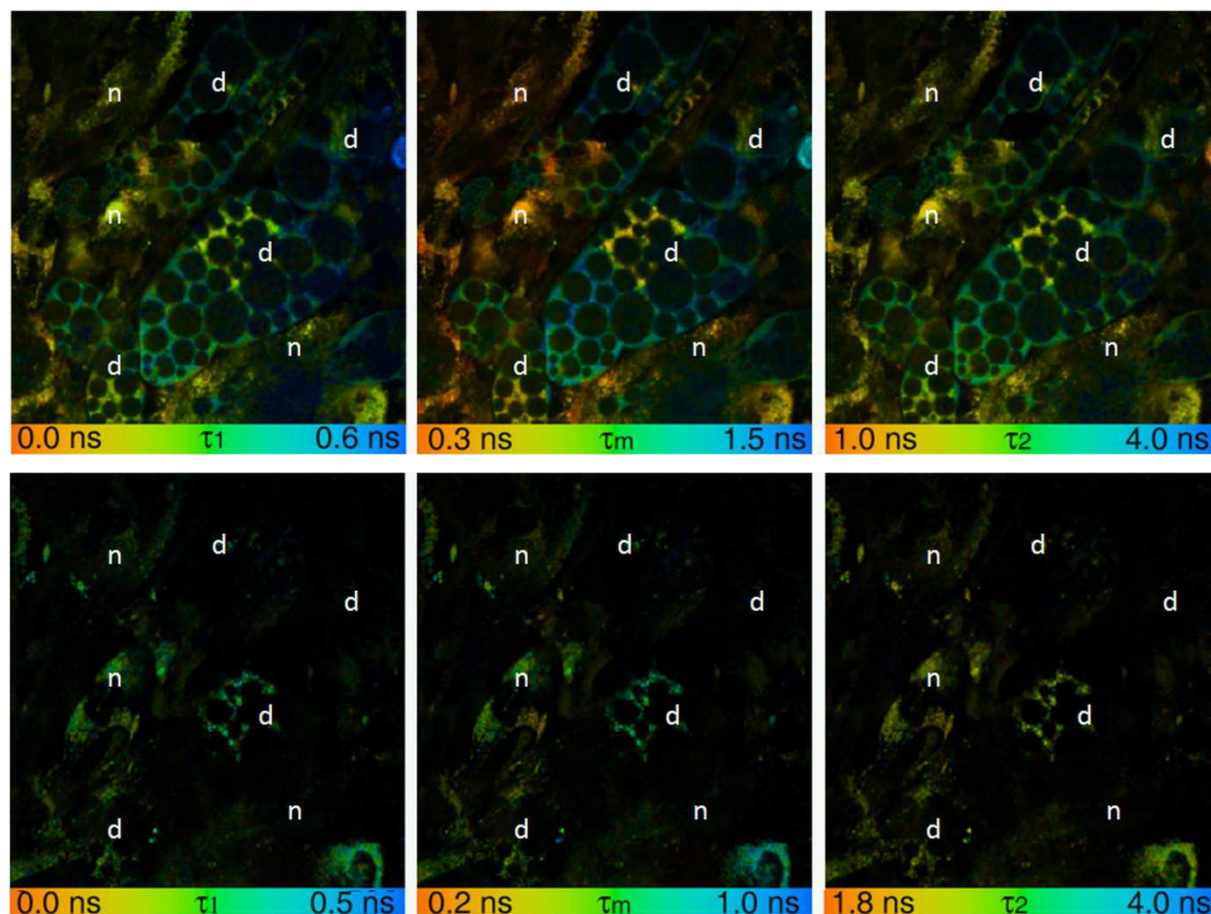


Fig. 3.18: False-color coded FLIM image of cells after adipogenic differentiation.

Upper image: 750 nm excitation wavelength, lower image: 900 nm excitation wavelength.

Non-differentiated cells (n) have a yellow-red color code in the τ_m and τ_2 image due to the shorter fluorescence lifetime compared to the “blue-green” differentiated cells (d). At longer excitation wavelength, NAD(P)H fluorescence is not observed. Mainly flavins in non-differentiated cells and further fluorophores (lysosomes, see fig. 3.19 and chapter 3.2.5) in differentiated cells appear during 900 nm excitation.

This region is the area of high accumulation of lysosomes as probed with the marker LysoTracker (Molecular Probes) (Fig. 3.19). Fig. 3.18 (upper image) was taken with an excitation wavelength of 750 nm. This wavelength is excellent to excite NAD(P)H. In order to get information on the contribution of flavins, a laser wavelength of 900 nm was chosen (Fig. 3.18 lower image). The 900 nm-excited autofluorescence image is much weaker due to the absence of NAD(P)H fluorescence. Only some fluorescent structures are seen. Interestingly, the small intracellular area with the shorter fluorescence lifetimes as described above (likely the region of lysosomes) can be imaged with both excitation wavelengths.

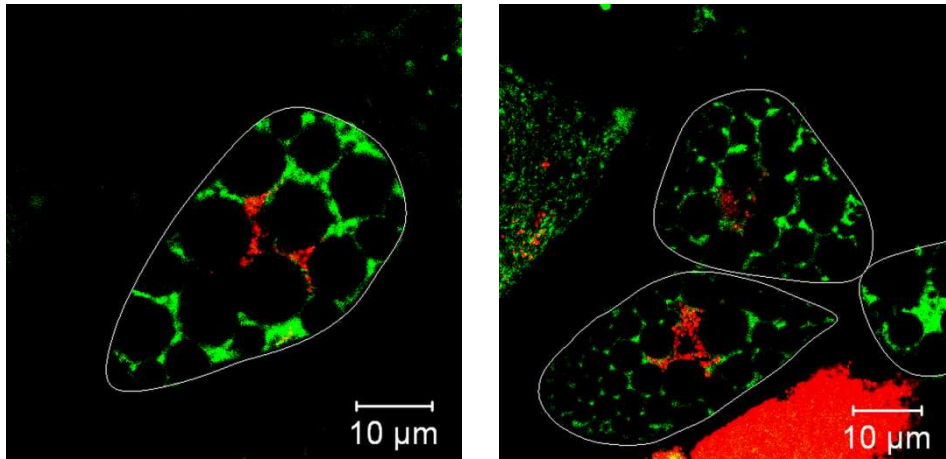


Fig. 3.19: Two-photon images of differentiated cells stained with probes to track mitochondria (green) and lysosomes (red). Cell membranes of differentiated cells are depicted (white).

3.2.4. SHG imaging

Alternative to two-photon excited fluorescence, two-photon microscopy allows the detection of SHG. Some molecules and tissue structures that lack a center of symmetry are able to generate SHG. SHG is an instantaneous process in which two photons are converted into a single photon of twice the energy. As shown in Fig. 3.20, the extracellular protein collagen II (powder, Sigma-Aldrich, Germany) can be excited by two-photon processes to emit fluorescence as well as SHG. The broad fluorescence has a maximum at 450 nm (750 nm excitation wavelength) whereas the SHG radiation is at half of the laser wavelength. For instance, when excited with 800 nm, SHG light can be detected at 400 nm wavelength. In contrast to the fluorescence, SHG occurs also at higher NIR excitation wavelengths.

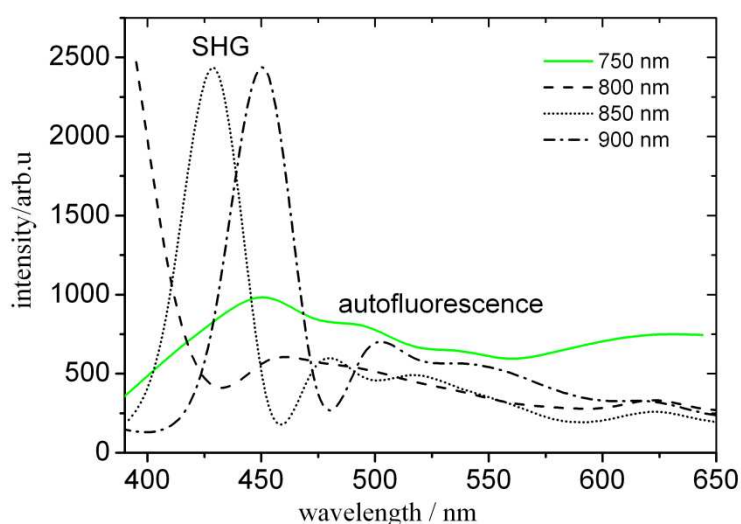


Fig. 3.20: Two-photon excited autofluorescence and SHG spectrum from collagen II (Sigma-Aldrich).

Fig. 3.21 left demonstrates fluorescence lifetimes of collagen II when excited at 750 nm. The autofluorescence decays of collagen can be fitted as a double exponential decay. The two components arise mainly from autofluorescence because the SHG signal in the UV is blocked by filters in the microscope and cannot reach the detector. The short component has a lifetime of about 0.26 ns with an amplitude of 58% whereas the longer component has a lifetime 2.6 ns with an amplitude of 42%. By contrast, at an excitation wavelength of 850-900 nm the signal is mainly based on SHG (98 %).

According to the control measurement with the purified powder collagen II, a laser wavelength of 870 nm has been chosen to investigate the biosynthesis of collagen from cells

during the differentiation process. The biosynthesis of collagen in 3D salivary gland and pancreatic stem/progenitor cell cultures has been monitored after incubation in differentiation medium by the occurrence of SHG signals in addition to two-photon autofluorescence.

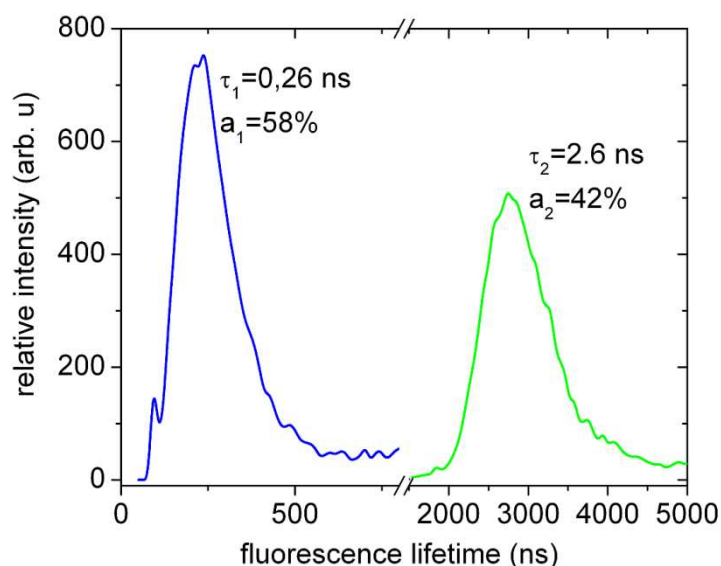


Fig. 3.21: Fluorescence lifetime distribution histogram of collagen II at 750 nm excitation.

The spheroids had dimensions of 0.2-2 mm in diameter. The differentiation process has been observed for a long time period up to 5 weeks by performing optical sectioning in z-steps of 5–10 μm several times a week (Fig. 3.22).

The occurrence of the first SHG signal was detected eight days after the introduction of the stimulating agent. As expected, the SHG signal from the biosynthesized extracellular matrix increased with time.

In order to differentiate between the different sources of luminescence (SHG and autofluorescence), SPC boards as well as different filters were used. With a BP 435/5 filter, collagen structures could be detected but no living cells and no other ECM proteins. When removing the filter, signals arose from a variety of fluorophores as well as from collagen (Fig. 3.22).

Results 3

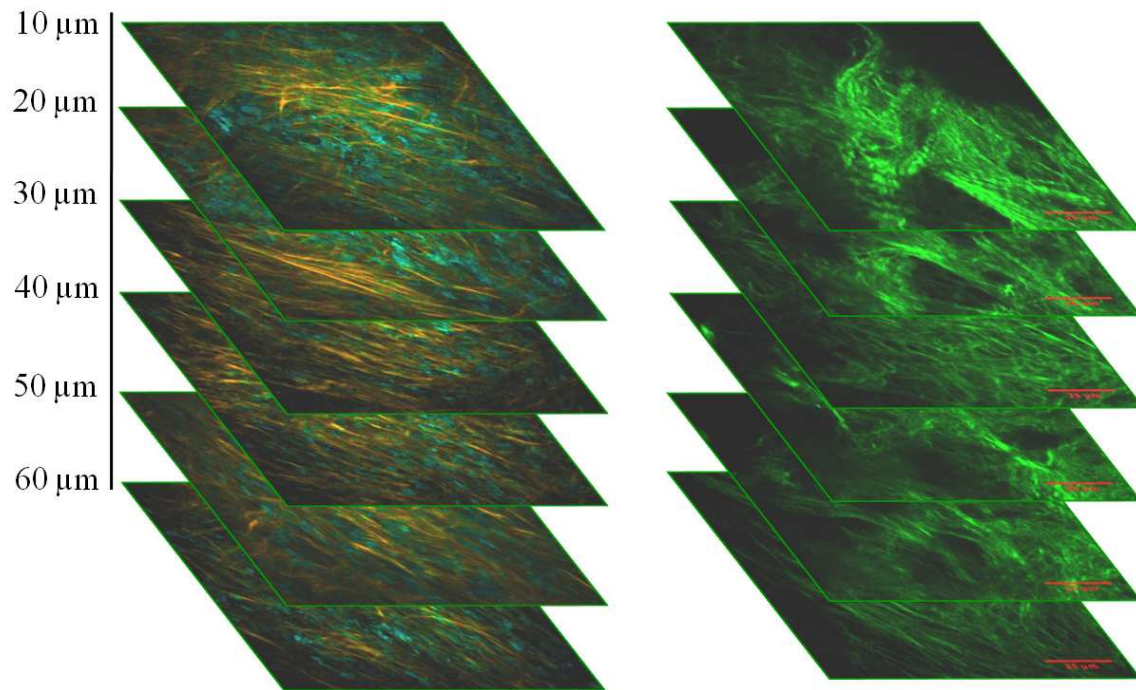


Fig. 3.22: SHG (yellow fibrils) and autofluorescence (blue-green) imaging of stem cell spheroids by optical sectioning without BP435/5 filter (left) and with bandpass filter (right). 40x/1.3 oil objective, 870 nm excitation.

False color FLIM images have been used to differentiate between SHG and autofluorescence. The SHG signal as well as a part of the autofluorescence was observed at the very short time interval between 0.0-0.3 ns (Fig. 3.23). SHG signals have no “lifetime” whereas the fluorescence lifetime is in the order of hundreds of picoseconds up to 5 ns (flavin mononucleotide, FMN) (König and Schneckenburger 1994; Lakowicz 1999; Skala *et al.* 2007). Some fluorescence photons always arrive within picoseconds immediately after excitation, even if the fluorescence lifetime is in the range of several nanoseconds. The artificial “lifetime” of SHG is due to the instrument response function and appears as an exponential component in the calculation.

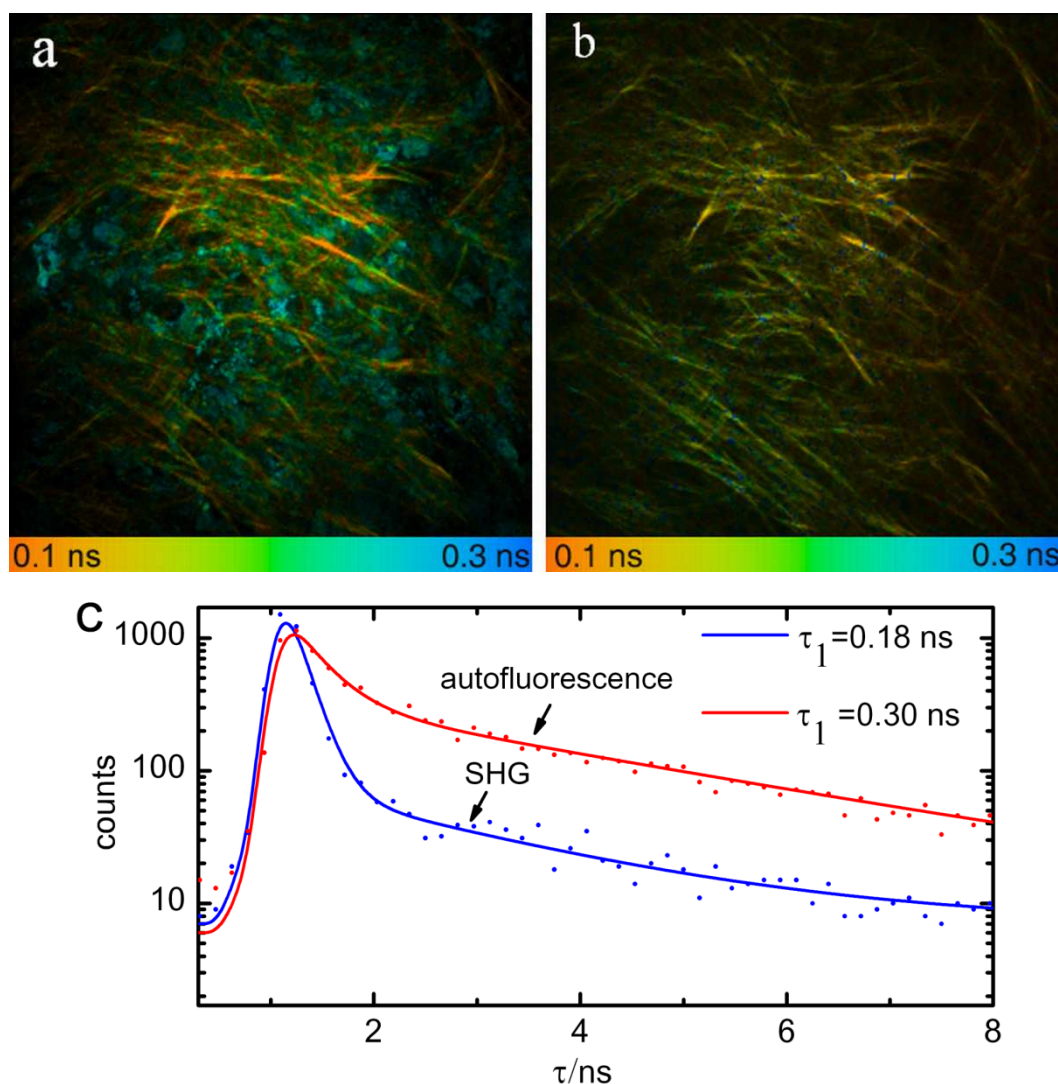


Fig. 3.23: False-color coded FLIM images from cells 4 weeks after onset of differentiation.

- Autofluorescence and SHG detection in the spectral range of 400-610 nm (870 nm excitation). Fluorescence (blue, green) arises mainly from cells, SHG (red, yellow) from collagen structures.
- The signal is dominated by SHG of collagen when using a bandpass 435/5 filter.
- Luminescence lifetime measurements of a fluorescent cellular organelle (red curve) and from a collagen structure (blue curve).

In addition, SHG radiation was detected after 3 weeks of osteogenic differentiation from pancreatic, salivary gland, and bone marrow mesenchymal stem cells.

Samples were stained for identification of the collagen type by immunocytochemistry. As demonstrated in Fig. 3.24, human mesenchymal stem cells produced collagen I as a result of osteogenic differentiation, whereas rat pancreatic cells biosynthesized collagen II after chondrogenic differentiation.

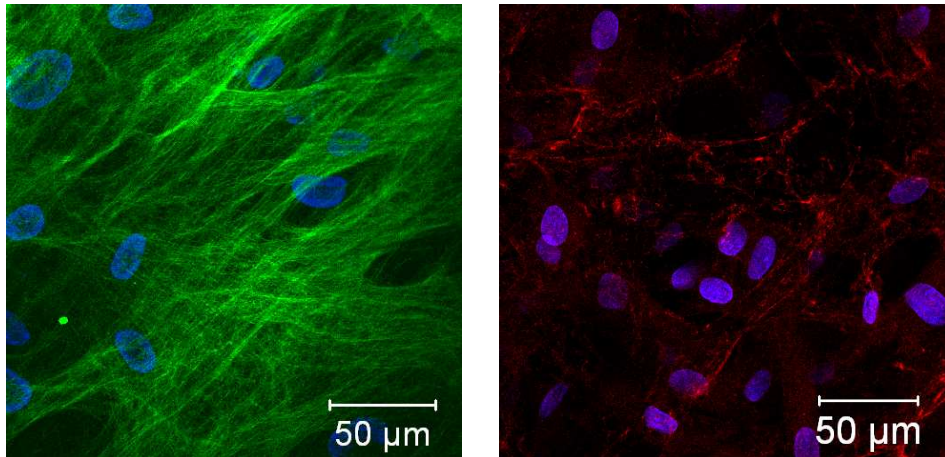


Fig. 3.24: Immunocytochemistry. Left: Mesenchymal stem cells produced collagen I after 3 weeks of osteogenic differentiation. Right: Rat pancreatic stem cell produced collagen II after 3 weeks of chondrogenic differentiation.

3.2.5. Two-photon imaging of lysosomes

Cells can accumulate non-degradable end products within lysosomal compartments when passaged and incubated for a long time. Within this work two-photon autofluorescence imaging was used to probe if the lysosomal compartments become visible. Interestingly, lysosomes in many of the investigated stem cells exhibited a bright autofluorescence after a variety of passages. Spectral imaging has shown that they fluoresce in the green-yellow spectral range. Usually the compartments are rounded (distinguishable from mitochondria) and have a more intense fluorescence (Fig. 3.25). In contrast to the NAD(P)H fluorescence in mitochondria, lysosomal autofluorescence can be excited efficiently in the spectral range from 750 nm to 900 nm.

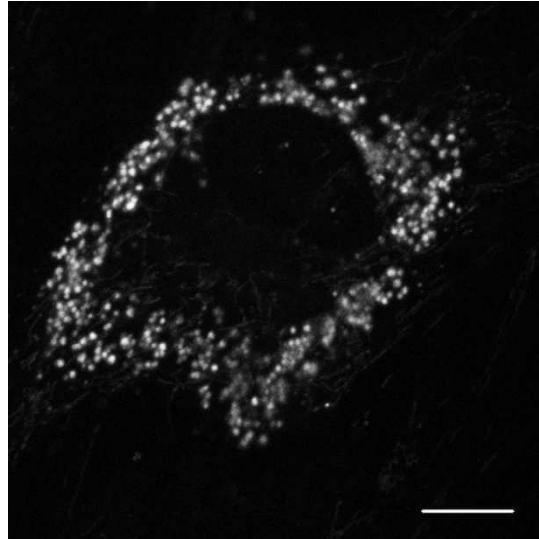


Fig. 3.25: Older stem cells exhibit a strong autofluorescence due to the presence of lysosomes. Note the weaker autofluorescence of the mitochondria (scale bar: 10 μm).

Fig. 3.26 shows two-photon excited cells labeled with the lysosome probe *Lysotracker* in comparison with the *MitoTracker* probe to detect mitochondria, and DAPI to image the nucleus.

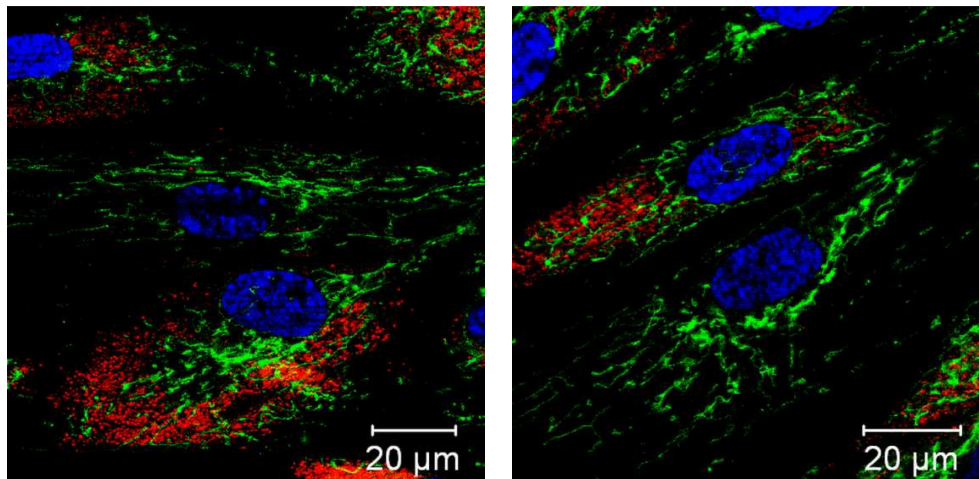


Fig. 3.26: Lysosomes (red), mitochondria (green) and nuclei (blue) of 2 weeks old stem cells.

3.3. Nanoprocessing

Within this chapter, the use of femtosecond laser scanning microscopes for both high-resolution non-destructive imaging and highly-destructive nanoprocessing without any collateral side effects was studied. In particular, the question was answered if the laser beam can be used to optically knock-out cells of no interest and to keep the cells of interest alive.

3.3.1. Nanosurgery of single cell in cell monolayers

The sub-20 fs as well as the 250 fs laser scanning microscopes were able to perform nanoprocessing by single point illumination (drilling) and cutting (line scanning) at mean powers in the milliwatt range and short exposure times. However, the use of sub-20 fs laser pulses required significant less power compared to the long 250 fs laser pulses.

In the beginning, nanoprocessing experiments by single point illumination of the perinuclear as well as the nuclear region of single cells in a monolayer have been performed. Typically, pulse energy of 2.6 nJ and 10 μ s irradiation time were chosen to expose a target cell when using 250 fs laser pulses. The destructive effect was assessed by probing the membrane integrity using the fluorescent marker Ethidium bromide. This DNA-binding dye cannot penetrate across the intact cell membrane and therefore stains cells after membrane damage only. Fig. 3.27 shows fluorescence images before and after exposure of a particular single rat pancreatic stem cell in a monolayer.

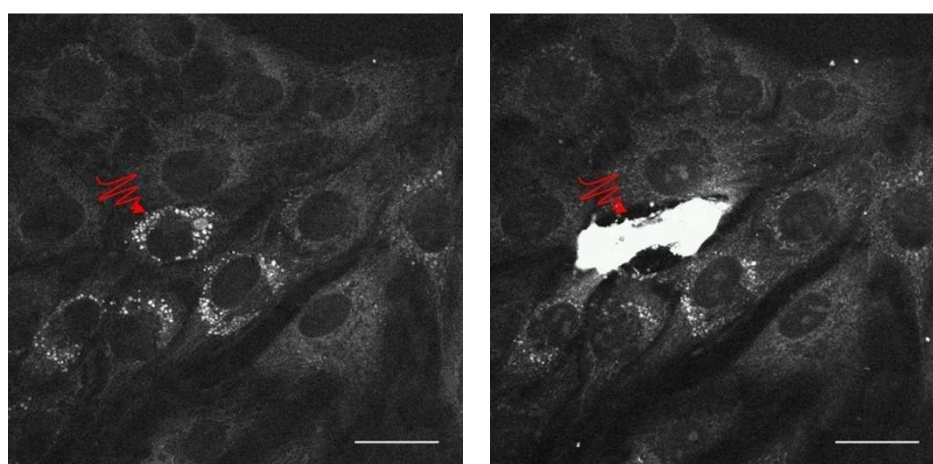


Fig. 3.27: Two-photon fluorescence of rat pancreatic stem cells before (left) and after single point illumination of one particular cell (arrow). The laser-exposed cell died and took up the dead-cell indicator Ethidium bromide (scale bar: 30 μ m).

Ethidium bromide was administered after laser exposure. The image (Fig. 3.27, left) taken before intense light exposure demonstrates the two-photon excited autofluorescence. The nuclei appeared dark. Four cells show a brighter luminescence than the surrounding cells. One bright cell (arrow) was chosen for the optical knock-out experiment. As seen in the figure taken 10 min after the intense single point illumination, Ethidium bromide accumulated in high concentration in the laser-exposed shrunken cell. The cell did not survive due to the laser exposure. In contrast, neighbour cells remained intact. Some of them demonstrated a very weak nuclear fluorescence.

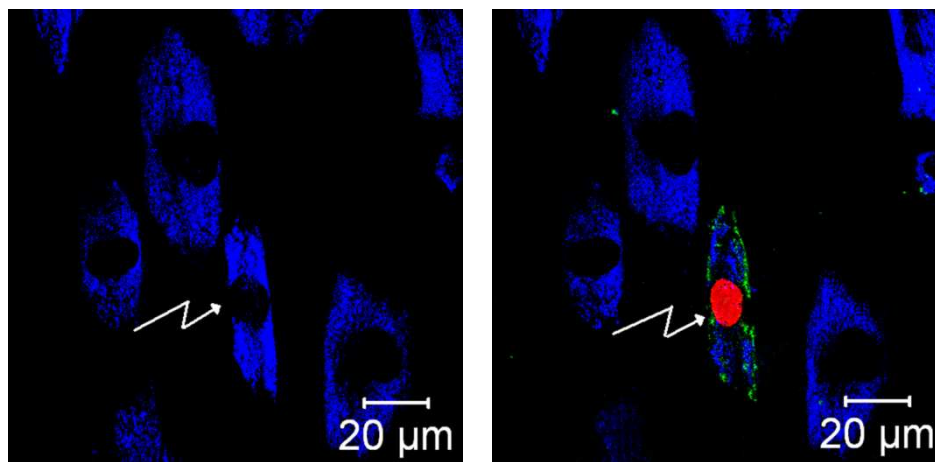


Fig. 3.28: Two-photon excited fluorescence of human mesenchymal stem cells before (left) and 1 min after intense single-point illumination of a particular cell (right, arrow) and administration of a fluorescent annexin probe (green) and Ethidium bromide (red). As a result of laser exposure, Phosphatidil-serine translocated to the outer leaflet of the membrane and bound to extracellular annexin V (Uchugonova *et al.* 2008c).

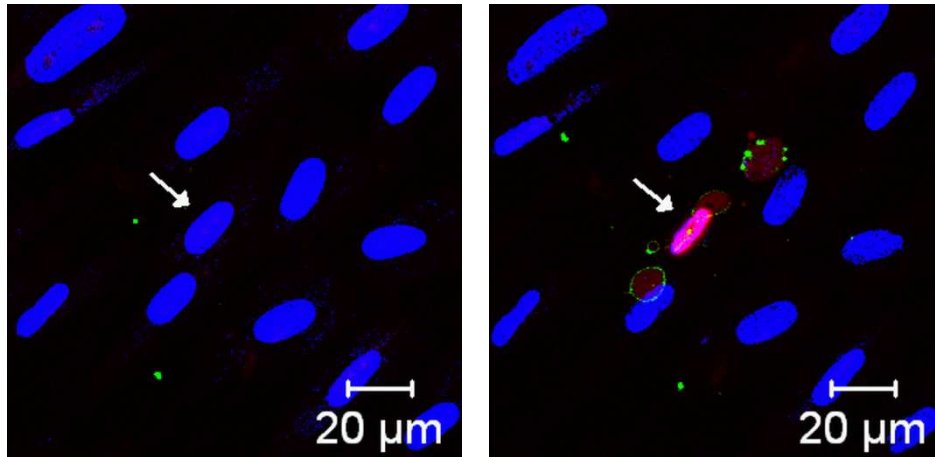


Fig. 3.29: Fluorescence images of human mesenchymal stem cells incubated with the DNA marker Hoechst (blue), the annexin probe (green) and Ethidium bromide (red) before (left) and 15 min after laser exposure. Only the cell which was exposed to high-power laser radiation emitted fluorescence from the dead-cell indicator Ethidium bromide and the annexin V probe. The laser-exposed cell was clearly fragmented.

Optically destroyed single cells were positive for ROS detection by carboxy- H_2DCFDA . If the laser power was not too high, surrounding cells survived and did not show any signs of ROS attack, membrane damage, nor modifications of their morphology. Also the probe for extracellular annexin V was found to be positive for the single laser-exposed cell in contrast to the surrounding cells (Fig. 3.28). During exposure, the morphology changed and microblebs occurred. Often fragmentations of the exposed cells were detected (Fig. 3.29).

Interestingly, also significant changes in the cellular autofluorescence occurred. Fig. 3.30 shows an example of the two-photon excited autofluorescence of stem cells before intense single point laser exposure with 12 fs laser pulses to one of these cells (left). The autofluorescence image taken after this procedure revealed a strong increase and a modified fluorescence pattern of the laser-exposed cell (right). Very likely, defects of internal membranes including the nuclear membrane occurred which resulted in the diffusion of (mitochondrial) NAD(P)H into the nucleus and the cytoplasm. In contrast, the autofluorescence of the surrounding cells did not change significantly.

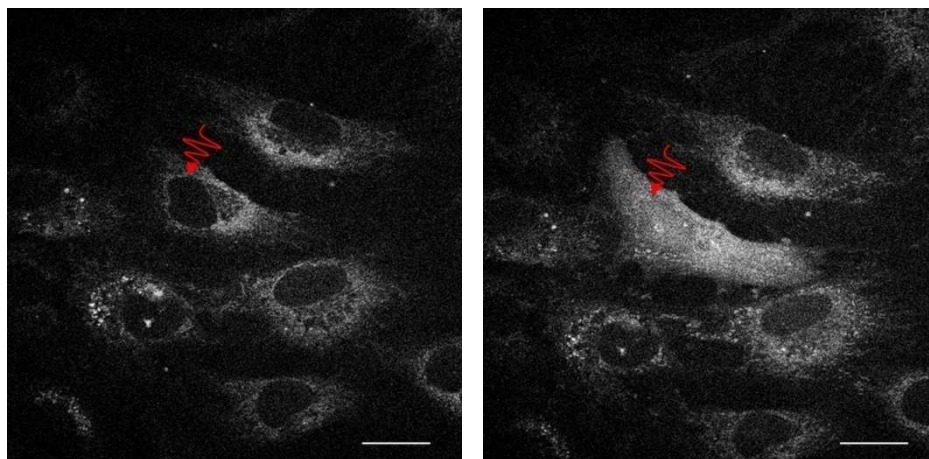


Fig. 3.30: Autofluorescence before and after single point illumination of human pancreatic stem cells. Right: The nucleus of the laser treated cell (7 mW, 12 fs pulse width, 0.5 s, single point illumination) became fluorescent likely due to the diffusion of NAD(P)H through laser-induced nuclear nanopores (scale bar: 30 μm).

Extremely precise cuts within the cytoplasm and the nucleus could be performed with low average powers as low as 7 mW when using 12 fs laser pulses. We observed by video-taping the formation of some small microbubbles with a lifetime of less than 2 seconds. The increase of the power up to 20 mW resulted in more destructive effects mainly induced by 1-3 bubbles with size up to 5 μm . The most efficient way to destroy a single cell of interest was scanning of the whole cell for few seconds (Fig. 3.31).

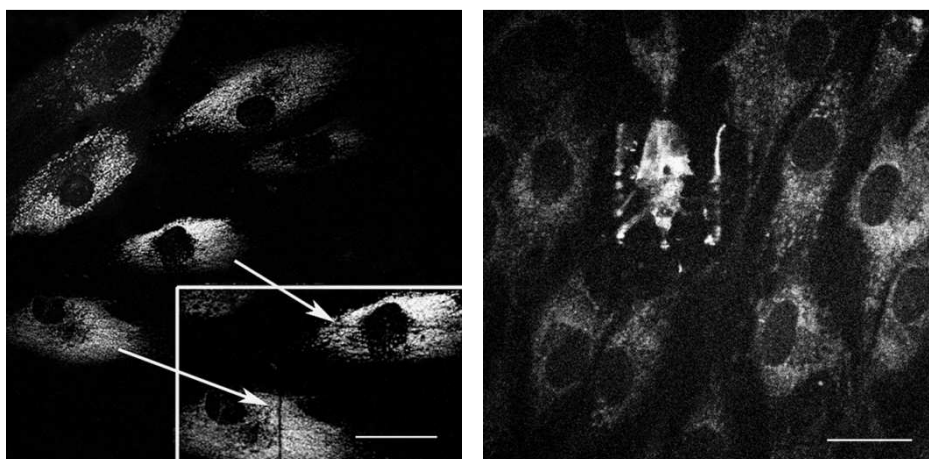


Fig. 3.31: Line scans with low powers down to 7 mW (12 fs laser pulses) produced tiny nanocuts (left image, arrows). Scanning of a whole cell within a cell monolayer destroyed the laser-exposed cell without collateral effects (right image) (scale bar: 30 μm).

3.3.2. Optical knock out of single cells in stem cell spheroids/clusters

To expose single cells inside the stem cell spheroids, at first three-dimensional two-photon autofluorescence images were obtained in z-stacks (0-60 μm) and z-intervals of 1-5 μm . Optical destruction was performed by single point illumination of a single cell of interest within the spheroids. Typically, the target cell was at the depth of about 20 μm within the cell cluster. In particular, one cell was exposed with high pulse energy of 2.6 nJ and an exposure time of 10 ms. Fig. 3.32 demonstrates the successful optical destruction of the laser-exposed cell without any damage to the neighbouring cells. The laser-exposed cell took up the dead-cell indicator Ethidium bromide and appeared as very bright fluorescent single cell at the depth of 20 μm .

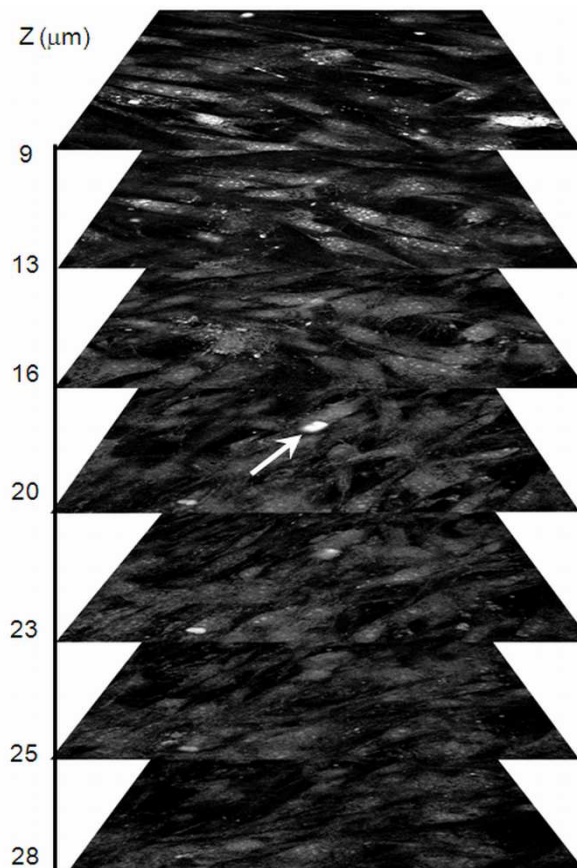


Fig. 3.32: Detection of the membrane integrity and cell viability probed by Ethidium bromide within a human pancreatic stem cell spheroid. One particular cell at a depth of 20 μm was exposed with an intense beam (2.6 nJ) by single-point illumination. The stack of two-photon images was taken within 1 minute after this laser procedure. Ethidium bromide stained this particular cell only.

Also the TUNEL assay was performed in the laser-exposed stem cell cluster in order to obtain information of the damaged condition of the surrounding non-exposed cells. No signs of DNA strand breaks were found in non-exposed neighbour cells.

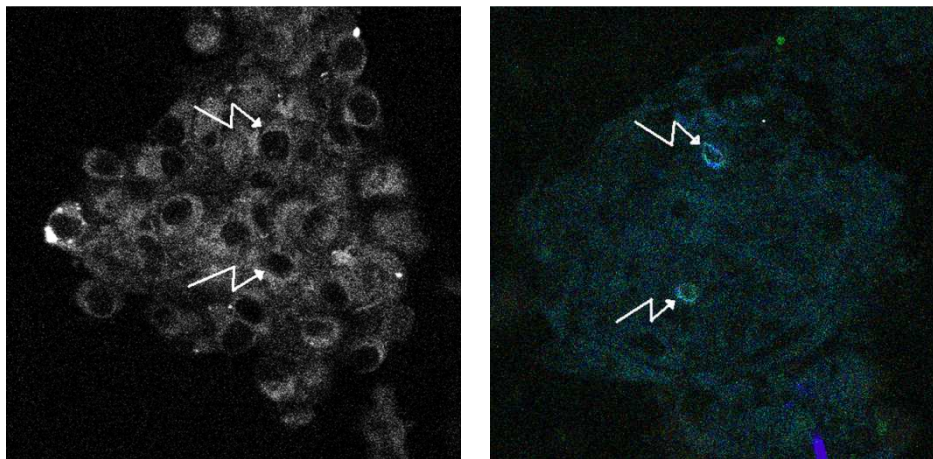


Fig. 3.33: Fluorescence image before (left) and after (right) destructive illumination of two intraspheroidal human pancreatic stem cells with intense laser pulses. The laser-exposed cells became highly fluorescent.

Interestingly, the laser exposure by intense single point illumination resulted in modifications of the luminescence property in the cell. Besides the two-photon autofluorescence due to NAD(P)H and flavins, a laser-induced autofluorescent product was detected (Fig. 3.33). In principle, the optical destruction of particular cells can be traced by two-photon autofluorescence imaging without any exogenous markers.

The method of selective optical destruction of a cell of interest can be described as optical knock out (Uchugonova *et al.* 2008c).

The method of optical knock out was used to demonstrate the possibility of “optical cleaning” of cell cultures. Stem cell cultures were cleaned in such a way that a particular cell of interest remained alive while the surrounding cells obtained a lethal laser exposure.

To isolate single cells of interest, most of the surrounding cells within a $0.7 \times 0.7 \text{ mm}^2$ area were exposed with 200 mW average power and ROI scanning. Significant changes of the morphology and the autofluorescence pattern of the laser exposed cells were monitored. The non-exposed cell of interest remained intact and was monitored over several days. A normal division of the isolated single living cell was detected as well as the migration of new cells to the laser-exposed area (Fig. 3.34).

A detailed description of these studies can be found in appendix B.

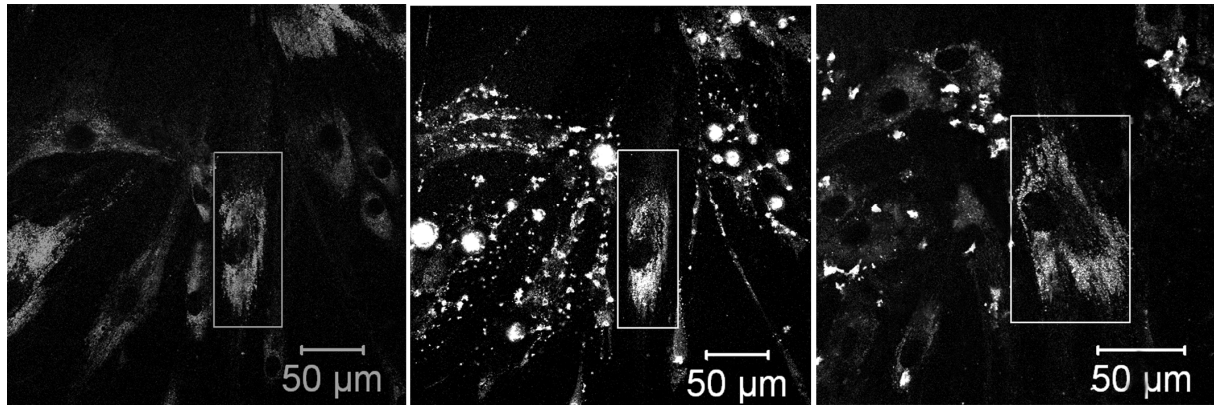


Fig. 3.34: Optical cleaning of stem cell cultures. One particular cell was kept alive whereas the surrounding cells were optically destroyed (left: autofluorescence image before intense ROI scanning, middle: autofluorescence 1 min after exposure). The non-exposed cell survived and started cell division (right).

3.4. Optical transfection of stem cells

Within this chapter, the possibility of a contact-free, chemical-free, gentle optical method was probed to realize targeted transfection of single stem cells without any lethal effect. Of high interest was the question if it would be possible to transfect with ultrashort laser pulses of extremely low picojoule pulse energy and low mean milliwatt laser power, respectively. For that purpose, a microscope with the world shortest laser pulse width in the focal plane of just 12 femtosecond was employed.

3.4.1. Optoinjection of fluorescent molecules

A particular stem cell was chosen by the video-detection of transmitted light as well as by two-photon autofluorescence which exactly confines the focal plane. Then, the laser beam was “parked” at the cellular membrane and the mean power was increased. Single point illumination was performed when opening the shutter for 50 ms which corresponds to 3.75 million pulses. In order to prove successful optoporation, Ethidium bromide was given to the medium in different experiments immediately as well as 2 min, 5 min, 10 min, 20 min, and 30 min after laser exposure. Interestingly, a low mean average power of 5 mW (66 pJ) was sufficient to provide a transient hole into the membrane as proven by the diffusion of the probe into the cell and into the nucleus. Fig. 3.35 shows two-photon images of two

optoporated cells after introduction of the membrane-impermeable fluorophore. When increasing the power to values higher than (14 ± 2) mW, the formation of microbubbles with a diameter of more than $5\ \mu\text{m}$ were observed. Often these cells changed their morphology and finally died.

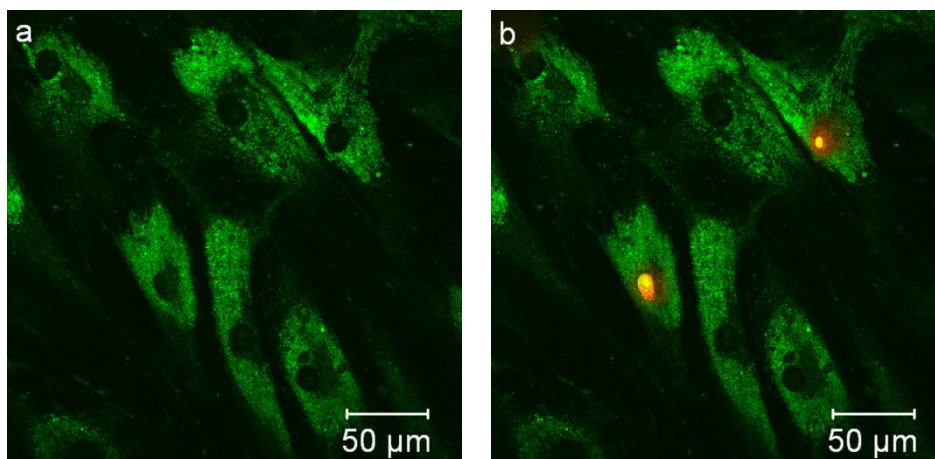


Fig. 3.35: (a) Two-photon autofluorescence image of human salivary gland stem cells. The major endogenous fluorophore is the reduced coenzyme NADH. (b) Cell fluorescence after optoporation of two cells and the application of Ethidium bromide. Non-exposed cells did not uptake the fluorescent probe.

3.4.2. Targeted transfection

After the determination of the optimal laser parameters such as 5-7 mW average power and 50-100 ms exposure time for optoporation of stem cells, transfection was performed with the DNA plasmid vector pEGFP-N1 from Clontech (4.7 kb, molar weight 3 MDa). The plasmid was injected into the extracellular 0.5 ml medium of GFP-MiniCeM cell chambers with a grid at the glass bottom. After laser exposure, the chambers were transferred to an incubator and maintained at 37°C in a 5% CO_2 humidified atmosphere for up to 8 days (appendix C). The laser-exposed stem cells and their surrounding cells were tracked by phase contrast microscopy and fluorescence imaging. In addition, spectral analysis was performed.

The formation of green fluorescent proteins with an emission maximum at 507 nm was first monitored for some cells 24 hours after exposure. When monitoring 48 hours later, all of the successfully transfected stem cells exhibited green fluorescence. Interestingly, all laser-exposed cells survived.

Results 3

Some transfected cells underwent cell division after 48 – 72 hours. The daughter cells exhibited also green fluorescence. Fig. 3.36 shows green fluorescent human salivary gland cells. The protein fluorescence indicates the successful GFP biosynthesis after introduction of the plasmid into the cytoplasm through the nanopore and the uptake into the cellular DNA as well as the reproduction of laser-exposed cells.

When calculating the number of green fluorescent cells to the number of exposed cells, a transfection efficiency of 70-80% was obtained for hPSC and hSGSC. Fig. 3.37 indicates an emission spectrum with a maximum at 510 nm for the transfected cell with the biosynthesis of GFP.

A more detailed description of this work on laser transfection can be found in appendix C.

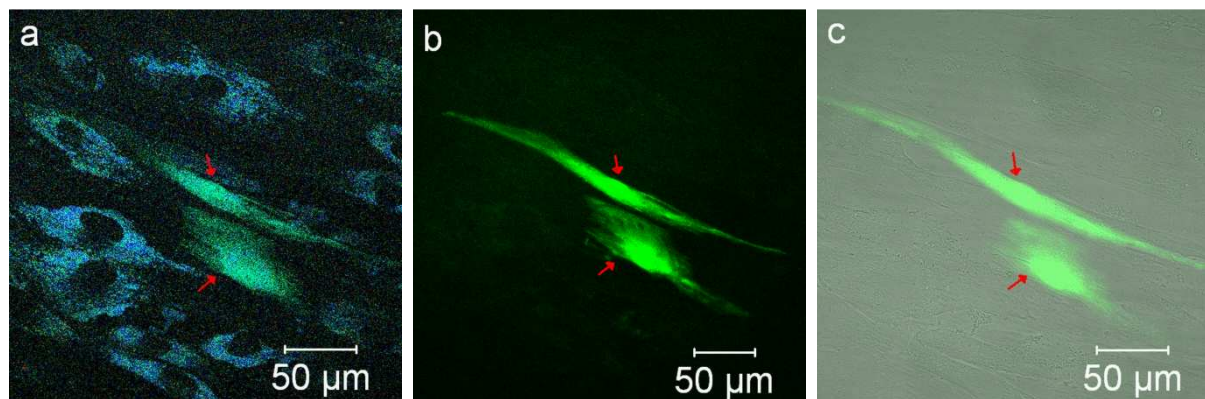


Fig. 3.36: Two-green fluorescent daughter cells 3 days after laser optoporation of a single human salivary gland stem cell. (a) Fluorescence image taken with a short pass filter 610 and an excitation wavelength of 750 nm. Both the natural autofluorescence as well as the GFP fluorescence are depicted. (b) The use of the GFP bandpass filter in combination with an excitation wavelength of 800 nm results mainly in the green fluorescence. (c) Overlay of the green fluorescence with the transmission image.

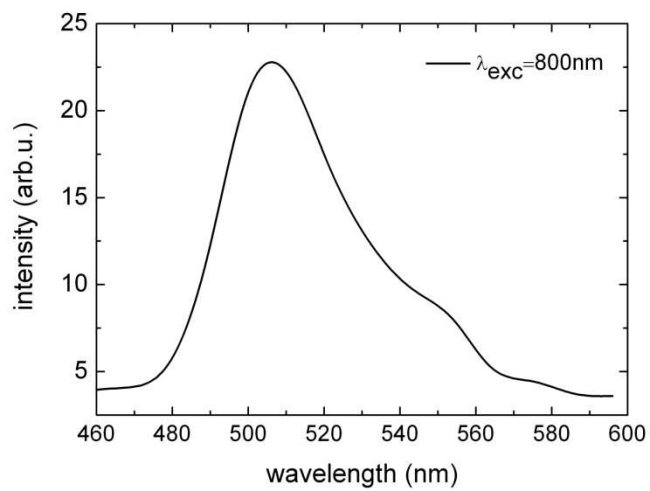


Fig. 3.37: Typical spectrum of intracellular GFP within transfected stem cells.

4. DISCUSSION AND CONCLUSION

In cell biology, especially in stem cell research, it is important to study and analyze living cells without significant input on metabolism, reproduction, and viability. Taking advantage of the marker-free multiphoton microscopy technique, the stem cells can be imaged over long periods of time without any collateral destructive effects. In this dissertation, stem cells and their development into specialized cells have been studied up to 5 weeks after introduction of a differentiation-stimulated medium. The cells and their extracellular microenvironment inside spheroids were investigated in three dimensions. Within one high-resolution optical section, approximately 15-20 cells were imaged in an area of $0.3 \times 0.3 \text{ mm}^2$. For a single optical section (512x512 pixel image), the laser beam dwell time was about (1.6-25.6) μs . This low beam dwell time and the low picojoule pulse energy prevented any damage to the cells under investigation. By autofluorescence/SHG imaging, the redox-state coenzymes NAD(P)H and flavin/flavoproteins as well as the structural protein collagen have been detected. An appropriate wavelength range to image stem cells was found to be 750–760 nm where the intramitochondrial endogenous fluorescent coenzymes can be imaged (see chapter 3.2). Radiation at 890-900 nm was preferred when imaging flavin/flavoproteins only. For collagen detection, a long wavelength such as 870 nm was employed. These near infrared wavelengths are safe due to the absence of significant absorbers. If the intensity reaches around $1 \text{ GW}/\text{cm}^2$, absorption starts by a two-photon excitation process. However, this high intensity occurs only for about 250 femtoseconds (or shorter) in a tiny sub-femtoliter excitation volume followed by a 48,000 times longer dark period of time of 12 ns (80 MHz pulse repetition frequency). The laser beam “parks” on a pixel for just some microseconds. As demonstrated in a variety of biosafety studies including the detection of DNA breaks, ROS formation, and the onset of apoptosis, stem cells can be scanned with intense 250 femtosecond laser pulses at average powers below 7 mW and typical μs beam dwell times per pixel without destructive effects. However, when applying the same average power for sub-20 fs laser pulses, irreversible cell damage occurred (Uchugonova *et al.* 2008a).

Discussion and Conclusion 4

The safe near infrared window for non-destructive stem cell imaging depends therefore mainly on the average power (intensity) and the pulse width. For the case of the sub-20 fs pulses an average power in the μW range was employed.

König *et al.* (1999a) reported on cell damage studies based on the exposure of Chinese hamster ovary cells (CHO), a worldwide used easy to handle cell type with 12 hours cell doubling intervals, with 170 fs – 2.2 ps laser pulses. A strong dependence of cell damage on pulse width was demonstrated. The authors laser-exposed thousands of single CHO cells and determined the cell cloning efficiency by monitoring the reproduction behavior and studying the morphology and autofluorescence of the daughter cells and further generations. First destructive effects with 250 fs were found at a mean power of 6 mW when applying 10 consecutive scans at 16 seconds per frame (König *et al.* 1999a). According to the results within this work, the investigated human and animal adult stem cells were found to be less sensitive to femtosecond NIR laser pulses than CHO cells. Very likely, stem cells are less sensitive to UV and NIR photostress than other cell lines due to their ability of efficient self-repair.

The stem cells can be scanned many times without any significant changes using near infrared light. Stem cell spheroids were scanned typically three times weekly when performing studies for up to 5 weeks. Optical sections were obtained in typical z-steps of 5 μm down to a total depth of 200 μm . A superior submicron spatial resolution enabled the imaging of single intracellular mitochondria. Mitochondria were found to be the brightest fluorescent structures and were imaged in all cells. During imaging it was observed that mitochondria had morphologically different structures and were distributed in the cytoplasm or formed aggregates in the perinuclear region. Researchers have shown that the morphological heterogeneity of mitochondria and their distribution reflects changes in the metabolic state of the cells. Aggregation of mitochondria in the perinuclear region has been detected in cancer cells (Hallmann *et al.* 2004) and as a result of the treatment with microtubule-active drugs (Kedzior *et al.* 2004). Sicter *et al.* (2005) have demonstrated that the mitochondrial distribution can change when the medium, substrates, or the ambient CO_2 conditions altered. Some authors showed that the perinuclear arrangement of mitochondria can be correlated with the function in certain somatic cells e.g. neurons and pancreatic cells (Johnson *et al.* 2003). There is a hypothesis that stem cells may retain the perinuclear arrangement of mitochondria, whereas an alteration of this pattern occurs during differentiation (Sicter *et al.* 2005; Lonergan

et al. 2006). In particular, an aggregated mitochondrial distribution pattern was found to be related to differentiation (Yaffe 2003; Lonergan *et al.* 2006).

Within this work, mitochondria have been studied by monitoring the changes in two-photon autofluorescence. Moreover, biochemical information can be gained by FLIM and emission spectroscopy techniques.

The major native fluorophore located in the mitochondria is NAD(P)H in free and bound form. Interestingly, the reduced form only emits visible light. The oxidized form NAD⁺ does not fluoresce in the visible spectral range. Spectral measurement and fluorescence lifetime measurements proved the existence of NAD(P)H and flavins in mitochondria when excited at 750 nm. NAD(P)H from within the cytoplasm has a lower quantum yield as in the mitochondria. Within the nucleus, NAD(P)H is present in very low concentrations only (Li *et al.* 2008). The emission maximum of free NAD(P)H is around 470 nm whereas the maximum is blue-shifted (440 nm) when binding to proteins occurs (König and Schneckenburger 1994). As demonstrated in this work, the human stem cells have a more intense autofluorescence than the animal stem cells. The autofluorescence intensity varied significantly among the cells from the same culture dish and within the same optical section which reflects the heterogeneity of the cell population. In future work the highly autofluorescent cells should be investigated by single cell immunocytochemistry.

Two major fluorophores could be identified based on time-resolved single photon counting and the calculation of fluorescence lifetimes as well as by spectral imaging. The detected two-photon autofluorescence with emission maxima at 460-490 nm and 530-535 nm and the long fluorescence lifetimes of 1.8 ns and 2.0 ns, respectively, appears to indicate the presence of the biomolecules NAD(P)H and flavins/flavoproteins.

Interestingly, the analysis of the short-lived component of human salivary gland stem cells was found to be very complex. Some cells exhibited only one short-lived fluorophore with a fluorescence lifetime of about 0.2 ns only (excellent bi-exponential fit with χ^2 of 1.00), whereas the majority of cells revealed an additional short-lived component with 0.7 ns fluorescence lifetime.

The interpretation of these two short-lived fluorophores is complicated. Free NAD(P)H has a short lifetime around 0.2-0.3 ns whereas a variety of flavoproteins have short picosecond lifetimes. The free flavin mononucleotide (FMN) has a typical lifetime of 4.7 ns - 5.2 ns (König and Schneckenburger 1994; Lakowicz 1999) while flavin adenine dinucleotide (FAD) has a lifetime of 2.3 ns – 2.8 ns (Lakowicz 1999; Skala *et al.* 2007; Russels *et al.* 2008).

Discussion and Conclusion 4

When binding to a variety of proteins, the fluorescence lifetime of NAD(P)H in a variety of cells and solutions shifts to higher values of about 2 ns (König and Schneckenburger 1994). Chia *et al.* (2008) reported on the presence of three NAD(P)H fluorophores in rat brain tissue: a very short one of 0.48 ns for the free (non-bound) coenzyme, a second short one of 0.77 ns and a long lifetime of 3 – 6 ns for bound NAD(P)H. When studying adipogenic differentiation in this work, a blue shifted autofluorescence spectrum and a decrease of the concentration of fluorescent flavins/flavoproteins were monitored during differentiation. The findings of Reyes *et al.* (2006) in the case of human mesenchymal stem cells during osteogenic differentiation are in agreement with the results of this work. They used a confocal microscope to detect the decrease of flavins/flavoproteins and of the ratio NAD(P)H/FAD during differentiation. Rice *et al.* (2007) reported also on a decrease of fluorescent flavins during the differentiation process of mesenchymal stem cells by measuring the mean of the fluorescence. On the contrary, Monici *et al.* (2002) showed for the case of differentiated leukemic cells that the bound form NAD(P)H shifted to the free form and that the concentration of fluorescent flavins increased. It would be of interest to study in the future autofluorescence modifications during differentiation in dependence on the stem cell type.

When studying adipogenic differentiation by means of FLIM within this work, the fluorescence lifetime of adipocytes was found to be increasing. A similar behavior was found by Guo *et al.* (2008) when studying osteogenic differentiation. Squirrell *et al.* (2008) studied embryonic stem cells and reported also on an increase of the fluorescence lifetime during differentiation.

Tab. 4.1 summarizes the 5D results of this work (intensity, FLIM, spectral imaging) regarding the autofluorescence behavior of stem cells and cells under adipogenic differentiation. During differentiation, the blue-shift of the emission maximum indicates the relative increase of bound NAD(P)H and an increase of the ratio bound NAD(P)H to free NAD(P)H, respectively. Monici *et al.* (2002) reported on lower bound NAD(P)H/free NAD(P)H ratio in anaerobic cells than aerobic cells. This is also confirmed by a relative increase of the long fluorescence lifetime component τ_2 which reflects bound NAD(P)H and an increase of the ratio of the amplitudes a_2/a_1 , respectively. Because there is an overall decrease of the fluorescence intensity during differentiation, the concentration of the reduced form NAD(P)H must drop compared to the oxidized form NAD(P)H. That means the oxygen consumption increases. This hypothesis is in accordance with data of Guo *et al.* (2008) who claim a decrease of NAD(P)H/NAD⁺ means an increased metabolism. The data in this work show also a decrease

of flavin fluorescence during adipogenic differentiation. Both, NAD(P)H fluorescence and flavin fluorescence dropped, however, the ratio NAD(P)H/flavins increased.

However, Reyes *et al.* reported in the same year on the decrease of this ratio for stem cells during osteogenic differentiation. Further studies on a variety of stem cells under different types of differentiation are required to figure out the exact metabolism during the differentiation process.

Tab. 4.1: Autofluorescence modifications of stem cells and cells after adipogenic differentiation measured by multiphoton spectral and fluorescence lifetime imaging within this work

Cells	NAD(P)H fluorescence intensity	Fluorescence maximum	Flavin fluorescence intensity	NAD(P)H/flavin	Fluorescence lifetime	Bound NAD(P)H/Free NAD(P)H
Stem cells	high	493 nm	high	low	short 0.22 /2.00 ns	low $a_2/a_1=0.28$
Diff. cells	low	blue shifted 460 nm	low	high	long 0.26/2.33 ns	high $a_2/a_1=0.50$

Future work needs to be done for the interpretation of the cellular FLIM data and the spectra with regard to the specific cellular metabolism and differentiation value. For that purpose, the particular imaged cell of interest should be also characterized with selective biochemical means such as antibody staining of the cell as well as the surrounding cells.

The bright fluorescent granules observed in older stem cell populations have been found to be lysosomes. This supports the hypothesis of the accumulation of lipopigments in stem cells. Lipopigments are characterized by a yellowish fluorescence. Crose *et al.* (1999) showed an increase of the fluorescence signal from lysosomes when the number of passages increased. The measurement of the fluorescence intensity and pattern of lysosomes in stem cells may therefore provide information on the ageing process.

Very interestingly, SHG can be used to detect the biosynthesis of collagen as a result of the differentiation process (Lee *et al.* 2006; Uchugonova *et al.* 2008d; Uchugonova and König 2008). Within this work, long-term studies of up to 35 days on 3D stem cell spheroids have been performed.

Discussion and Conclusion 4

The expression of the extracellular matrix protein has been successfully monitored. The possibility of non-destructive marker-free imaging allows the study of the organization and development of the ECM structure and of feedback mechanisms. Recently it was shown that human embryonic stem cell cultured on type IV collagen induces vascular cell differentiation (Gerecht-Nir *et al.* 2003; Schenke-Layland *et al.* 2007).

State of the art two-photon fluorescence imaging is performed with pulses of 200-300 fs or even around 1 ps pulse width depending on the two-photon microscope manufacturer. The signal in two-photon microscopy depends on a P^2/τ relation with power P and pulse width τ . Because of this relation, picosecond laser microscopes require just a relatively small increase in laser power to obtain similar images as for femtosecond laser microscopes, e.g. 1 ps systems require three times higher laser power than 110 fs systems.

However, in the case of nanoprocessing based on multiphoton ionisation processes where several photons are involved (e.g. 5 NIR photons and 6.5 eV, respectively, are required to induce an optical breakdown in water (Venugopalan *et al.* 2002; Vogel and Venugopalan 2003)), the shortening of the laser pulse width would significantly improve the desired destructive effect. The non-distorted delivery of sub-15 fs through a microscope objective and even sub-10 fs pulses by compensation of quadratic and cubic dispersion terms has been demonstrated and employed so far for nonlinear imaging (Larson and Yeh 2006; Tempea *et al.* 2007).

As shown in this work, sub-20 fs laser scanning microscopes can be realized and employed for nanoinjection and optical transfection of human stem cells. Interestingly, low mean powers of 5–7 mW (66-93 pJ @ 75 MHz), which is more than one order less power as in current femtosecond laser nanoprocessing tools, were sufficient to realize transient high TW/cm^2 intensities and successful stem cell manipulation. The use of a sub-10 mW power guarantees also the absence of any destructive thermal effects and disturbing trapping effects. The potential use of low power systems may open also the chance for the manufacturing of miniaturized sub-20 fs laser systems for nanoprocessing and imaging without bulky expensive pump lasers.

Within this work, multiphoton ionisation at transient TW/cm^2 intensities was also used for “optical cleaning” of the cell cluster. For example, optical inactivation of a single target cell within the spheroid without collateral side effects to neighbour cells was realized. Also neighbour cells can be optically destroyed while keeping a cell of interest alive.

The novel method provides the possibility to control the development of stem cells in three dimensions, to destroy undesired cells and to isolate stem cells of interest.

A transient nanohole could be created by optoporation where the destructive highly focused laser beam was “parked” on the cellular membrane by single point illumination for about 50 ms. The membrane stayed open for few seconds before self-repair processes occurred. During this short time interval extracellular chemicals such as GFP plasmids can be passively introduced to the cytoplasm. In order to transfer the plasmid to the nuclear region, a further single point illumination of the nuclear membrane could be performed. However, more easily is just to wait until replication (mitosis) where the nuclear membrane became disintegrated. At that time the GFP plasmid can be incorporated in the cell’s DNA. Therefore it takes some days to verify the successful targeted transfection of stem cells by the onset of the green fluorescence.

When using extremely short laser pulses, high transfection efficiencies were realized. All laser-exposed cells survived and 3 out of 4 treated human stem cells have been transfected. The cells exhibited normal reproduction behaviour (cell division after 2-3 days) and the daughter cells became also green fluorescent. The human stem cells used for these preliminary experiments were obtained from a human pancreas and submandibular glands. They possess a remarkable potential for self-renewal and multilineage differentiation including the development into specialized cells of all three germ layers (Kruse *et al.* 2004; Kruse *et al.* 2006). So far, no other transfection studies have been conducted with these new types of stem cell sources.

One major reason for the very efficient transfection with sub-20 fs laser pulses is likely the very low mean power of less than 10 mW. Another interesting effect is the high stability of the laser beam position. The novel dispersion technology overcomes the problems of beam positioning fluctuations observed in femtosecond laser systems based on prism technology.

Transfection of stem/primary cells is a major problem in up-to-date technology based on chemical, mechanical or electrical means. Safety concerns have been raised with the application of these approaches on human (Well 2004; Newmann and Bettinger 2007; Tsen *et al.* 2009). The non-invasive gentle creation of a transient nanohole in the cellular membrane by low mean power sub-20 fs laser pulses without any collateral damage and disturbance of the self-repairing potency overcomes this problem.

Femtosecond laser manipulation of stem cells opens new ways for stem cell based gene therapy, the generation of stable cell lines, and transplantation technology. In particular, the

Discussion and Conclusion 4

induction of specific genes may improve the efficiency of controlled differentiation. Cell types of interest may be collected using specific marker genes. Tracking of stem cells derived after engraftment could be facilitated by tracer genes. Furthermore, cells can be reprogrammed by injection corrective genetic materials, so an appropriate type of cell can be created to develop replacement tissues.

5. OUTLOOK/FUTURE DIRECTIONS

Investigations on various aspects of stem cells became an important aspect in scientific research, particularly in the area of tissue engineering, biotechnology, pharmacy, and therapy. Stem cells are currently in a stage from “bench to bedside” in the area of myocardial infarction, neurological diseases such as Alzheimer and Parkinson, diabetes, and cancer. Earlier this year the United States Food and Drug Agency (FDA) gave the permission to the Californian Company *Geron Corporation* to perform a clinical trial based on the use of human embryonic stem cells (Jaishankar and Vrana 2009). This world’s first human embryonic stem cell therapy on patients with spinal cord injuries will cause lots of interest.

There are a variety of approaches to harvest embryonic or adult stem cells as well as to reprogram cells. For example, the nucleus of a somatic cell is transferred into a denucleated egg and developed into blastocytes with pluripotent cells in the case of somatic cell nuclear transfer (SCNT). In addition, somatic cells can be reprogrammed to *induced pluripotent stem cells* (iPSC) (i) by genetic manipulation transfection methods based on viruses (Takahashi *et al.* 2007; Kaji *et al.* 2009) or (ii) by the employment of recombinant proteins (Zhou *et al.* 2009).

Major problems remain such as the lack of a well-controlled differentiation process and a method to harvest a “contamination-free” pool of well-defined specific human cells.

Current stem cell therapy is based on the employment of adult stem cells. However, the recruitment of the limited number of endogenous adult stem cells and their restricted locations is extremely difficult. Furthermore, the stem cells of the patient to be treated will also carry the genetic effect in genetically based diseases such as Alzheimer or Huntington disease.

There is a hope that the optical technologies, in particular multiphoton imaging and nanoprocessing tools, can be employed to trace and manipulate the stem cells as well as to monitor the differentiation process.

In this dissertation, the basic interaction of femtosecond laser pulses with some animal and human stem cells have been studied. Marker-free high-resolution imaging has been

demonstrated on stem cell layers and stem cell spheroids. However, future work on a large number of different animal and human adult stem cells within their native tissue environment has to be conducted to answer the question if the rare stem cells can be identified due to their characteristic autofluorescence behavior. One paper recently published discusses the prospective isolation of bronchiolar stem cells from facultative transit-amplifying cells by autofluorescence detection (Teisanu *et al.* 2009). Results from frozen tissue sections demonstrated also a different autofluorescence behavior of stem cells in the hair follicle bulge compared to the surrounding cells (Wu *et al.* 2005). Multiphoton microscopes have also been used to monitor the migration of neural stem/progenitor cells (NSCs/NPCs) in the brain of mice (Zhao *et al.* 2007). This allows us to understand how NSCs/NPCs respond to cortical brain ischemia and to distinguish migrating from non-migrating cells as well as to trace the migration direction within the brain.

In this dissertation, the first multiphoton investigations performed on stem cells show that the ratio of fluorescent flavoproteins to the fluorescent coenzyme NAD(P)H as well as the mean fluorescence lifetimes are different from typical mature laboratory cell lines. Interestingly, the autofluorescence behavior also changes during differentiation processes. It was found that certain fluorescence parameters such as the fluorescence lifetime and the emission spectrum can be used to monitor the onset of differentiation as well as the biosynthesis of chemical compounds as a unique function of a particular specialized cell type. Within this work, the cell's fabrication and transport of lipids and collagen has been monitored as a function of time after incubation with the differentiation medium. Further work is needed to answer the question as to which types of collagen can be detected using second harmonic generation (SHG) and what are the best laser excitation parameters. It would be also of interest to study the autofluorescence behavior of adult stem cells versus embryonic stem cells and to perform optical sections of embryonic stem cell bodies.

As demonstrated, multiphoton techniques such as two-photon excited autofluorescence and SHG can be employed as valuable non-destructive imaging tools to trace stem cells and to optimize the differentiation process. Current multiphoton microscopes enable the study of stem cells *in vitro*. However, first two-photon tomographs for skin imaging are in clinical use (König 2008). There is a chance to trace adult stem cells in the basal cell layer of the epidermis and along the hair shafts. In the near future, two-photon microendoscopes will be available (König *et al.* 2008) which can be employed to trace stem cells inside the body.

Interestingly, a multiphoton system can not only be used as a high-contrast and high-resolution imaging system but also as highly precise nanoprocessing tool. The successful targeted transfection has been demonstrated by means of low picojoule sub-20 femtosecond laser pulses of an ultracompact turn-key microscope (Uchugonova *et al.* 2008a-c). So far, the DNA plasmid eGFP only was introduced in human stem cells by the optical generation of a transient nanohole. In the future, it will be interesting to see the efficient way of transfecting the stem cells with a variety of more important genes.

Furthermore, the optical generation of transient nanoholes will open a novel way to deliver other different molecules and chemicals such as RNA, recombinant proteins, nanoparticles, and drugs into the living cell without destructive collateral effects. Very recently it was demonstrated that the same apparatus *FemtOgene*TM can be employed successfully to deliver superquencher molecular beacon (SQMB) probes into living cells (Földes-Papp *et al.* 2009).

A current problem of the multiphoton microscope is the limitation to a low number of transfected adherent cells within a certain time period and highly experienced personnel. Future engineering work may be of interest such as fiber-based systems automatic miniaturized high-throughput femtosecond laser systems, e.g. (Tsampaoula *et al.* 2008). It is likely that the combination of femtosecond laser systems with laser tweezers (optical trapping) enables the transfection of non-adherent and large numbers of cell populations (Baumgart *et al.* 2009). It would be also of high interest to probe if slow growing primary cells and non-dividing cells (cardiomyocytes, neurons, hepatocytes, chondrocytes) can be laser transfected by means of a second optoporation of the nuclear membrane. Moreover, transfection can be performed inside 3D structures e.g. embryonic stem cell bodies. Tsen *et al.* (2009) have recently demonstrated the potential use of femtosecond laser pulses *in vivo* DNA delivery for the skin.

In conclusion, multiphoton femtosecond laser systems will open up new opportunities in the investigation of stem cells and its application in medicine. They can provide morphological and biochemical information about stem cells in their native environment as well as can be used to manipulate the cells, the intracellular compartments, and the extracellular microenvironment in three dimensions.

6. BIBLIOGRAPHY

- Baumgart J, Bintig W, Ngezahayo A, Willenbrock S, Murua Escobar H, Ertmer W, Lubatsschowski H, Heisterkamp A (2009) Quantified femtosecond laser based opto-perforation of living cells. Proceedings of LPM2008-the 9th International Symposium on Laser Precision Microfabrication.
- Becker W (2005) Advanced time-correlated single-photon counting techniques. Springer, Berlin Heidelberg New York.
- Becker W (2008) The bh TCSPC handbook, 3rd edition. Becker & Hickl GmbH. Available on www.becker-hickl.com
- Becker AJ, McCulloch EA, Till JE (1963) Cytological demonstration of the clonal nature of spleen colonies derived from transplanted mouse marrow cells. *Nature* 197:452–4
- Bjornson C, Rietze R, Reynolds B, Magli M, Vescovi A (1999) Turning brain into blood: A hematopoietic fate adopted by adult neural stem cells *in vivo*. *Science* 283:534–537
- Bruder SP, Jaiswal N, Haynesworth SE (1997) Growth kinetics, selfrenewal, and the osteogenic potential of purified human mesenchymal stem cells during extensive subcultivation and following cryopreservation. *Journal of Cellular Biochemistry* 64:278-94
- Bugiel I, König K, Wabnitz H (1989) Investigations of cells by fluorescence laser scanning microscopy with subnanosecond time resolution. *Lasers in the Life Sciences* 3:47-53
- Camporesi S (2007) The context of embryonic development and its ethical relevance. *Biotechnology Journal* 2:1147-1153
- Case J, Horvath TL, Ballas CB, March KL, Srour EF (2008) In vitro clonal analysis of murine pluripotent stem cells isolated from skeletal muscle and adipose stromal cells. *Experimental Hematology* 36:224-234
- Cecchini M, Bumma G, Serresi M, Beltram F (2007) PC12 differentiation on biopolymer nanostructures. *Nanotechnology* 18:505103

Bibliography 6

- Chance B, Schoener B, Oshino R, Itshak F, Nakase Y (1979) Oxidation-reduction ratio studies of mitochondria in freeze-trapped samples. *Journal of Biological Chemistry* 254:4764-4771
- Chia TH, Williamson A, Spencer DD, Levene MJ (2008) Multiphoton fluorescence lifetime imaging of intrinsic fluorescence in human and rat brain tissue reveals spatially distinct NADH binding. *Optics Express* 16:4237-4249
- Chung S, Shin B-S, Hedlund E, Pruszek J, Ferree A, Kang UJ, Isacson O, Kim K-S (2006) Genetic selection of sox1GFP-expressing neural precursors removes residual tumorigenic pluripotent stem cells and attenuates tumor formation after transplantation. *Journal of Neurochemistry* 97:1467-1480
- Cox G, Moreno N, Feijo J (2005) Second harmonic imaging of plant polysaccharides. *Journal of Biomedical Optics* 10:024013
- Croce AC, Spano A, Locatelli D, Barni S, Sciola L, Bottiroli G (1999) Dependence of fibroblast autofluorescence properties on normal and transformed condition. Role of the metabolic activity. *Photochemistry and Photobiology* 69:367-374
- David R, Groebner M, Franz WM (2005) Magnetic Cell Sorting Purification of Differentiated Embryonic Stem Cells Stably Expressing Truncated Human CD4 as Surface Marker. *Stem Cells* 23:477-482
- De Coppi P, Bartsch G, Siddiqui MM, Xu T, Santos CC, Perin L, Mostoslavsky G, Serre AC, Snyder EY, Yoo JJ, Furth ME, Soker S, Atala A (2007) Isolation of amniotic stem cell lines with potential for therapy. *Nature Biotechnology* 25:100–6
- Denk W, Strickler JH, Webb WW (1990) Two-photon laser scanning fluorescence microscopy. *Science* 248:73-76
- Demos SG, Bold R, White R de Vere, Ramsamooj R (2005) Investigation of Near-Infrared autofluorescence Imaging for the detection of Breast Cancer. *IEEE Journal of Selected Topics in Quantum Electronics* 11:791-798
- Dimitrow E, Riemann I, Ehles A, Koehler J, Norgauer J, Elsner P, König K, Kaatz M (2009) Spectral fluorescence lifetime detection and selective melanin imaging by multiphoton laser tomography for melanoma diagnosis. *Experimental Dermatology* 18:509-15
- Diskinson ME, Bearman G, Tille S, Landsford R, Fraser SE (2001) Multi-spectral imaging linear unmixing add a whole new dimension to laser scanning fluorescence microscopy. *BioTechniques* 31:1272-1278

- Eglitis MA, Mezey E (1997) Hematopoietic cells differentiate into both microglia and macroglia in the brains of adult mice. *Proceedings of the National Academy of Sciences of the USA* 94:4080–4085.
- Evans MJ, Kaufman MH (1981) Establishment in culture of pluripotential cells from mouse embryos. *Nature* 292:154-156
- Friedenstein AJ, Petrakova KV, Kurolesova AI, Frolova GP (1968) Heterotopic transplants of bone marrow. Analysis of precursor cells for osteogenic and hematopoietic tissues. *Transplantation* 6:230-247
- Freund I, Deutsch M (1996) 2nd harmonic microscopy of biological tissue. *Optics Letters* 11:94-96
- Foote CS (1999) Definition of type I and type II photosensitized oxidation. *Photochemistry and Photobiology* 54:659
- Fournier LS, Lucidi V, Berejnoi K, Miller T, Demos SG, Brasch CR (2006) In-vivo NIR autofluorescence imaging of rat mammary tumors. *Optics Express* 14:6713-6723
- Földes-Papp Z, König K, Studier H, Bückle R, Breunig HG, Uchugonova A, Kostner GM (2009) Trafficking of mature miRNA into the nucleus of life liver cells. *Current Pharmaceutical Biotechnology* 10, in press
- Ge D, Liu X, Wu J, Tu Q, Shi Y, Chen H (2009) Chemical and physical stimuli induce cardiomyocyte differentiation from stem cells. *Biochemical and Biophysical Research Communications* 381:317-21
- Gimble JM, Guilak F (2003) Adipose-derived adult stem cells: isolation, characterization, and differentiation potential. *Cytotherapy* 5:362–9
- Gerecht-Nir S, Itskovitz-Eldor J (2004) Cell therapy using human embryonic stem cells. *Transplant Immunology* 12:203-209
- Gerecht-Nir S, Ziskind A, Cohan S, Itskovitz-eldor J (2003) Human embryonic stem cells as an *in vitro* model for human vascular development and the induction of vascular differentiation. *Laboratory investigation* 83:1811-1820
- Gorjup E, Danner S, Rotter N, Habermann J, Brassat U, Brummendorf T, Wien S, Meyerhans A, Wollenberger B, Kruse C, Briesen von H (2009) Glandular tissue from human pancreas and salivary gland yields similar stem cell population. *European Journal of Cell Biology* 88:409-421
- Göppert-Mayer M (1929) Über die Wahrscheinlichkeit des Zusammenwirkens zweite Lichtquanten in einem Elementarakt. *Die Naturwissenschaften* 17:932

Bibliography 6

- Gritti A, Parati EA, Cova L, Frolichsthal P, Galli R, Wanke E, Faravelli L, Morassutti DJ, Roisen F, Nickel DD, Vescovi AL (1996) Multipotential Stem Cells from the Adult Mouse Brain Proliferate and Self-Renew in Response to Basic Fibroblast Growth Factor. *Journal of Neuroscience* 16:1091-100
- Guan K, Nayernia K, Maier LS, Wagner S, Dressel R, Lee JH, Nolte J, Wolf F, Li M, Engel W, Hasenfuss G (2006) Pluripotency of spermatogonial stem cells from adult mouse testis. *Nature* 440:1199-1203
- Guo H-W, Chen C-T, Wei Y-H, Lee OK, Gukassyan V, Kao F-J, Wang H-W (2008) Reduced nicotinamid adenine dinucleotide fluorescence lifetime separates human mesenchymal stem cells from differentiated progenies. *Journal of Biomedical Optics Letters* 13:050505(1-3)
- Haleem-Smith H, Derfoul A, Okafor C, Tuli R, Olsen D, Hall DJ, Tuan RS (2005) Optimization of high-efficiency transfection of adult human mesenchymal stem cells *in vitro*. *Molecular Biotechnology* 3:09-19
- Hallmann A, Milczarek R, Lipinski M, Kossowska E, Spodnik JH, Wozniak M, Wakabayashi T, Klimek J (2004) Fast perinuclear clustering of mitochondria in oxidatively stressed human choriocarcinoma cells. *Folia Morphologica* 63:407-412
- Hamm A, Krott N, Breibach I, Blindt R, Bosserhof AK (2002) Efficient transfection method for primary cells. *Tissue Engineering* 8:1-13
- Heisterkamp A, Maxwell IZ, Mazur E, Underwood JM, Nickerson JA, Kumar S, Ingber DE (2005) Pulse energy dependence of subcellular dissection by femtosecond laser pulses. *Optics Express* 13:3690-3696
- Henderson BW, Dougherty TJ (1992) How does photodynamic therapy work? *Photochemistry and Photobiology* 55:145-157
- Hisatomi Y, Okumura K, Nakamura K, Matsumoto S, Satoh A, Nagano K, Yamamoto T, Endo F (2004) Flow cytometric isolation of endodermal progenitors from mouse salivary gland differentiate into hepatic and pancreatic lineages. *Hepatology* 39:667-675
- Hoffman RM (2006) The pluripotency of hair follicle stem cells. *Cell Cycle* 5:232-233
- Huang S, Ahmed A, Heikal A, Webb WW (2002) Two-photon fluorescence spectroscopy and microscopy of NAD(P)H and Flavoproteins. *Biophysical Journal* 82:2811-2825
- Hussain MA, Theise ND (2004) Stem cell therapy for diabetes mellitus. *Lancet* 364:203-205

- In 'K Anker PC, Noort WA, Scherjon SA, Der Keur CK, Kruisselbrink AB, Van Bezooijen RL, Beekhuizen W, Willemze R, Kanhai HH, Fibbe WE (2003) Mesenchymal stem cells in human secondtrimester bone marrow, liver, lung and spleen exhibit a similar immunophenotype, but a heterogeneous multilineage differentiation potential. *Haematologica* 88:845-852
- Jaenisch R, Young R (2008) Stem cells, the molecular circuitry of pluripotency and nuclear reprogramming. *Cell* 132:567-582
- Jaishankar A, Vrana KE (2009) Emerging molecular approaches in stem cell biology. *BioTechniques* 46:367-371
- Jasara J, Rudolph W (1999) Characterisation of sub-10-fs pulse focusing with high numerical aperture microscope objectives. *Optics Letters* 24:777-779
- Johnson PR, Dolman NJ, Vaillant C, Peterson OH, Tepkin AV, Erdemli G (2003) Non-uniform distribution of mitochondria in pancreatic acinar cells. *Cell Tissue Research* 313:37-45
- Joshi SS, Tarantolo SR, Kuszunski CA, Kessinger A (2000) Antitumor therapoitec potential of activated umbilical cord blood cells against leukaemia and breast cancer. *Clinical Cancer Research* 6:4351-4358
- Ju Z, Rudolph KL (2006) Telomeres and Telomerase in Stem Cells during Aging and Disease. *Genome Dynamics* 1:84-103
- Kedzior J, Masaoka M, Kurono C, Spondnik JH, Hallmann A, Majczak A, Niemczyk E, Trzonkowski P, Mysliwski A, Soji T, Wakabayashi T (2004) Changes in physicochemical properties of microtubules lead to the formation of a single spherical structures of mitochondrial assembly enveloping nuclear chromatins. *Journal Electron Microscopy* 53:659-670
- Kaji K, Norrby K, Paca A, Mileikovsky M, Mohseni P, Woltjen K (2009) Virus-free induction of pluripotency and subsequent excision of reprogramming factors. *Nature*. doi:10.1038/nature07864
- Kim JB, Sebastiano V, Wu G, Agauzo-Bravo MJ, Sasse P, Gentile L, Ko K, Ruau D, Ehrich M, D van den Boom, Meyer J, Hübner K, Bernemann C, Ortmeier C, Zenme M, Fleischmann BK, Zaehres H, and Schöler HR (2009) Oct4-Induced Pluripotency in Adult Neural Stem Cells. *Cell* 136:411-419
- Kirschstein R, Skirboll RL (2001) Stem Cells: Scientific Progress and Future Research Directions. Department of Health and Human Services. </info/scireport/2001report>

Bibliography 6

- Kruse C, Birth M, Rohwedel J, Assmuth K, Goepel A, Wedel T (2004) Pluripotency of adult stem cells derived from human and rat pancreas. *Applied Physics A* 76:1617-1724
- Kruse C, Kajahn J, Petschnik AE, Maass A, Klink E, Rapoport DH, Wedel T (2006) Adult pancreatic stem/progenitor cells spontaneously differentiate *in vitro* into multiple cell lineages and form teratoma-like structures. *Annals of Anatomy* 188:503-517
- Kohli V, Elezzabi A, Acker JP (2005) Cell nanosurgery using ultrashort (femtosecond) laser pulses: applications to membrane surgery and cell isolation. *Lasers in Surgery and Medicine* 37:227-230
- Kohli V, Elezzabi AY (2008) Laser surgery of zebrafish (*Danio rerio*) embryos using femtosecond laser pulses: Optimal parameters for exogenous material delivery, and the laser's effect on short- and long-term development. *BMC Biotechnology* 8:7
- Korbling M, Korbling, Katz R, Khanna A, Ruifrok A, Rondon G, Albitar M, Champlin R, Estrov Z (2002) Hepatocytes and epithelial cells of donor origin in recipients of peripheral-blood stem cells. *New England Journal of Medicine* 346:738-746
- König K, Schneckenburger H (1994) Laser-Induced Autofluorescence for Medical Diagnosis. *Journal of Fluorescence* 4:17-40
- König K (1999) Biomedizinische Applikationen der optischen Mikromanipulation und Zweiphotonen-Anregung vitaler Zellen mittels Naher-Infrarot Laser-Mikroskopie. Shaker Verlag Aachen
- König K, Becker W, Fischer P, Riemann I, Halbhuber K-J (1999a) Pulse-length dependence of cellular response to intense near-infrared laser pulses in multiphoton microscopes. *Optics Letters* 24:113-115
- König K, Riemann I, Fischer P, Halbhuber KJ (1999b) Intracellular nanosurgery with near infrared femtosecond laser pulses. *Cellular and Molecular Biology* 45:195-201.
- König K (2000a) Multiphoton Microscopy in life sciences. *Journal of Microscopy* 200:83-104
- König K (2000b) Robert Feulgen Prize Lecture 2000. Laser Tweezers and Multiphoton Microscopes in Life Sciences. *Histochemistry and Cell Biology* 114:79-92
- König K, Riemann I, Fritzsche W (2001) Nanodissection of human chromosomes with near infrared femtosecond laser pulses. *Optics Letters* 26:819-821
- König K, Krauss O, Riemann I (2002) Intratissue surgery with 80 MHz nanojoule femtosecond laser pulses in the near infrared. *Optics Express* 10:171-176
- König K, Schenke-Layland K, Riemann I, Stock UA (2005a) Multiphoton autofluorescence imaging of intratissue elastic fibers. *Biomaterials* 26:495-500

- König K, Riemann I, Stracke F, Le Harzic R (2005b) Nanoprocessing with nanojoule near-infrared femtosecond laser pulses. *Medical Laser Application* 20:169-184
- König K (2006) Cell damage during multi-photon microscopy. In: J.B. Pawley (ed.). *Handbook of biological confocal microscopy*, 3rd edition. Springer, NY, pp 680-689
- König K (2008) Clinical multiphoton tomography. *Journal of Biophotonics* 1:13-23
- König K, Weinigel M, Hoppert D, Bückle R, Schubert H, Köhler MJ, Kaatz M, Elsner P (2008) Multiphoton tissue imaging using high-NA microendoscopes and flexible scan heads for clinical studies and small animal research. *Journal of Biophotonics* 1:506-513
- Lakowicz JA (1999) *Principles of Fluorescence Spectroscopy*. 2nd ed. Springer Science/Business Media, New York
- Larson AM, Yeh AT (2006) Ex vivo characterization of sub-10 fs pulses. *Optics Letters* 31:1681-1683
- Lechner A, Habener JF (2003) Stem/progenitor cells derived from adult tissues:potential for the treatment of diabetes mellitus. *Journal of Physiological Endocrinology and Metabolism* 284:E259-E266
- Lee HS, Teng SW, Chen HC, Lo W, Sun Y, Lin TY, Chiou LL, Jiang CC, Dong CY (2006) Imaging the bone marrow stem cells morphogenesis in PGA scaffold by multiphoton autofluorescence and second harmonic (SHG) imaging. *Tissue Engineering* 12:2835-2842
- Li D, Zheng W, Qu JY (2008) Time-resolved spectroscopic imaging reveals the fundamentals of cellular NADH fluorescence. *Optics Letters* 33:2365-2367
- Lohergan T, Brenner C, Bavister B (2006) Differentiation-related changes in mitochondrial properties as indicators of stem cell competence. *Journal of Cellular Physiology* 208:149-153
- Loncar D (1992) Ultrastructural analysis of differentiation of rat endoderm *in vitro*: Adipose vascular-stromal cells induce endoderm differentiation, which in turn induces differentiation of the vascular-stromal cells into chondrocytes. *Journal of Submicroscopic Cytology and Pathology* 24:509-519
- Martin GR (1981) Isolation of a pluripotent cell line from early mouse embryos cultured in medium conditioned by teratocarcinoma stem cells. *Proceeding of the National Academic Sciences of the USA* 78:7634-7638.

Bibliography 6

- Masters BR, So PT, Gratton E (1997) Multiphoton excitation fluorescence microscopy and spectroscopy of *in vivo* human skin. *Biophysical Journal* 72:2405-2412
- Maximow A (1909) Der Lymphozyt als gemeinsame Stammzelle der verschiedenen Blutelemente in der embryonalen Entwicklung und im postfetalen Leber der Säugetiere. *Folia Haematologica* 8:125–141
- Mezey E, Chandross KJ, Harta G, Maki RA, McKercher SR (2000) Turning blood into brain: cells bearing neuronal antigens generated *in vivo* from bone marrow. *Science* 290: 1779–1782.
- Mezey E, Key S, Vogelsang G, Szalayova I, Lange GD, Crain B (2003) Transplanted bone marrow generates new neurons in human brains. *Proceedings of the National Academic Sciences of the USA* 100:1364-1369
- Minguell JJ, Erices A, Conget P (2001) Mesenchymal stem cells. *Experimental Biology and Medicine* 226:507-520
- Miller HR (2006) The promises of stem cells for neural repair. *Brain research* 1091:258-264
- Monici M, Agati G, Fusi F, Pratesi R, Paglierani M, Santini V, Bernabei PA (2002) Dependence of leukemic cell autofluorescence pattern on the degree of differentiation. *Photochemical and Photobiological Sciences* 2:981-987
- Morshead CM, Reynolds BA, Craig CG, McBurney MW, Staines WA, Morassutti D, Weiss S, van der Kooy D (1994) Neural stem cells in the adult mammalian forebrain: a relatively quiescent subpopulation of subependymal cells. *Neuron* 13:1071–1082.
- Murry CE, Wiseman RW, Schwartz SM, Hauschka SD (1996) Skeletal myoblast transplantation for repair of myocardial necrosis. *Journal of Clinical Investigation* 98: 2512–2523.
- Muschler GF, Nakamoto C, Griffith LG (2004) Engineering principles of clinical cell based tissue engineering. *Journal of Bone Joint Surgery* 86:1541-1558
- Müller M, Squier J, Wolleschensky R, Simon U, Brakenhoff J (1997) Dispersion precompensation for high numerical aperture objectives. *Journal of Microscopy* 191:141-150
- Neeley WL, Redenti S, Klassen H, Tao S, Desai T, Young MJ, Langer R (2008) A microfabricated scaffold for retinal progenitor cell grafting. *Biomaterials* 29:418-426
- Newmann CM, Bettinger T (2007) Gene therapy and prospects: ultrasound for gene transfer. *Gene therapy* 14:465-475

- Niesner R, Peker B, Schlüsche, Gericke (2004) Noniterative bi-exponential fluorescence lifetime imaging in the investigation of cellular metabolism by mean of NAD(P)H autofluorescence. *Physical Chemistry and Chemical Physics* 5:1141-1149
- Nuttall M E, Patton AJ, Olivera DL, Nadeau DP, Gowen M (1998) Human trabecular bone cells are able to express both osteoblastic and adipocytic phenotype: implications for osteopenic disorders. *Journal of Bone and Mineral Research* 13:371 -382.
- Oh B-K, Lee C-H, Park C, Park YN (2004) Telomerase regulation and progressive telomere shortening of rat hepatic stem-like epithelial cells during *in vitro* aging. *Experimental Cell Research* 298:445-454
- Orlic D, Kajstura J, Chimenti S, Jakoniuk I, Anderson SM, Li B, Pickel J, McKay R, Nadal-Ginard B, Bodine DM, Leri A, Anversa P (2001) Bone marrow cells regenerate infarcted myocardium. *Nature* 410:701-705.
- Palmer TD, Markakis EA, Willhoite AR, Safar F, Gage FH (1999) Fibroblast growth factor-2 activates a latent neurogenic program in neural stem cells from diverse regions of the adult CNS. *Journal of Neuroscience* 19:8487–8497
- Palumbo G, Caruso M, Crescenzi E, Tecce MF, Roberti G, Colasanti A (1996) Targeted gene transfer in eukaryotic cells by dye-assisted laser optoporation. *Journal of Photochemistry and Photobiology* 36:41-46
- Paterson L, Agate B, Comrie M, Ferguson R, Lake TK, Morris JE, Carruthers AE, Brown CTA, Sibbett W, Bryant PE, Gunn-Moore F, Riches AC, Dholakia K (2005) *Optics Express* 13:595-600
- Periasamy A (2001) *Methods in Cellular Imaging*. Oxford University Press, Oxford New York
- Periasamy A, Clegg RM (2009) *FLIM Microscopy in Biology and Medicine*. Taylor and Francis Group (CRC Press), Boca Raton London New York
- Pittenger MF, Mackay AM, Beck SC, Jaiswal RK, Douglas R, Moska JD, Moorman MA, Simonetti DW, Craig S, Marshak DR (1999) Multilineage potential of adult human mesenchymal stem cells. *Science* 284:143-147
- Priller J, Flügel A, Wehner T, Boentert M, Haas CA, Prinz M, Fernandes-Klett F, Prass K, Bechmann I, Bauke A. de Boer, Frotscher M, Kreutzberg GW, Persons DA, Dirnagl U (2001) Targeting gene-modified hematopoietic cells to the central nervous system: use of green fluorescent protein uncovers microglial engraftment. *Nature Medicine* 7:1356-1361

Bibliography 6

- Rapoport DH, Danner S, Kruse C (2009) Glandular stem cells are a promising source for much more than β -cell replacement. *Annals of Anatomy* 191:62-69
- Rebecca MW, Warren RZ, Watt WW (2001) Multiphoton microscopy in biological research. *Current Opinion in Chemical Biology* 5:603-608
- Reyes MG, Fermanian S, Yang F, Zhou SY, Herretes S, Murphy DB, Elisseeff JH, Chuck RS (2006) Metabolic changes in mesenchymal stem cells in osteogenic medium measured by autofluorescence spectroscopy. *Stem Cells* 24:1213-1217
- Rice WL, Kaplan DL, Georgakoudi I (2007) Quantitative biomarkers of stem cell differentiation based on intrinsic two-photon excited fluorescence. *Journal of Biomedical Optics Letters* 12:060504(1-3)
- Rotter N, Oder J, Schlenke P, Lindner U, Böhrnsen F, Kramer J, Rohwedel J, Huss R, Brandau S, Wollenberg B, Lang S, (2008) Isolation and Characterization of Adult Stem Cells from Human Salivary Glands. *Stem Cells and Development* 17:509-518
- Rubio D, Garcia-Castro J, Martin MC, Fuente R, Cigudosa J, Lloyd AC, Bernad A (2005) Spontaneous human adult stem cell transformation. *Cancer Research* 65:3035-3039
- Russels JA, Diamond KR, Collins TJ, Tiedje HF, Hayward JE, Farrell TJ, Patterson MS, Fang Q (2008) Characterization of Fluorescence Lifetime of Photofrin and Delta-Aminolevulinic Acid Induced Protoporphyrin IX in Living Cells Using Single- and Two-Photon Excitation. *IEEE Journal of Quantum Electronics* 14:158-166
- Sacconi L, Tolic-Norrelykke I, Antolini R, Pavone FS (2005) Combined intracellular three-dimensional imaging and selective nanosurgery by a nonlinear microscope. *Journal of Biomedical Optics* 10:14002
- Sakaguchi Y, Sekiya I, Yagishita K, Muneta T (2005) Comparison of human stem cells derived from various mesenchymal tissues: Superiority of synovium as a cell source. *Arthritis and Rheumatism* 52:2521-2529
- Sauer H, Rahimi G, Hescheler J, Wartenberg M (1999) Effects of electrical fields on cardiomyocyte differentiation of embryonic stem cells. *Journal of Cellular Biochemistry* 75:710-723
- Schenke-Layland K, Riemann I, Damour O, Stock UA, König K (2006) Two-photon microscopes and *in vivo* multiphoton tomographs- Powerful diagnostic tools for tissue engineering and drug delivery. *Advanced Drug Delivery Reviews* 58:878-896

- Schenke-Layland K, Ekaterini A, Rhodes KE, Hagvall SH, Mikkola HK, MacLellan WR (2007) Collagen IV Induces Trophoectoderm Differentiation of Mouse Embryonic Stem cells. *Stem Cells* 25:1519-1538
- Schneckenburger H, Hendinger A, Sailer R, Schmitt M (2002) *Journal of Biomedical Optics* 7:410-416
- Seaberg RM, Smukler SR, Kieffer TJ, Enikolopov G, Asghar Z, Wheeler MB, Korbitt G, van der Kooy D (2004) Clonal identification of multipotent precursors from adult mouse pancreas that generate neural and pancreatic lineages. *Nature Biotechnology* 22:1095-1096
- Shimada T, Watanabe W, Matsunaga S, Higashi T, Ishii H, Fukui K, Isobe K, Itoh K (2005) *Optics Express* 13:9869-9880
- Shirahata Y, Ohkohchi N, Itagak H, Satomi S (2001) New technique for gene transfection using laser irradiation. *Journal of Investigated Medicine* 49:184-190
- Sicter S, Reyers JMG, Moon CS, Suwan-Apichon O, Elisseeff JH, Chuck RS (2005) Noninvasive mitochondrial imaging in life cell culture. *Photochemistry and Photobiology* 81:1569-1571
- Siminovitch L, McCulloch EA, Till JE (1963) The distribution of colony-forming cells among spleen colonies. *Journal of Cellular Physiology* 62:327–336
- Skala MC, Riching KM, Bird DK, Gendron-Fitzpatrick A, Eickhoff J, Eliceiri KW, Keely PJ, Ramanujam N (2007) *In vivo* multiphoton fluorescence lifetime imaging of protein-bound and free nicotinamide adenine dinucleotide in normal and precancerous epithelia. *Journal of Biomedical Optics* 12:024014(1-10)
- Smith J, Ladi E, Mayer-Proschel M, Noble M (2000) Redox state is a central modulator of the balance between self-renewal and differentiation in a dividing glial precursor cells. *Proceedings of the National Academy of Sciences of the U.S.A.* 97:10032-10037
- Songtao Shi *et al.* (2003) Adult Human Dental Pulp Stem Cells *in vitro* and *in vivo* Dr. Songtao Shi *et al.* (NIDCR) U.S. Patent Application No. 10/333,522 filed 17 Jan 2003 (HHS Reference No. E-233-2000/0-US-03)
- Squirrell JM, Wokosin DL, White JG, Bavister BD (1999) Long-term two photon fluorescence imaging of mammalian embryos without compromising viability. *Nature Biotechnology* 17:763-767
- Squirrell JM, Eliceiri KW, Kamp TJ, Lyons CE (2008) Application of Multiphoton and Fluorescence Lifetime Microscopy of Endogenous Fluorescence to the Study of

Bibliography 6

- Differentiation in Mouse Embryonic Stem Cells. *Microscopy and Microanalysis* 14:1472-1473
- Stamm C, Westphal B, Kleine HD, Petzsch M, Kittner C, Klinge H, Schümichen C, Nienaber CA, Freund M, Steinhoff G (2003) Autologous bone marrow stem cell transplantation for myocardial regeneration. *Lancet* 361:45-46
- Stevenson DJ, Agate B, Tsampoula X, Fischer P, Brown CTA, Sibbett W, Riches A, Gunn-Moore F, Dholakia K (2006) Femtosecond optical transfection of cells: viability and efficiency. *Optics Express* 14:7125-7133
- Stingle A, Spielmann C, Krausz F, Szipöcs R (1994) Generation of 11-fs pulses from a Ti:sapphire laser without the use of prism. *Optics Letters* 19:204-206
- Suwa T, Yang L, Hornsby PJ (2001) Telomerase activity in primary cultures of normal adrenocortical cells. *Journal of Endocrinology* 170:677-684
- Takahashi K, Tanabe K, Ohnuki M, Narita M, Ichisaka T, Tomoda K, Yamanaka S (2007) Induction of Pluripotent Stem Cells from Adult Human Fibroblasts by Defined Factors. *Cell* 131:861-872
- Taylor DA, Atkins BZ, Hungspreugs P, Jones T, Reedy M, Hutcheson K, Glower D, Kraus W (1998) Regenerating functional myocardium: improved performance after skeletal myoblast transplantation. *Nature Medicine* 4:929-933
- Teisanu RM, Lagasse E, Whitesides JF, Stripp BR (2009) Prospective isolation of bronchial stem cells based upon immunophenotypic and autofluorescence characteristic. *Stem cells* 27:612-622
- Tempea G, Považay V, Assion A, Isemann A, Pervak W, Kempe M, Stingl A, Drexler W (2007) Undistorted delivery of sub-15 fs pulses via high-numerical-aperture microscope objectives. *Proceedings of the SPIE* 6442:64420P-1-5
- Thomas T, Nowka K, Lan L, Derwahl M (2006) Expression of endoderm stem cell markers: evidence for the presence of adult stem cells in human thyroid glands. *Thyroid* 16:537-544
- Thomson JA, Kalishman J, Golos TG, Durning M, Harris CP, Becker RA, Hear. JP (1995) Isolation of a primate embryonic stem cell line. *Proceedings of the National Academy of Sciences of the USA* 92:7844-7848
- Thomson JA, Itskovitz-Eldor J, Shapiro SS, Waknitz MA, Swiergiel JJ, Marshall VS, Jones JM (1998) Embryonic stem cell lines derived from human blastocysts. *Science* 282:1145-1147

- Till JE, McCulloch EA (1980) Hematopoietic stem cell differentiation. *Biochim. Biophys. Acta* 605:431-59
- Tirlapur UK, König K (2002) Targeted transfection by femtosecond laser. *Nature* 418:4295-4298
- Tomita S, Li RK, Weisel RD, Weisel RD, MD; Mickle DAG, MD; Kim EJ, Sakai T, Jia ZQ (1999) Autologous transplantation of bone marrow cells improves damaged heart function. *Circulation* 100:247-256
- Tsampoula X, Garces-Chavez V, Comrie M, Stevenson DJ, Agate B, Brown CTA, Gunn-Moore F, Dholakia K (2007) Femtosecond cellular transfection using a nondiffracting light beam. *Applied Physics Letters* 91:053902
- Tsampoula X, Taguchi K, Gizmar T, Garces-Chaves V, Ma N, Mohanty S, Mohanty K, Gunn-Moore G, Dholakia (2008) Fibre based cellular transfection. *Optics Express* 16:17007-170013
- Tsen S-WD, Wu C-Y, Meneshian A, Pai SI, Hung C-F, Wu T-C (2009) Femtosecond laser treatment enhances DNA transfection efficiency *in vivo*. *Journal of Biomedical Sciences* 16:36
- Uchugonova A, König K (2008) Two-photon autofluorescence and second-harmonic imaging of adult stem cells. *Journal of Biomedical Optics* 13:054068
- Uchugonova A, König K, Bückle R, Isemann A, Tempea G (2008a) Targeted transfection of stem cells with sub-20fs laser pulses. *Optics Express* 16:9357-9364
- Uchugonova A, Müller J, Bückle R, Tempea G, Isemann A, Stingl A, König K (2008b) Negatively-chirped laser enables nonlinear excitation and nanoprocessing with sub 20fs pulses. *Proceedings of the SPIE* 6860:686015
- Uchugonova A, Isemann A, Gorjup E, Tempea G, Bückle R, Watanabe W, König K (2008c) Optical knock out of stem cells with extremely ultrashort femtosecond laser pulses. *Journal of Biophotonics* 1:463-469
- Uchugonova A, Gorjup E, Riemann I, Sauer S, König K (2008d) Two-photon imaging of stem cells. *Proceedings of the SPIE* 6860:68601W-1-10
- Venugopalan V, Guerra A, Nahen K, Vogel A (2002) Role of laser-induced plasma formation in pulse cellular microsurgery and micromanipulation. *Physical Review Letters* 88:078103
- Vogel A, Venugopalan V (2003) Mechanism pulsed laser ablation of biological tissues. *Chemical Reviews* 103:577-644

Bibliography 6

- Vogel A, Noack J, Hüttman G, Paltauf G (2005) Mechanisms of femtosecond laser nanosurgery of cells and tissues. *Applied Physics B* 81:1015-1047
- Wagner DR, Lindsey DP, Li KW, Tummala P, Chandran SE, Smith RL Longaker MT, Carter DR, Beaupre GS (2008) Hydrostatic pressure enhances chondrogenic differentiation of human bone marrow stromal cells in osteochondrogenic medium. *Annals of Biomedical Engineering* 36:813-20
- Watanabe W, Matsunaga S, Shimada T, Higashi T, Fukui K, Itoh K (2005) Femtosecond laser disruption of mitochondria in living cells. *Medical Laser Application* 20:185-191
- Weiss S, Dunne C, Hewson J, Wohl C, Wheatley M, Peterson AC, Reynolds BA (1996) Multipotent CNS stem cells are present in the adult mammalian spinal cord and ventricular neuroaxis. *Journal of Neuroscience* 16:7599–7609
- Well DJ (2004) Gene therapy progress and prospects: electroporation and other physical methods. *Gene therapy* 11:101-107
- Wilson T, Sheppard C (1984) *Theory and practice of scanning optical microscopy*. San Diego, CA: Academic Press
- Wu BP, Tao Q, Lyle S (2005) Autofluorescence in the stem cell region of the hair follicle bulge. *Journal of Investigative Dermatology* 124:860-862
- Yaffe M (2003) The cutting edge of mitochondrial fusion. *Nature Cell Biology* 5:497-499
- Yim EKF, Pang SW, Leong KW (2007) Synthetic nanostructures inducing differentiation of human mesenchymal stem cells into neuronal lineage. *Experimental Cell Research* 313:1820-1829
- Young HE, Steele TA, Bray RA, Hudson J, Floyd JA, Hawkins K, Thomas K, Austin T, Edwards C, Cuzzourt J, Duenzl M, Lucas PA, Black AC (2001) Human reserve pluripotent mesenchymal stem cells are present in the connective tissues of skeletal muscle and dermis derived from fetal, adult, and geriatric donors. *Anatomical Record* 264:51-62.
- Yu D, Silva GA (2008) Stem cell sources and therapeutic approaches for central nervous system and neural retinal disorders. *Neurosurgical Focus* 24:E10
- Zhao L-R, Nam SC (2007) Multiphoton microscope imaging: The behavior of neural progenitor cells in the rostral migratory stream. *Neuroscience Letters* 425:83-88
- Zhang JC, Savage HE, Sacks PG, Delohery T, Alfano RR, Katz A, Schantz SP (1997) Innate Cellular Fluorescence Reflects Alteration in Cellular Proliferation. *Lasers in Surgery and Medicine* 20:319-331

- Zhou H, Wu S, Joo JY, Zhu S, Han DW, Lin T, Trauger S, Bien G, Yao S, Zhu Y, Siuzdac G, Schöler HR, Duan L, Ding S (2009) Generation of pluripotent stem cells using recombinant proteins. *Cell Stem Cell*. doi:10.1016/j.stem.2009.04005
- Zipfel WR, Williams RM, Webb WW (2003) Nonlinear magic: Multiphoton microscopy in the biosciences. *Nature Biotechnology* 21:1369-1377
- Zou G-M, Chen J-J, Ni J (2006) Light induces differentiation of mouse embryonic stem cells associated with activation of ERK5. *Oncogene* 25:463-469
- Zoumi A, Yen A, Tromberg BJ (2002) Imaging cells and extracellular matrix *in vivo* by using second harmonic generation and two-photon excited fluorescence. *Proceedings of the National Academy of Sciences of the USA* 99:11014-11019
- Zuk PA, Zhu M, Mizuno H, Huang J, Futrell JW, Katz AJ, Benhaim P, Lorenz HP, Hedrick MH (2001) Multilineage cells from human adipose tissue: implications for cell-based therapies. *Tissue Engineering* 7:211-228.

Frequently Used Abbreviations

abbr.	expanded abbreviation
AOTF	acousto-optical tunable filter
ATCC	American type culture collection
BMP	bone morphogenic growth factor
BP	bandpass
BS	beam splitter
Carboxy-H ₂ DCFDA	5-(and-6)-carboxy-2',7'-dichlorodihydrofluorescein diacetate
CCD	charge coupled device
CHO	Chinese hamster ovary
DAPI	4',6-diamidino-2-phenylindol
DBS	dichroic beam splitter
DEAE-dextran	diethylaminoethyl-dextran
DMEM	Dulbecco's modified Eagle's medium
DM	dispersive mirror
DMSO	dimethylsulfoxide [(CH ₃) ₂ SO]
DNA	desoxyribonucleic acid
ECM	extracellular matrix
ESC	embryonic stem cell
Eth. Bromide	Ethidium bromide (C ₂₁ H ₂₀ N ₃ Br)
FACS	fluorescence-activated cell sorting
FAD	flavin adenine dinucleotide
FLIM	fluorescence lifetime imaging
FMN	flavin mononucleotide
FSC	fetal calf serum
fs	femtosecond
FWHM	full-width half-maximum
GaAsP	gallium-arsenide-phosphide
GDD	group delay dispersion
GFP	green fluorescence protein
hBM-MSC	human bone marrow mesenchymal stem cell
HDM	highly-dispersive mirror
HOD	higher order dispersion
hDPSC	human dental pulp stem cell

Frequently Used Abbreviations

hSGSC	human salivary gland stem cell
hPSC	human pancreatic stem cell
iPSC	induced pluripotent stem cell
IRF	instrumental response function
kDa	kilodalton
LipDH	lipoamide dehydrogenase
LSM	laser scanning microscope
MACS	magnetic-activated cell sorting
MPM	multiphoton microscope
NAD(P)H	nicotinamide adenine (phosphate) dinucleotide
NA	numerical aperture
NDD	non-descanned detector
NGS	normal goat serum
NIR	near infrared
NL-PD	non-linear photodiode
NSC	neural stem cells
PBS	phosphate buffered saline
PCR	polymerase chain reaction
Pen/Strep	penicillin/streptomycin
PMT	photomultiplier tube
ps	picosecond
rPSCs	rat pancreatic stem cell
PtK2	rat kangaroo kidney 2
ROS	reactive oxygen species
SD	standard deviation
SHG	second harmonic generation
SP	short pass filter
TBP	time-bandwidth product
TBHP	tert-butyl hydroperoxide
TCSPC	time correlated single photon counting
TGF- β 3	transforming growth factor- β 3
TUNEL	terminal deoxynucleotidil transferase (TdT) – mediated dUTP nick-end labeling
UV	ultraviolet

List of Figures

Figure	Title	Page
1.1	Scheme of the ESCs isolation process and examples for embryonic stem cell-derived cell types.	4
1.2	Illustration of tissue specific stem cells from the skin. Stem cell populations have been identified in the epidermis (stratum basale), the hair follicle, and in the sebaceous gland.	5
1.3	Immunocytochemistry approach. Cells are stained with fluorophore-labeled antibodies. A primary antibody binds to a cellular specific antigen (receptor). This complex binds to a secondary fluorescent antibody which can be detected by fluorescence microscopy and FACS.	12
1.4	Methods for cell transfection.	16
1.5	Principle of one- and two-photon excitation. In the case of one-photon excitation of molecules, short-wavelength radiation with high energy photons are required. In two-photon excitation, two low-energy photons are absorbed simultaneously. The absorption from the ground state S_0 to the first excited electronic state S_1 occurs within femtoseconds (fs), whereas the vibrational relaxation within S_1 takes picoseconds (ps). The fluorescence of biomolecules occurs typically within some hundred picoseconds up to 10 nanoseconds (ns) after excitation.	18
1.6	Comparison of excitation volumes. In contrast to one-photon excitation (left), two-photon excitation occurs in a tiny sub-femtoliter focal volume only due to the required high GW/cm^2 light intensity. In one-photon microscopy, excitation (fluorescence) occurs in a large double cone shaped excitation volume.	19
1.7	Two photon excited fluorescence (TPF) versus SHG. SHG occurs immediately, at exactly half the laser wavelength λ_1 , and in forward direction whereas the fluorescence occurs some nanoseconds after excitation, at a wavelength range between $\lambda_1/2$ and λ_1 , and in isotropic direction.	20
1.8	(a) Femtosecond laser nanodissection and nanodrilling of human chromosomes. (b) Femtosecond-laser induced nanoholes in the cellular membrane for targeted transfection. (c) Ablation of single mitochondria in a living cell. (d) Disruption of cell-cell connections by femtosecond laser pulses (Tirlapur and König 2002; König <i>et al.</i> 2005b).	24

List of Figures

Figure	Title	Page
2.1	Images of a stem cell spheroid attached to a cover slip. Left: phase contrast image, Right: fluorescence image (blue: Hoechst 33342, red: Rhodamine 123).	30
2.2	Experimental setup of the modified ZEISS LSM510-NLO (META) multiphoton microscope and photograph of the microscope with the SHG detection module. BS-beam splitter; PMT-photomultiplier tube; AOTF-acousto-optical tunable filter; SP-short pass filter; BP-bandpass filter.	36
2.3	Experimental setup and photograph of the sub-20 femtosecond laser microscope FemtOgene. The beam emitted by the 12-fs oscillator passes a pair of high dispersion mirrors (HDM) before coupling into the scanning microscope via a dispersion-balanced Michelson scanning interferometer.	38
2.4	The spectrum and the autocorrelation function demonstrate the output laser parameters 12 fs, 80 nm full-width half-maximum (FWHM), 153 nm full-width tenth-maximum (FWTM), and the emission maximum at 792 nm.	39
2.5	Fluorescence decay curves. The green dotted curve reflects the mono-exponential fluorescence decay with a long fluorescence lifetime of 4.0 ns, whereas the blue dotted mono-exponential curve reflects a fluorophore with a short lifetime of 1.6 ns. Typically, the “real” autofluorescence decay of a stem cell is a bi-exponential (red curve) with two fluorophores with lifetimes $\tau_1 \approx 0.30$ ns and $\tau_2 \approx 2$ ns, respectively. The black curve reflects the instrumental response function (IRF).	41
2.6	Measured IRF from collagen II.	42
3.1	Absorption spectra of the major tissue components water, oxidized hemoglobin (HbO ₂), and melanin. The molar extinction coefficients and the absorption coefficient of water are depicted. The region of 600 nm – 1200 nm is referred as optical window due to the low absorption/extinction coefficients and the low scattering coefficients (König 1999).	44
3.2	Principle of multiphoton ionization (generation of free electrons and ions) and ROS formation during the multiphoton absorption process. S ₀ , S ₁ , and S ₂ are the ground state and higher energy excited electronic states, and T ₁ is the lowest energy triplet state for the molecule. ISC is intersystem crossing to the triplet state. Multiphoton ionization requires multiple photons (e.g. 4) and TW/cm ² intensities, respectively, to remove electrons from the molecule. Two-photon excitation at lower GW/cm ² intensities results in heat, fluorescence, and the occupation of the triplet state. The triplet state with a relatively long lifetime of some microseconds enables chemical reactions including oxygen which results in the formation of ROS.	45

Figure	Title	Page
3.3	(a) Positive control of ROS formation. Green fluorescence indicates generation of ROS. Additionally, the nuclei were stained with blue-fluorescent Hoechst 33342. (b) ROS negative cells after femtosecond laser exposure at 800 nm. The nuclear fluorescence due to Hoechst shows up only. (c) Normalized fluorescence spectra of carboxy-H ₂ DCFDA and Hoechst at 800 nm excitation.	48
3.4	Overlay of the green nuclear fluorescence and the transmission image of TUNEL positive cells after exposure to 250 fs laser pulses at 800 nm (60 mW, 1 scan). The spectrum shows the emission of the two-photon excited TUNEL assay probe.	49
3.5	The green fluorescence indicates laser-induced alterations of the membrane structure. The blue fluorescence in the cytoplasm depicts autofluorescence, whereas the nuclear fluorescence in the right image originates from the DNA stain Hoechst.	50
3.6	750 nm excited autofluorescence images of hSGSCs (left) and rPSCs (right). The beam splitter HFT KP 650 and the short pass filter KP 685 were employed for the detection.	51
3.7	Autofluorescence images of (a) rat pancreatic stem cells (rPSC), (b) human pancreatic stem cells (hPSC), (c) human dental pulp stem cells (hDPSC) and (d) human salivary gland stem cells (hSGSC) at 750 nm excitation wavelength (Uchugonova and König 2008).	52
3.8	Autofluorescence images of rPSC cells. Note that some cells (<5 %) exhibited a very intense autofluorescence (750 nm excitation wavelength).	52
3.9	Spectral analysis of hSGSC stem cells obtained from 32 images in the spectral range of 382 nm to 714 nm. Excitation wavelength was 750 nm (40x objective, the beam splitter HFT KP 650 was employed in front of the PMT array to avoid the detection of backscattered laser light).	53
3.10	(a) Spectral measurement of hSGSC stem cells. Four excitation wavelengths were employed. The emission peak shows a red-shift with increasing excitation wavelength due to the preferred two-photon excitation of flavins versus NAD(P)H. (b) The 750 nm/800 nm excited emission spectra can be considered as an overlay of the two fluorophores NAD(P)H and flavins (dotted lines, spectral unmixing).	54
3.11	FLIM of stem cells (hSGSC). The depicted decay curve is from an intracellular “pixel” of the right cell (cross), the τ_2 -histogram from the whole frame.	56

List of Figures

Figure	Title	Page
3.12	Histograms for the distribution of the fluorescent components (a) τ_1 , (b) τ_2 and (c) τ_m at 750 nm and 900 nm of hSGSC stem cells calculated from the frame in Fig. 3.11	57
3.13	Left: Average FLIM data of a particular cell were obtained from a region of interest (white rectangle). Right: The histogram reveals two short-lived components with two fluorescence lifetime maxima at 0.238 ns and 0.783 ns, respectively. The fluorophores with a lifetime in the range of 0.00-0.50 ns are depicted red and the fluorophores with a lifetime of 0.51-1.40 ns are shown green in the false color τ_1 image.	59
3.14	Adipocytes stained with red oil O (scale bar: 30 μ m).	59
3.15	Transmission and two-photon autofluorescence images of cells after adipogenic differentiation. In the transmission image the cell membrane of two adipocytes are marked (white line).	60
3.16	Spectral image (left) and spectra (right) of the cells 7 days after incubation in the adipogenic medium. Differentiated cells showed an increase of NAD(P)H and a decrease of flavins/flavoproteins compared to the non-differentiated cells as well as a decrease of the total fluorescence intensity of more than 60%. The dotted line is the normalized spectrum of the differentiated cells in order to indicate the blue shift compared to the non-differentiated cells (750 nm excitation wavelength).	61
3.17	ROI histogram distributions (τ_1 , τ_m , τ_2) and typical decay curves from differentiated cells and non-differentiated cells. Differentiated cells have a larger distribution of the short and long fluorescent component (large FWHM of the histogram) and a significantly larger fluorescence lifetime τ_2 compared to the non-differentiated cells.	62
3.18	False-color coded FLIM image of cells after adipogenic differentiation. Upper image: 750 nm excitation wavelength, lower image: 900 nm excitation wavelength. Non-differentiated cells (n) have a yellow-red color code in the τ_m and τ_2 image due to the shorter fluorescence lifetime compared to the “blue-green” differentiated cells (d). At longer excitation wavelength, NAD(P)H fluorescence is not observed. Mainly flavins in non-differentiated cells and further fluorophores (lysosomes, see fig. 3.19 and chapter 3.2.5) in differentiated cells appear during 900 nm excitation.	63
3.19	Two-photon images of differentiated cells stained with probes to track mitochondria (green) and lysosomes (red). Cell membranes are depicted (white).	64

Figure	Title	Page
3.20	Two-photon excited autofluorescence and SHG spectrum from collagen II (Sigma-Aldrich).	65
3.21	Fluorescence lifetime distribution histogram of collagen II at 750 nm excitation.	66
3.22	SHG (yellow fibrils) and autofluorescence (blue-green) imaging of stem cell spheroids by optical sectioning without BP435/5 filter (left) and with bandpass filter (right). 40x/1.3 oil objective, 870 nm excitation.	67
3.23	False-color coded FLIM images from cells 4 weeks after onset of differentiation. (a) Autofluorescence and SHG detection in the spectral range of 400-610 nm (870 nm excitation). Fluorescence (blue, green) arises mainly from cells, SHG (red, yellow) from collagen structures. (b) The signal is dominated by SHG of collagen when using a bandpass 435/5 filter. (c) Luminescence lifetime measurements of a fluorescent cellular organelle (red curve) and from a collagen structure (blue curve).	68
3.24	Immunocytochemistry. Left: Mesenchymal stem cells produced collagen I after 3 weeks of osteogenic differentiation. Right: Rat pancreatic stem cell produced collagen II after 3 weeks of chondrogenic differentiation.	69
3.25	Older stem cells exhibit a strong autofluorescence due to the presence of lysosomes. Note the weaker autofluorescence of the mitochondria (scale bar: 10 μ m).	70
3.26	Lysosomes (red), mitochondria (green) and nuclei (blue) of 2 weeks old stem cells.	70
3.27	Two-photon fluorescence of rat pancreatic stem cells before (left) and after single point illumination of one particular cell (arrow). The laser-exposed cell died and took up the dead-cell indicator Ethidium bromide (scale bar: 30 μ m).	71
3.28	Two-photon excited fluorescence of human mesenchymal stem cells before (left) and 1 min after intense single-point illumination of a particular cell (right, arrow) and administration of a fluorescent annexin probe (green) and Ethidium bromide (red). As a result of laser exposure, Phosphatidil-serine translocated to the outer leaflet of the membrane and bound to extracellular annexin V (Uchugonova <i>et al.</i> 2008c).	72

List of Figures

Figure	Title	Page
3.29	Fluorescence images of human mesenchymal stem cells incubated with the DNA marker Hoechst (blue), the annexin probe (green) and Ethidium bromide (red) before (left) and 15 min after laser exposure. Only the cell which was exposed to high-power laser radiation emitted fluorescence from the dead-cell indicator Ethidium bromide and the annexin V probe. The laser-exposed cell was clearly fragmented.	73
3.30	Autofluorescence before and after single point illumination of human pancreatic stem cells. Right: The nucleus of the laser treated cell (7 mW, 12 fs pulse width, 0.5 s, single point illumination) became fluorescent likely to the diffusion of NAD(P)H through laser-induced nuclear nanopores (scale bar: 30 μm).	74
3.31	Line scans with low powers down to 7 mW (12 fs laser pulses) produced tiny nanocuts (left image, arrows). Scanning of a whole cell within a cell monolayer destroyed the laser-exposed cell without collateral effects (right image) (scale bar: 30 μm).	74
3.32	Detection of the membrane integrity and cell viability probed by Ethidium bromide within a human pancreatic stem cell spheroid. One particular cell at a depth of 20 μm was exposed with an intense beam (2.6 nJ) by single-point illumination. The stack of two-photon images was taken within 1 minute after this laser procedure. Ethidium bromide entered this particular cell only.	75
3.33	Fluorescence image before (left) and after (right) destructive illumination of two intraspheroidal human pancreatic stem cells with intense laser pulses. The laser-exposed cells became highly fluorescent	76
3.34	Optical cleaning of stem cell cultures. One particular cell was kept alive whereas the surrounding cells were optically destroyed (left: autofluorescence image before intense ROI scanning, middle: autofluorescence 1 min after exposure). The non-exposed cell survived and started cell division (right).	77
3.35	(a) Two-photon autofluorescence image of human salivary gland stem cells. The major endogenous fluorophore is the reduced coenzyme NADH. 250x250 μm^2 image. (b) Cell fluorescence after optoporation of two cells and the application of Ethidium bromide. Non-exposed cells did not uptake the fluorescent probe.	78

Figure	Title	Page
3.36	Two-green fluorescent daughter cells 3 days after laser optoporation of a single human salivary gland stem cell. (a) Fluorescence image taken with a short pass filter 610 and an excitation wavelength of 750 nm. Both the natural autofluorescence as well as the GFP fluorescence are depicted. (b) The use of the GFP bandpass filter in combination with an excitation wavelength of 800 nm results mainly in the green fluorescence. (c) Overlay of the green fluorescence with the transmission image.	79
3.37	Typical spectrum of intracellular GFP within transfected stem cells.	80

List of Tables

Table	Title	Page
3.1	Typical laser and exposure parameters used for two-photon imaging of stem cells.	46
3.2	Intracellular FLIM data obtained from 10 decay curves within the cytoplasm of the stem cell with the cross in Fig. 3.11 (Uchugonova and König 2008).	56
3.3	Average FLIM data calculated from 10 regions of interest covering one single cell in each region. “x”- no component was detected.	58
3.4	FLIM data obtained from 750 nm excited non-differentiated cells and cells with fat droplets.	61
4.1	Autofluorescence modifications of stem cells and cells after adipogenic differentiation measured by multiphoton spectral and fluorescence lifetime imaging within this work.	85

Appendix A

Published paper: Uchugonova A and König K (2008) Two-photon autofluorescence and second harmonic imaging of adult stem cells. *Journal of Biomedical Optics* 16:054068-8

Abstract Human and animal stem cells (rat and human adult pancreatic stem cells, salivary gland stem cells, human dental pulp stem cells) are investigated by femtosecond laser 5-D two-photon microscopy. Autofluorescence and second harmonic generation (SHG) are imaged with submicron spatial resolution, 270 ps temporal resolution, and 10 nm spectral resolution. In particular, the reduced coenzyme nicotinamide adenine (phosphorylated) dinucleotide [NAD(P)H] and flavoprotein fluorescence was detected in stem cell monolayers and stem cell spheroids. Major emission peaks at 460 nm and 530 nm with typical long fluorescence lifetimes (τ_2) of 1.8 ns and 2.0 ns, respectively, are measured using spectral imaging and time-correlated single photon counting. Differentiated stem cells produced the extracellular matrix (ECM) protein collagen, detected by SHG signals at 435 nm. Multiphoton microscopes may become novel non-invasive tools for marker-free optical stem cell characterization and for on-line monitoring of differentiation within a 3-D microenvironment.

Keywords: stem cell, 5D two photon imaging, autofluorescence, second harmonic generation

© 2008 Society of Photo-Optical Instrumentation Engineers

The article is available online via <http://dx.doi.org/10.1117/1.3002370>

Appendix B

Published paper: Uchugonova A, Isemann A, Gorjup E, Tempea G, Bückle R, Watanabe W, König K (2008) Optical knock out of stem cells with extremely ultrashort femtosecond laser pulses. *Journal of Biophotonics* 1:463-469

Abstract Novel ultracompact multiphoton sub-20 femtosecond near infrared 85 MHz laser scanning microscopes and conventional 250 fs laser microscopes have been used to perform high spatial resolution two-photon imaging of stem cell clusters as well as selective intracellular nanoprocessing and knock out of living single stem cells within an 3D microenvironment without any collateral damage. Also lethal cell exposure of large parts of cell clusters was successfully probed while maintaining single cells of interest alive. The mean power could be kept in the milliwatt range for 3D nanoprocessing and even in the microwatt range for two-photon imaging. Ultracompact low power sub-20 fs laser systems may become interesting tools for optical nanobiotechnology such as optical cleaning of stem cell clusters as well as optical transfection.

Key words: femtosecond laser, optical knock out, stem cell, nanoprocessing, multiphoton microscopy

© 2008 by WILEY-VCH Verlag GmbH & Co. KGaA, Weinheim

The article is available online via [http://doi: 10.1002/jbio.200810047](http://doi:10.1002/jbio.200810047)

Appendix C

Published paper: Uchugonova A, Isemann A, Tempea G, Bückle B, and König K (2008) Targeted transfection of stem cells with sub-20 femtosecond laser pulses. *Optics Express* 16: 9357-9364

Abstract Multiphoton microscopes have become important tools for non-contact sub-wavelength three-dimensional nanoprocessing of living biological specimens based on multiphoton ionization and plasma formation. Ultrashort laser pulses are required, however, dispersive effects limit the shortest pulse duration achievable at the focal plane. We report on a compact nonlinear laser scanning microscope with sub-20 femtosecond 75 MHz near infrared laser pulses for nanosurgery of human stem cells and two-photon high-resolution imaging. Single point illumination of the cell membrane was performed to induce a transient nanopore for the delivery of extracellular green fluorescent protein plasmids. Mean powers of less than 7 mW (<93 pJ) and low millisecond exposure times were sufficient to transfect human pancreatic and salivary gland stem cells. Ultracompact sub-20 femtosecond laser microscopes may become optical tools for nanobiotechnology and nanomedicine including optical stem cell manipulation.

OCIS codes: (140.3538) Lasers, pulsed; (180.4315) Nonlinear microscopy; (000.1430) Biology and medicine; (020.4180) Multiphoton processes; (140.7090) Ultrafast lasers; (170.3890) Medical optics instrumentation

© 2008 *Optical Society of America*

The article is available online via <http://doi:10.1364/OE.16.009357>

Acknowledgements

First and foremost, I would like to thank Professor Karsten König for providing me the opportunity to join the scientific world in Europe. Dear Professor König, thank you very much for your teaching in the fascinating area of laser microscopy, for your guidance into the research field “femtosecond laser - stem cell interaction”, and for your permanent scientific inspiration and technical supports. I would like to point that I am very thankful for the very interesting proposal of my PhD work.

Dear Professor Günter Fuhr, thank you very much for providing me generous financial supports to realize my PhD work and for giving me the opportunity to work at the Fraunhofer Institute of Biomedical Engineering. Especially, I thank you for your teaching, motivations, and the organization of the “Doktorandenseminar” where I gained a huge experience in research discussions and training in giving scientific presentations.

Furthermore, I would like to thank Erwin Gorjup from the IBMT Department *Biohybride* for the characterization of stem cells and for helping me with stem cell handling. Thanks, I enjoyed working with you. I also like to thank Professor Katja Schenke-Layland (UCLA, USA) for sharing with me her expertise on stem cells and many discussions on the differentiation of stem cells. I thank also for providing me the possibility to practice methods on stem cells in the *Cardiovascular Stem Cell Research Center* at the UCLA.

I have profited in multiple ways from supports by my colleagues in the *Biomedical Optics Group*, in particular Dr. Iris Riemann, Dr. Frank Stracke, Dr. Ronan LeHarzic, Daniel Dörr, David Brunell, Juliette Müller, Martin Schwarz and most notable Daniel Sauer who helped me to adjust the microscopes and lasers and took assistance during many experiments. I thank Iris and Frank for their helpful comments regarding this dissertation and my ex-colleague Dr. Alexander Ehlers for teaching FLIM.

I wish to thank Professor Ammasi Periasamy (Director of the Keck Center at the University of Virginia) for many discussions on FLIM.

I would like to thank the Deutsche Akademische Austauschdienst (DAAD) for financial support, the German Research Foundation (Deutsche Forschungsgemeinschaft; DFG) for travel grants to attend the two important conferences *Photonics West* in California during which I presented parts of this dissertation, as well as for the fellowship to visit the *Cardiovascular Stem Cell Research Center* at UCLA.

Acknowledgements

I happily thank my friends who provided me with the environment to enjoy my research.

Finally, I thank my family members Batina, Gulmairam, Gulzada, Bakutbek, Gulnara, Baktugul, and Nurlan for their supports, their encouragements and for giving me confidence. I love you and miss you.

The same goes to my father Asan and to my mother Basira to whom this dissertation is dedicated. Words fail to express my feelings. Thank you for your LOVE.

Own Publication List

Peer-reviewed papers

1. **Uchugonova A**, Kadyraliev TK, Kaliev RR, Zakirov DZ, Jumagulova A (2002) Morphophysiological changes in kidneys under the influence of hypoxic hypoxia. Vestnic of KNU 2002:139-145
2. **Uchugonova A**, Kadyraliev TK (2003) Structural-functional changes in kidneys under the influence of hypobaric hypoxia. Vestnic of KNU 2003:184-186
3. Kadyraliev TK, Raymbecov NK, **Uchugonova A** (2004) Morphological changes of pulmonary vessels at the high-altitude pulmonary arterial hypertension. Central Asian Medicine Journal 10:22-24
4. **Uchugonova A**, Isemann A, Tempea G, Bückle B, König K (2008) Targeted transfection of stem cells with sub-20 femtosecond laser pulses. Optics Express 16:9357-9364
5. **Uchugonova A**, König K (2008) Two-photon autofluorescence and second harmonic imaging of adult stem cells. Journal of Biomedical Optics 13:054068-8
6. **Uchugonova A**, Isemann A, Gorjup E, Tempea G, Bückle R, Watanabe W, König K (2008) Optical knock out of stem cells with extremely ultrashort femtosecond laser pulses. Journal of Biophotonics 1:463-469
7. Földes-Papp Z, König K, Studier H, Bückle R, Breunig HG, **Uchugonova A**, Kostner GM (2009) Trafficking of mature miRNA into the nucleus of liver cells. Current Pharmaceutical Biotechnology 10, in press

Proceedings

1. **Uchugonova A**, Riemann I, Stracke F, Martin S, König K (2007) The influence of NIR femtosecond laser radiation on the viability of 3D stem cell clusters and tumor spheroids. Proceedings of the SPIE 6442:64421Z-1
2. Riemann I, Stracke F, **Uchugonova A**, Martin S, Bückle R, König K (2007) Optical nano-injection into cells and 3D stem cell clusters via a NIR femtosecond laser. Proceedings of the SPIE 6442:64421F-1

Own Publication List

3. **Uchugonova A**, Riemann I, Stracke F, LeHarzic R, König K (2007) Optical knocking out of single cells in tumor spheroids by femtosecond laser. WLT Proceedings 2007, 887-889
4. **Uchugonova A**, Gorjup E, Riemann I, Sauer D, König K (2008) Two photon imaging of stem cell. Proceedings of the SPIE 6860:68601W-1
5. **Uchugonova A**, König K, Bückle R, Tempea G, Isemann A, Stingl A (2008) Negatively-Chirped Laser Enables Nonlinear Excitation and Nanoprocessing with sub-20-fs Pulses. Proceedings of the SPIE 6860:686015-1
6. **Uchugonova, A**, Isemann, A, Bückle R, Watanabe W, König K (2009) Two-photon imaging and nanoprocessing of stem cells. Proceedings of the SPIE 7183:71831A-6
7. **Uchugonova A**, König K (2009) Multiphoton imaging and 3D nanoprocessing of stem cells. Proceedings of the II International Symposium “Topical Problems of Biophotonics 2009”, 82-83

Book chapters

1. König K, Bauerfeld F, Sauer D, Schuck H, **Uchugonova A**, Lei E, Stark M, Velten T, Bückle R, LeHarzic R (2007) Femtosecond laser nanomachining of silicon wafers and two-photon nanolithography for stem cell research. In: Masuhara H, Kawata S (eds.) Handai Nano Biophotonics 3. Elsevier, Amsterdam Oxford, pp 287-296
2. König K, **Uchugonova A** (2009) Multiphoton Fluorescence Lifetime Imaging at the Dawn of Clinical Application. In: Periasamy A, Clegg RM (eds.) FLIM Microscopy in Biology and Medicine. Taylor & Francis Group (CRC Press), Boca Raton London New York, pp 165-187

Declaration

I hereby declare that this thesis is the result of my own independent investigation and that all contributions from other sources are duly acknowledged. No part of this thesis was previously submitted for a degree at this or another university.

Ich erkläre hiermit an Eides statt, dass ich die vorliegende Arbeit ohne unzulässige Hilfe Dritter und ohne Benutzung anderer als der angegebenen Hilfsmittel angefertigt habe. Die aus anderen Quellen direkt oder indirekt übernommenen Daten und Konzepte sind unter Angabe der Quelle gekennzeichnet.

Die Arbeit wurde bisher weder im Inland noch im Ausland in gleicher oder ähnlicher Form in einem anderen Verfahren zur Erlangung des Doktorgrades einer anderen Prüfungsbehörde vorgelegt.

Aisada Uchugonova

Saarbrücken, 18 August 2009

Curriculum Vitae

Aisada Uchugonova

born May 3, 1977 in Naryn (Kyrgyzstan)

Education

School «B. Kalenderov», Naryn, Kyrgyzstan Grade: “excellent”	1984-1994
National Medical College, Bishkek, Kyrgyzstan, Medical Assistant of the Laboratory of Clinical Diagnostics; Grade: “excellent”	1995-1997
Kyrgyz National University, Bishkek, Kyrgyzstan, Bachelor of Biology; Grade: “excellent”	1997-2001
Kyrgyz National University, Bishkek, Kyrgyzstan, Master of Biology, Specialization: Biomedical Science; Grade: “excellent”	2001-2003

Professional experience

Student assistant, National Center of Cardiology and Internal Medicine (NCCIM), Bishkek, Kyrgyzstan (Prof. Dr. T. Kadyraliev)	June 1, 2001- July 30, 2003
Researcher, Institute of Molecular Biology and Medicine (IMBM) at the National Center of Cardiology and Internal Medicine (NCCIM), Bishkek, Kyrgyzstan (Prof. Dr. A. Aldashev)	August 1, 2003 - July 30, 2005
Researcher, Fraunhofer Institute of Biomedical Technology (IBMT), St. Ingbert, Germany (Prof. Dr. K. König)	October 1, 2005 - June 30, 2006
Researcher, JenLab GmbH, Jena, Germany	July 1- October 15, 2006
Qualification as Laser Safety Officer (Laserschutzbeauftragter), Universität des Saarlandes, UoS, Saarbrücken	October 16, 2005 – February 28, 2006
Researcher, Fraunhofer Institute of Biomedical Technology (IBMT), St. Ingbert and Saarland University (UoS), Germany (Prof. Dr. G. Fuhr and Prof. Dr. K. König)	October 16, 2006 - October 31, 2009

Curriculum Vitae

Presentations

- Cytometry 16th, Annual meeting of German Society for Cytometry (DGFZ), Leipzig, Germany. “*In vivo* multiphoton imaging of single cells in human skin using femtosecond laser pulses”. October 18-21, 2006
- Conference Focus on Microscopy, Valencia, Spain. “Optical knocking out of single cells in tumor spheroids and stem cell clusters using nanojoule femtosecond laser pulses”. April 10-13, 2007
- International Workshop on Advanced Multiphoton and Fluorescence Lifetime Imaging Techniques 2007, St. Ingbert, Germany. “The influence of NIR femtosecond laser radiation on the viability of three dimensional stem cell clusters”. June 13-15, 2007
- WLT Conference Laser in Manufacturing, Laser 2007, München, Germany. “Optical knocking out of single cells in tumor spheroids by femtosecond laser”. June 20-21, 2007
- Conference Photonics West, “International Society for Optical Engineering” (SPIE), BiOS, 2007. San Jose, CA, USA. “The influence of NIR femtosecond laser radiation on the viability of 3D stem cell clusters and tumor spheroids”. January 20-25, 2007
- Conference Photonics West, “International Society for Optical Engineering” (SPIE), BiOS, 2008. San Jose, CA, USA. “Two photon imaging of stem cells”. January 16-24, 2008
- International Workshop on Advanced Multiphoton and Fluorescence Lifetime Imaging Techniques 2008, Saarbrücken, Germany. “Optical knock out and targeted trasfection of stem cells with sub-20 femtosecond laser pulses”. June 30-July 2, 2008
- International Seminar, Cardiovascular Stem Cell Research Center, University of California, Los Angeles (UCLA), USA “Two-photon autofluorescence and second harmonic generation (SHG) imaging of stem cells”. February, 2008
- Conference Photonics West, “International Society for Optical Engineering” (SPIE), BiOS, 2009. San Jose, CA, USA. “Two-photon imaging and nanoprocessing of stem cells”. January 24-29, 2009
- II International Symposium on Topical problems of Biophotonics, 2009, Nizhny Novgorod, Russia “Multiphoton imaging and 3D nanoprocessing of stem cells”. July 19-24, 2009

Awards and Grants, Fellowships

Fellowship of the “Deutsche Akademische Austauschdienst“ (DAAD)	October 01, 2005 – June 30, 2006
SPIE Award: “Best Poster Prize” (Photonics West, BIOS, San Jose, CA, USA)	January 16, 2008
Travel Grant of the “Deutsche Forschungsgemeinschaft” (DFG); Photonics West, San Jose, CA, USA	January 16-24, 2008
Fellowship of the “Deutsche Forschungsgemeinschaft” (DFG); Cardiovascular Stem Cell Research Center, University of California, Los Angeles (UCLA), CA, USA	February, 2008
Travel Grant of the “Deutsche Forschungsgemeinschaft” (DFG); Photonics West, San Jose, CA, USA	January 23-29, 2009

